March 2018

Structure-Property Relationships of Polymer Films and Hydrogels to Control Bacterial Adhesion

Kristopher W. Kolewe
University of Massachusetts Amherst

STRUCTURE-PROPERTY RELATIONSHIPS OF POLYMER FILMS AND HYDROGELS TO CONTROL BACTERIAL ADHESION

A Dissertation Presented

by

KRISTOPHER W. KOLEWE

Submitted to the Graduate School of the
University of Massachusetts Amherst in partial fulfillment
of the requirements for the degree of

DOCTOR OF PHILOSOPHY

February 2018

Chemical Engineering

STRUCTURE-PROPERTY RELATIONSHIPS OF POLYMER FILMS AND HYDROGELS TO CONTROL BACTERIAL ADHESION

A Dissertation Presented

by

KRISTOPHER W. KOLEWE

Approved as to style and content by:

_____
Jessica D. Schiffman, Chair

_____
Shelly R. Peyton, Member

_____
Maria M. Santore, Member

_____
Susan C. Roberts, Member

_____
John Klier, Department Head
Chemical Engineering

ACKNOWLEDGEMENTS

I would like to thank the Chemical Engineering Department at UMass Amherst for giving me the opportunity to pursue my Ph.D. This work was partially funded by the National Research Service Award T32 GM008515 from the National Institutes of Health, the James M. Douglas Career Development Faculty Award, and Armstrong Fund for Science.

I would like to thank my advisor, Dr. Jessica Schiffman, for all the time and seemingly endless patience she invested in me over the years. I'm thankful for her support as I pursued the many side projects and collaborative studies that supplemented by thesis work. Her enthusiasm for science and dedication to her students has been inspirational and helped me grow both as a person and as a scientist. I also want to thank my committee members Prof. Shelly Peyton, Prof. Susan Roberts, and Prof. Maria Santore for valuable insights and contributions with my research. Special thanks to Prof. Santore for her guidance throughout our collaborative work and for essentially adopting me as a member of her group. I want to thank Dr. Mike Imburgia, Sami Fakhouri, and Vijesh Tanna for training in the mechanical characterization instrumentation and techniques I used throughout my thesis. I also want to thank the professors and students I collaborated with during my thesis: Prof. Maria Santore, Dr. Surachate Kalasin, Prof. Todd Emrick, Dr. Chia-Chih Chang, Dr. Ying Bai, Prof. Stephen Nonnenmann, Jiaxin Zhu, Prof. Shelly Peyton, Dr. Lauren Barney, Prof Alejandro Briseno, Dr. Leonardo Gonzalez, Edmund Burnett, Victor Champagne, Prof. James Watkins, Feyza Dundar, Prof. Kenneth Carter, Dr. Yinyong Li, Prof. Neil Forbes, Abhinav Sharma, Vishnu Raman, Prof. Sarah Perry, and Shuo Sui.

I would like to thank the former and current members of the Schiffman Lab whom I've had the opportunity to work with over the years Dr. Katrina A. Rieger, Dr. Nathan P. Birch, Kerianne M. Dobosz, Xiangxi Meng, Thomas C. DiGiovanni, Irene Kurtz, Mungfei Huang, Dr. Guozhen Yang, and Dr. Yuan Liu. The group has made coming to the lab every day a productive yet fun and eventful experience. Special thanks to Katrina, Kerianne, and Nate for their help on various projects over the years. I would like to thank the undergraduate students who I've had the chance to mentor and work with Eric Rice, Natalie Mako, R.J. Roth, Robin Levinson, and Annuli Okoye.

I want to thank my friends and family for their support over the years, especially my parents, Nancy and Diethard, and my siblings, Korwyn and Martin. Finally, I would like to express my love and appreciation for my wife Emily and my excitement for whatever the future holds.

ABSTRACT

STRUCTURE-PROPERTY RELATIONSHIPS OF POLYMER FILMS AND HYDROGELS TO CONTROL BACTERIAL ADHESION

FEBRUARY 2018

KRISTOPHER W. KOLEWE

B.S., SYRACUSE UNIVERSITY

Ph.D., UNIVERSITY OF MASSACHUSETTS - AMHERST

Directed by: Professor Jessica D. Schiffman

The emergence and spread of antibiotic resistance across microbial species necessitates the need for alternative approaches to mitigate the risk of infection without relying on commercial antibiotics. Biofilm-related infections are a class of notoriously difficult to treat healthcare-associated infections that frequently develop on the surface of implanted medical devices. As biofilm formation is a surface-associated phenomenon, understanding how the intrinsic properties of materials affect bacterial adhesion enables the development of structure-property relationships that can guide the future design of infection-resistant materials. Despite lacking visual, auditory, and olfactory perception, bacteria still manage to sense and attach to surfaces. Previously, it has been reported that bacteria can detect and differentiate the surface chemistry and topography of surfaces; however, the influence of the stiffness and thickness on bacterial-surface interactions remains unknown.

In this thesis, the effect that the fundamental material properties of polymer films and hydrogels (stiffness, thickness, and chemistry) have on the adhesion and surface-associated transport of bacteria was investigated. By decoupling the effect of the hydrogel's

stiffness and thickness from their chemistry, we suggest a key takeaway design rule: to optimize fouling-resistance, hydrogel coatings should be thick and soft. Two chemically distinct hydrogels, poly(ethylene glycol) and agar, were synthesized over a 1-1000 kPa range of Young's modulus. Static adhesion experiments, conducted on 150 μm thick hydrogels, determined that *Escherichia coli* and *Staphylococcus aureus* colony surface coverage correlated positively with an increase in Young's modulus. Notably, a substantial increase in adhesion occurred for both bacteria when the thickness of the hydrogels was reduced to 10 μm. The stiffness of poly(ethylene glycol) brushes and hydrogels was also found to influence the length and frequency of *Staphylococcus aureus* surface-associated transport via dynamic shear flow experiments. Furthermore, a universal hydrogel functionalization platform was developed for instances where mechanical properties of hydrogels are not adjustable. The incorporation of the fouling-resistant polymer zwitterion, poly(2-methacryloyloxyethyl phosphorylcholine), enhanced resistance to bacterial adhesion without altering the mechanical properties of covalently or physically crosslinked hydrogels. This thesis demonstrates that by combining structure-property relationships with fouling-resistant zwitterionic chemistry, the adhesion of proteins and microorganisms to polymer hydrogels is reduced.

TABLE OF CONTENTS

Page

LIST OF TABLES

Table **Page**

LIST OF FIGURES

Figure **Page**

LIST OF ABBREVIATIONS

AFM: atomic force microscopy

CDC: Center for Disease Control and Prevention

CLSM: confocal laser scanning microscopy

E. coli: *Escherichia coli*

EPS: extracellular polymeric substances

FTIR: Fourier transform infrared spectroscopy

GFP: green fluorescent protein

HAIs: healthcare-associated infections

LB: Difco Luria-Bertani broth

M9: M9 minimal salt media

MPC: 2-methacryloyloxyethyl phosphorylcholine

MRSA: Methicillin-resistant *Staphylococcus aureus*

MSCRAMM: microbial surface components recognizing adhesive matrix molecules

NaOH: sodium hydroxide

NOA60: Norland optical adhesive 60

P. aeruginosa: Pseudomonas aeruginosa

PBS: phosphate buffered saline

PDA: polydopamine

PEG: poly(ethylene glycol)

PEG: poly(ethylene glycol) dimethacrylate

PEM: polyelectrolyte multilayer

PET: polyethylene terephthalate

PI: propidium iodide

PMMA: poly(methyl methacrylate)

PMPC: poly(2-methacryloyloxyethyl phosphorylcholine)

PVT: physical vapor transport

RGB: red/green/blue

S. aureus: Staphylococcus aureus

SAOS: small amplitude oscillatory shear rheology

SEM: scanning electron microscopy

SHS: superhydrophobic surface

SLIPS: Slippery Liquid-Infused Porous Surfaces

TEM: transmission electron microscopy

TRIS: sodium periodate tris(hydroxymethyl)aminomethane

TSB: tryptic soy broth

Wt %: weight percent

XPS: X-ray photoelectron spectroscopy

ZnPc: zinc phthalocyanine

CHAPTER 1

INTRODUCTION

1.1 Crisis of Antibiotic Resistance and Healthcare-Associated Infections

At the turn of the 20th century, the most common causes of death in the U.S. were due to infectious diseases. The discovery of the first antibiotic penicillin, by Alexander Fleming, changed the course of modern medicine.[1] Antibiotics are small molecule drugs that effectively kill or inhibit the proliferation of bacteria. For the first time in human history, a minor scrape or ear infection was not a cause for concern, rather an inconvenience easily remedied through a regimen of antibiotics. However, the incorrect and overuse of antibiotics accelerated the evolutionarily driven development of resistance in bacterial species as a survival mechanism.[2] Today, resistance has been observed for every antibiotic ever developed and bacterial infections are once again a threat to human health.

The global consequences of antibiotic resistance are profound, thus developing technology to mitigate the further spread of resistance is considered one of the preeminent challenges of the 21st century.[3] The potential consequences of antibiotic resistance on the practice of modern medicine was eloquently summarized by the acting Director-General of the World Health Organization (WHO), Dr. Margaret Chen. She wrote that "the world is heading towards a post-antibiotic era in which common infections will once again kill. If current trends continue, sophisticated interventions, like organ transplantation, joint replacements, cancer chemotherapy, and care of pre-term infants, will become more difficult or even too dangerous to undertake. This may even bring the end of modern medicine as we know it. We need to act now to make sure this does not happen." To prevent

this doomsday scenario, technological innovation must continue to develop new strategies to mitigate bacterial infections without the use of antibiotics.

1.1.1 Biofilm-Associated Medical Device Infections

The population that faces the greatest risk from bacterial infections are those that are the most susceptible. Following admittance to a hospital, patients have a 5% chance of acquiring a Healthcare-Associated Infection (HAI). In the United States alone, over 2 million people are diagnosed with an HAI, resulting in approximately 23,000 deaths annually.[4] Further, HAIs are a $40 billion financial burden on the U.S. healthcare system.[5] HAIs are most commonly found on the surfaces of medical devices and as complications of surgical procedures. Although medical devices are invaluable tools in modern medicine; device implantation bypasses a patient's skin, providing microbes direct access into the body. The medical device and associated placement location of the most common device-related infections are provided in Figure 1. Catheters, for example, are the most frequently used medical device, yet are the leading source of device-related HAIs.[6] Although a life-saving tool for critically-ill patients, intravascular catheters are the source of up to 80% of all bloodstream infections, resulting in an associated mortality rate of 12-25%.[7,8]

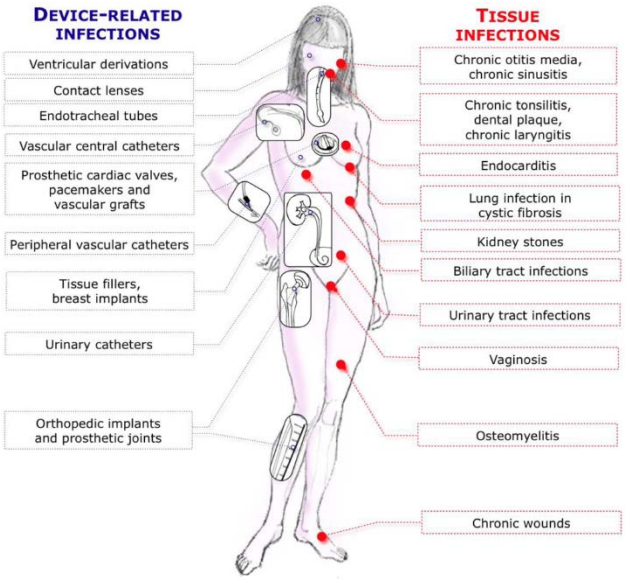

Figure 1: Medical-device related biofilm infections and associated tissue infections. Figure from Römling *et al*.[9]

Catheter-related infections typically arise because a patient's naturally occurring skin-flora colonizes and develops into a surface-associated community of bacteria on the catheter. Over 50% of infections are due to this "biofilm",[10] the most important survival mechanisms of bacteria.[11–13] Living within a biofilm community provides bacteria with enhanced tolerance against antibiotics and other antimicrobials, making biofilm-associated infections exceptionally difficult to fully eradicate. Drug-eluting coatings are the most widely used approach for limiting bacterial colonization on catheters and other medical devices today. Although successful at lowering the rate of infections, the preemptive release of antibiotics perpetuates the evolutionary development of antibiotic resistance. To extend the viability of antibiotics, the Center for Disease Control and Prevention (CDC) recommended curtailing the use of antibiotics as a preventative measure, rather than limiting their use as a reactive solution for diagnosed bacterial infections.[5] This initiative has increased interest in alternative surface modification strategies to limit bacterial adhesion and colonization without the use of antibiotics.

1.1.2 Bacterial Adhesion

Adhesion is the initial step in the colonization of bacteria on a surface. By overcoming energy barriers and fluid boundary layers, free-floating or planktonic bacteria initially engage a surface through physicochemical interactions.[14,15] Due to their size (0.5-2 μm) bacteria are considered "living colloids," and therefore can be described using theories of colloidal-surface interaction. For example, the reversible adhesion of colloidal particles, and subsequently bacteria, can be modeled by the change in Gibbs free energy of two bodies by the Derjaguin, Landau, Verwey, and Overbeek (DLVO) theory.[15,16] Extensions of the DLVO theory, including a thermodynamic model, further refine this approach with a precise understanding of a materials surface chemistry and physical properties of a surface.[17] However, there are two primary limitations with colloidal modeling of bacterial adhesion: 1) bacteria are living organisms with a heterogenous surface consisting of a multitude of protein adhesins and extracellular appendages and 2) the actual interface in real systems has been modified by the surrounding environment.[18] Once exposed to biological fluids, protein and other biomacromolecules passively adsorb and "condition" the surface of a material, effectively masking the original surface chemistry. In reality, this adsorbed protein layer is the true interface bacteria engage with and presents the optimal conditions for irreversible bacterial attachment.[19]

Irreversible adhesion or attachment occurs through specific surface adhesin receptor proteins and extracellular organelle. For example, *Staphylococcus aureus* (*S. aureus*) contains a family of surface adhesins, "microbial surface components recognizing adhesive matrix molecules" (MSCRAMM), that facilitate adhesion to common extracellular-matrix proteins in humans including collagen, fibrinogen, and fibronectin.[20,21]

Bacteria that can express extracellular surface organelle possess an additional means for surface adhesion. Numerous studies have demonstrated the use of pili, culi, and fimbriae both as a means for surface-sensing and to facilitate permanent attachment.[22–25] Once adhered, bacteria begin to proliferate and mature into biofilms.

1.1.3 Biofilm Formation

Biofilm formation occurs ubiquitously on nearly all surfaces.[12,26,27] In nature, 99% of bacteria exist in biofilms and pose an immense financial burden in an array of industries including water remediation,[28] food processing,[29] and as previously mentioned, healthcare devices/surfaces.[10] The transition from a free-floating planktonic cell to a surface-associated biofilm is a dynamic process that can be described in 5 stages of development (Figure 2): (1) initial reversible adhesion, (2) irreversible attachment, (3) early colony formation, (4) mature biofilm formation, and (5) dispersion into the local environment. The transition from single cell to colony formation is dependent on a variety of variables including environmental nutrition, presence of flow, and bacterial strain to highlight a few key contributors.

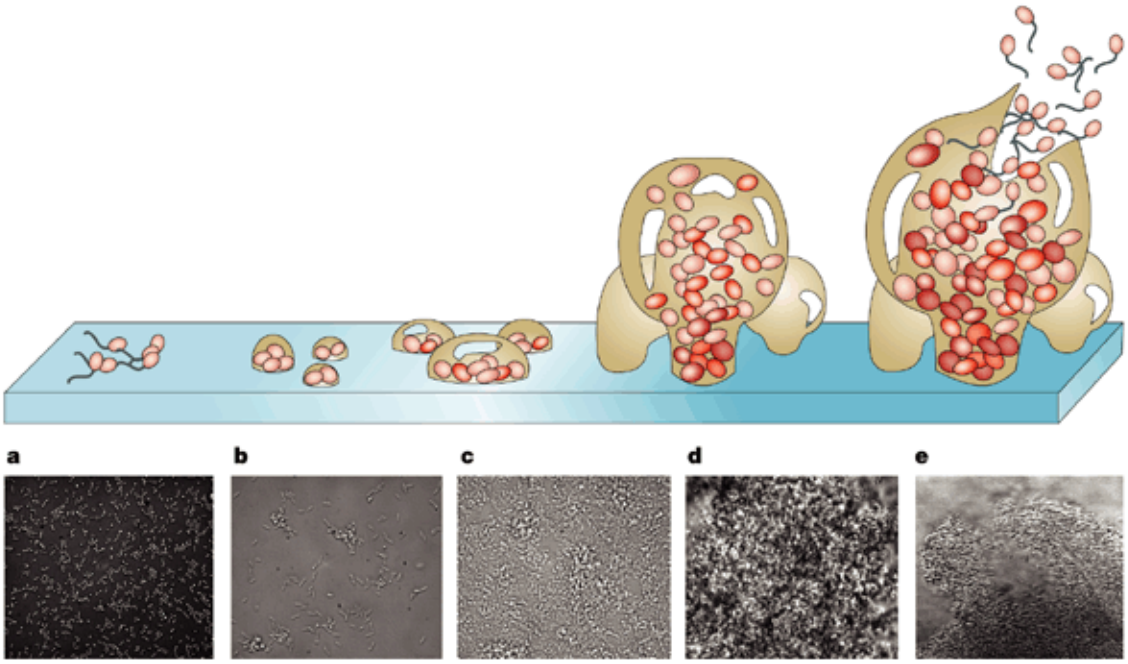

Figure 2: Biofilm formation is a dynamic process that transforms bacteria from free-floating planktonic cells to community-associated organisms living in complex differentiated structures. Figure from *Davies*.[30]

As micro-colonies develop, bacteria secrete a protective matrix of extracellular polymeric substances (EPS) composed of biopolymers and proteins that encases the bacteria providing protection from environmental stresses.[31,32] Once encased in EPS, bacteria develop into a community that further improves antibiotic tolerance in even susceptible cells by 1000 times.[33] This increased resistance is hypothesized to be associated through three potentially synergistic mechanisms: slow diffusion of antibiotics through EPS, development of dormant "persistor" cells, and the formation of altered microenviroments.[34] Biofilm maturation occurs over the course of days or weeks, depending on environmental factors.[35] During maturation, clusters of cells encased in EPS are released to colonize other surfaces downstream. The bacteria in these clusters retain the enhanced antibiotic tolerance of biofilms while displaying increased propensity for adhesion due to the presence of EPS. This tolerance to antimicrobials occurs at a community level and is independent of antibiotic resistance developed by individual

bacteria through genetic mutations. Together, the individual bacteria and biofilm mediated mechanisms of antibiotic tolerance synergistically enable mature biofilms to resist antimicrobial therapies while eluding the immune system. As biofilms reduce the efficacy of conventional antimicrobial therapies, there is a pressing need to develop new preventative approaches that can alleviate reliance on antibiotics to treat these challenging infections.

1.2 Materials Strategies to Prevent Biofilm Formation

The materials typically used for catheter fabrication are inexpensive and flexible, like latex and silicone, but are prone to protein adsorption and bacterial adhesion.[36] Thus, coatings are used to improve the fouling resistance of the base material without disrupting their function. Surface coatings will either kill bacteria through direct contact and/or the release of biocidal compounds (antibacterial) or resist bacterial adhesion (antifouling). Several strategies have been developed to modify surfaces to be antifouling or antibacterial, Figure 3.

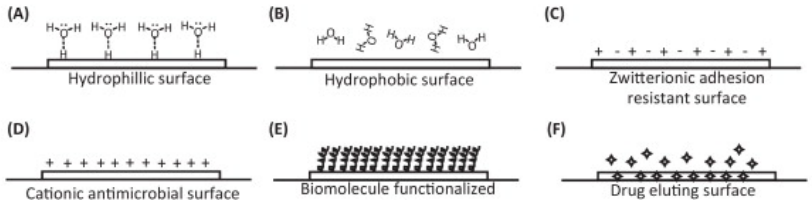

Figure 3: Surface modification strategies to limit biofilm formation through (A-C) adhesion resistant antifouling surfaces or (D-F) antibacterial modifications that kill bacteria. Figure from *Harding et al*.[37]

1.2.1 Antibacterial Materials

Antibacterial or biocidal materials are broadly classified as any material that can kill bacteria. There are two general mechanisms of biocidal action: (1) active release of biocidal compounds and (2) passive surface-contact associated contact. The release of biocidal molecules occurs either as a function of the material properties (passive active release) or through a triggered event i.e., a change in the pH value. Contact based biocidal materials function following bacterial adhesion through specific chemical or physical interactions with the outer membrane of the bacteria.

1.2.1.1 Active-Release Materials

Release materials either passively or actively dispense biocidal molecules into an aqueous environment to kill bacteria in solution. There are a wealth of biological and synthetic small molecules that have antibacterial properties including, antibiotics, metal ions, and essential oils to name a few.[38–40] Preemptive release of antibiotics from coatings is the most common and effective preventive strategy associated with medical devices, however this perpetuates the development of antibiotic resistance and is now reserved for only the highest risk patients.[5] Therefore, many devices are now impregnated with other releasable antimicrobial agents. Silver ions can effectively inactivate microbes and thus, are currently used clinically in catheters and stents.[41] The mechanism of inactivation is well-understood.[42,43] Unfortunately, bacteria have developed resistance to silver ions.[44–46] Further, silver coated catheters have not demonstrated a significant improvement in reducing the number of infections compared to untreated catheters in clinical studies. Other metal ions, including copper and zinc, have excellent antibacterial properties and are commercially used today in biocidal paints on ship hulls. However, the release of metal

ions into the ocean has raised numerous environmental concerns due to the non-specific killing action of these release agents. Due to the prevalence of UV light in nature, photocatalytic materials such as titanium dioxide (TiO_2) are a popular alternative to metal paints for marine applications. Following exposure to light photocatalytic materials, for example titanium dioxide TiO_2, release ions that kill bacteria.[47,48] The primary concerns of all release-based antibacterial materials are the evolutionary development of resistance through low concentration exposure (as occurred with antibiotics) and environmental toxicity concerns (in humans and nature).

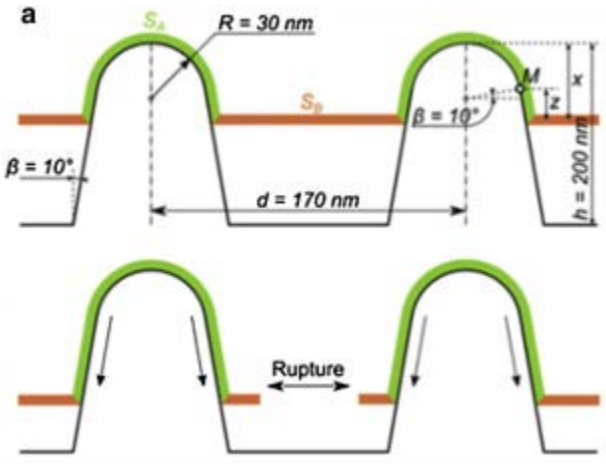

Figure 4: The biophysical model of the mechanism for the mechanical rupture of bacteria through interaction with the nanostructures on cicada wings. Membrane rupture occurs once the membrane is stretched enough to induced sufficient tension. Figure adapted from *Pogodin et al.*[49]

1.2.1.2 Passive Contact-Associated Materials

Contact biocidal materials are a unique subset of nanostructured surfaces that were first discovered as a defense mechanism employed by cicadas and dragonflies to prevent the adhesion of bacteria on their wings.[50] When bacteria adhere to the nanostructured surface of cicada wings, the bacteria's membrane stretches between each nanostructure inducing tension on their membrane. If enough tension is induced on the membrane then it will

rupture, releasing the cell's intracellular fluid thus killing the microbe, Figure 4.[49] This mechanism is driven through physical interactions, so is theorized to be less susceptible to the evolutionary development of resistance by bacteria. Although first observed on the biologically developed nanostructures on insects, surfaces have since been synthetically fabricated from inorganic black silicon.[51,52]

1.2.2 Antifouling Materials

All antifouling materials and surface modifications are designed to passively prevent bacterial adhesion and protein adsorption. High surface energy, hydrophilic, materials exhibit strong interactions with water which create an osmotic repulsion that prevents potential foulants from reaching the surface. Alternatively, low surface energy, hydrophobic, surfaces are designed to repel water and biomacromolecule adsorption through the integration of functional groups that are unable to hydrogen bond with water. Controlling the roughness and topography of surfaces is a form of physical surface modification that has also been used to control bacterial adhesion, but ineffective at resisting protein adsorption.

1.2.2.1 Hydrophilic Polymers

Hydrophilic polymers are water soluble due to the presence of polar or charge moieties in their chemical structure. Once immobilized onto a surface, most hydrophilic polymers interact with free water in the surrounding environment, through hydrogen bonding or electrostatic interactions, to create a boundary layer of water commonly referred to as a "hydration layer." Common hydrophilic polymers including, poly(ethylene glycol) (PEG), polyurethanes, and polyamides, are electrically neutral and contain functional

groups capable of hydrogen-bonding. Zwitterionic polymers are a class of polymers that contain both positive and negative charges, yet they are overall net neutral. PEG and zwitterionic polymers will be the primary polymers used throughout this work and will be discussed in detail below.

1.2.2.1.1 Poly(ethylene glycol) (PEG)

PEG is a biocompatible hydrophilic polymer widely used commercially for its fouling resistance, Figure 5. PEG is non-toxic and is considered a "stealth" polymer for its ability to resist recognition by the immune system.[53] The term PEG refers to polymers with a molecular weight below 20,000 Da while poly(ethylene oxide) (PEO) refers to higher molecular weight polymers with the same monomeric structure.

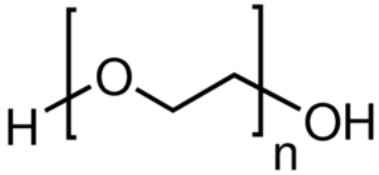

Figure 5: The structure of polyethylene glycol, the most commonly used fouling-resistant hydrophilic polymer.

A primary component in a wide variety of products from coatings to laxatives, PEG is considered the "gold-standard" antifouling polymer for its ability to resist protein adsorption. PEG inhibits protein adsorption and bacterial adhesion through a combination of two mechanisms, steric hindrance and the formation of a hydration boundary layer. As a protein approaches a PEGylated surface, the polymer chains compress creating a repulsive elastic force that acts against the approaching fouling species.[54] This steric hindrance has been extensively studied and occurs most effectively by maximizing the density of PEG chains on the surface. Additionally, when in an aqueous environment the

polyether structure of PEG readily hydrogen bonds with surrounding water molecules, hydrating the polymer chains and creating a hydration layer or boundary layer of water.[55,56] As the polymer chains compress, water molecules are removed from the hydrated polymer chains creating a negative osmotic penalty. The combined repulsive elastic and osmotic forces are especially effective in the prevention of protein adsorption, classifying PEG as a non-fouling protein resistant surface.

The use of PEG as an antifouling hydrogel or surface has some drawbacks. The more complex adhesion mechanisms of bacteria enable them to adhere to PEG-coated surfaces despite the resistance to protein adsorption. Thus, PEG is classified as a low-fouling rather than a completely non-fouling surface modification. Further, when exposed to oxygen present in biologically relevant media, PEG will auto-oxidize to form aldehydes and ethers effectively reducing its ability to prevent protein adsorption.[57] This limits the long-term efficacy of PEG and inspired a wealth of research into other surface chemistries that exploit similar antifouling mechanisms.

1.2.2.1.2 Polymer Zwitterions

A zwitterionic polymer contains both positive and negative charges, but overall net neutral. There are two classes of zwitterionic polymers: *polybetaines* which carry a positive and negative charge on the same monomer unit and polyampholytes which carry a 1:1 charge distribution on consecutive monomer units such as amino acids.[58] The cationic group, positive charge, is usually a quaternary ammonium while the anionic, negative charge, is either a carboxylate, sulfonate, or phosphate. These charged groups strongly interact with water leading to a robust electrostatically induced hydration layer. Due to the increased strength of the electrostatically driven interactions over hydrogen bonding, the

subsequent osmotic penalty upon potential fouling species is significantly greater for zwitterionic polymers than conventional hydrophilic polymers.[59,60] Additionally, upon exposure to aqueous sodium chloride (NaCl) potential interaction with zwitterionic polymers are further reduced, improving fouling resistance in salt conditions where other hydrophilic polymers, like PEG, have been demonstrated to be less effective.

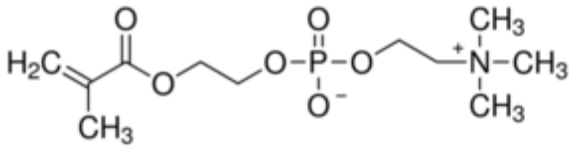

Figure 6: Structure of 2-methacryloyloxylethyl phosphocholine (MPC).

Drawing inspiration from the protein-resistant zwitterionic phospholipid membrane of red blood cells, Nakabayashi *et al.* developed a synthetic phosphorylcholine analog, 2-methacryloyloxylethyl phosphocholine (MPC), Figure 6.[61] Composed of a phosphocholine head-group and various polymer backbones poly(2-methacryloyloxyethyl phosphorylcholine) (pMPC) displays excellent fouling resistance and does not degrade in biological media. Other polybetaines including sulfobetaine methacrylate and carboxybetanine mechacrylate have been extensively studied and also demonstrate ultra-low fouling when exposed to protein solutions and serum.[62,63] Although hydrogels comprised of zwitterionic polymers effectively limit biofouling, they generally exhibit poor mechanical strength.[62,64–66] Modification strategies to bulk zwitterionic materials have been implemented to enhance the mechanical strength by 2-3× that of the original material including; clay-nanocomposites,[67] double-networks,[68] functional crosslinkers,[69] and pH-responsive monomers.[70] Copolymerized pMPC materials including hydroxyethyl methacrylate-MPC are currently used commercially as contact lenses and MPC-butyl

methacrylate in catheter coatings. Alternatively, surface coatings derived from silane chemistry, self-assembled monolayers (SAMs), layer-by-layer assembly (LBL), and specific peptide linkages have been developed as chemical surface modifications. However, these surface modification strategies require specific substrate properties thus are not extensively commercially viable. Thus, if a more versatile platform was developed, zwitterionic functionality could be incorporated to any surface to improve its biocompatibility and biofouling resistance.

1.2.2.2 Physical Surface Modifications

Microtopographic patterned surfaces have been proposed as a non-toxic antifouling strategy to inhibit the adhesion of bacteria and larger microogransisms.[71–73] Engineered roughness index has been proposed as a possible explanation for the reduction of microbial adhesion, however, the general mechanism remains poorly understood.[74] Nanotopographic patterning and biomimetic surfaces can also limit bacterial adhesion.[75] For example, independent of feature dimensions (square, rectangular, or circular posts), it was reported that organized topography significantly reduces bacterial attachment.[76] Drawing inspiration from natural antifouling defense of sharks, biomimetic Sharklet™ was engineered to mimic the ordered topography of sharkskin and to inhibit biofilm formation of bacteria and larger microogransisms.[72] Another naturally antifouling surface that has been synthetically recreated are lotus leaves. The remarkable hydrophobicity and subsequent fouling resistance of lotus leaves is derived from the ordered nanotopography on the leaf, referred to as the lotus effect.[77] In practice, physical surface modifications are primarily created using the elastomer, poly(dimethylsiloxane) (PDMS), due to its flexibility and mechanical integrity. However, the high polymer-water interfacial energy

of PDMS causes proteins and other amphiphilic molecules to preferentially adsorb in a thermodynamically favorable process.

1.3 Materials of Interest: Polymer Hydrogels

Hydrogels are a class of three-dimensional crosslinked hydrophilic materials, that swell in size when exposed to water and collapse when dried. Crosslink points are the junction of polymer chains and can be formed through covalent, ionic, or physical interactions. The space between crosslink points or the mesh size, dictates the diffusion limited size of objects within the network. One unique property of hydrogels is their ability to swell in the presence of water. As depicted in Figure 7, the polymer network expands in the presence of water resulting in a larger mass of water than polymer at thermodynamic equilibrium. The network structure of hydrogels is intrinsically tied to the polymerization technique and the type of polymer used in hydrogel synthesis, so the size and form factor of the hydrogel can be modified without altering the network structure and resulting properties.

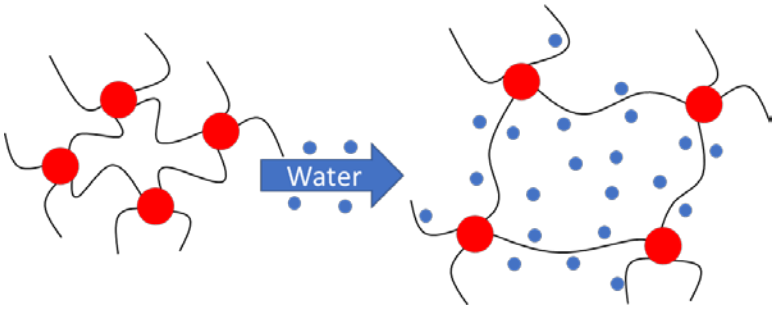

Figure 7: Schematic representation of hydrogel network swelling in the presence of water.

The high-water content and hydrophilic nature of hydrogels provides properties that are attractive for many medical applications due to their biocompatibility, protein adsorption resistance, and elasticity.[78] Depending on the fabrication process used, hydrogels can be prepared at a variety of thicknesses applicable for various applications.[79] For example, thin hydrogels are used as coatings on catheters to supplement fouling resistance and lubrication of the catheter while free-standing thick hydrogels are used as contact lenses. There are a variety of natural and synthetic polymers that can be used to form covalent, ionic, or physically crosslinked hydrogels.

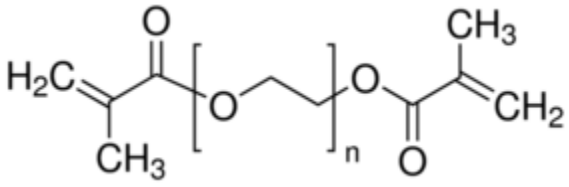

Figure 8: Structure of PEG dimethacrylate. A linear hydrophilic polymer that is the basis for PEG hydrogels used in this thesis.

1.3.1 PEG Hydrogels

The chemical structure of PEG makes the polymer an ideal backbone of chemically crosslinked hydrogels. Depending on the desired application, the network structure of PEG hydrogels can be controlled through the polymerization technique and the structure of each polymer unit. Linear PEG polymers including mono-functionalized diacrylates and duel-functionalized dimethacrylates can be polymerized through radical initiated polymerization, Figure 8. A popular method for hydrogel polymerization, photoinitiated free-radical polymerization or photopolymerization provides direct control over the extent of hydrogel crosslinking through the exposure duration of UV light. However, due to the nature of chain polymerization, the network structure of hydrogels created by radical polymerization is not uniform. Thus, theoretical models of the network's mesh size

determine an expected average based on the mass of the swollen hydrogel at equilibrium and the associated dry polymer content. While hyperbranched star polymers enable exquisite control over network structure not all applications require this degree of precision and cost.

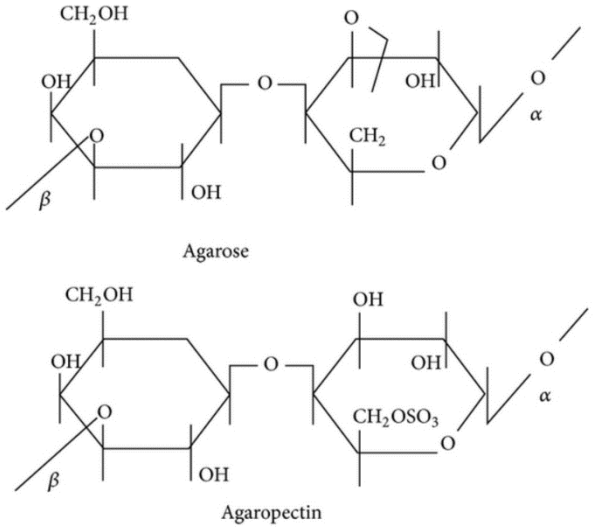

Figure 9: Structure of the two polymeric components of agar, agarose and agaropectin.[80]

1.3.2 Agar Hydrogels

The biopolymer agar is a polysaccharide derived from the cell wall of algae, comprised of sulphated polysaccharides, the specific structure of agar is dependent on the species of seaweed it was harvested from, Figure 9. Agar is comprised of two separate polymers, agarose and agarpectin. Insoluble in cold water, agar will dissolve when heated and set into a gel when cooled. When dissolved in water, the hydrophobic regions of agarose interact in helical conformations to create a physically crosslinked structure that is stabilized through the occurrence of hydrogen bonding with water at the polar regions of the polymer.[81,82] Hydrogels comprised of agar are commonly used as a solid-culture medium for bacterial growth and an inexpensive separation system for DNA and proteins.

Due to the large molecular weight (MW) of agar, this physically entangled network structure creates large regions of space or pores that can be characterized through size exclusion electrophoretic mobility measurements or scanning electron microscopy (SEM).[83]

CHAPTER 2

DISSERTATION OBJECTIVES

2.1 Broad Scope

In this dissertation, the chemical and mechanical properties of polymer hydrogels will be engineered to determine if structure-property relationships can be used to control bacterial adhesion. Although the effect of surface chemistry on bacterial adhesion has been extensively researched, specific bacterial-surface interactions arising the stiffness and thickness of materials has not yet been explored. The focus of this work is to first understand how these fundamental material properties influence *E. coli* and *S. aureus* adhesion and interaction, then use these structure-property relationships in conjunction with novel chemistries to develop materials that can control bacterial adhesion and biofilm formation. The specific objectives are briefly summarized below whereas later chapters provide details on the methods, results, discussion, conclusions, and future work pertaining to each objective.

2.2 Objective 1: Effect of Hydrogel Stiffness on Bacterial Adhesion

We are specifically interested in the effect that hydrogel stiffness has on bacterial adhesion, as stiffness is an intrinsic property associated with any hydrogel coating. To complete this objective, a library of PEG and agar hydrogels will be synthesized with comparable mechanical properties to decouple the effect of hydrogel chemistry and stiffness. Two diverse bacterial pathogens, *E. coli* and *S. aureus,* will be exposed to the hydrogels to elucidate the specific effect of hydrogel stiffness on bacterial adhesion and

early biofilm formation. The work corresponding to this objective can be found in Chapter 4 and 5.

2.3 Objective 2 Effect of Hydrogel Thickness on Bacterial Adhesion

Thickness is a design parameter that can be controlled for all hydrogel materials. Thus, we are interested in understanding whether the thickness of hydrogels has an influence on bacterial-surface interactions. To accomplish this, the stiffness and thickness of PEG hydrogels will be independently tuned to decouple these parameters and systematically evaluate any confounding secondary effects arising from each material property. By fabricating the hydrogels on a hard glass support, we introduce a second stiffness stimulus separated from the bacteria by a soft coating. The depth-dependent surface-sensing of two bacterial species will be used to evaluate the effect of hydrogel thickness on bacterial adhesion. The work corresponding to this objective is described in Chapter 5.

2.4 Objective 3: Effect of Hydrogel Stiffness on Dynamic Bacterial Adhesion

A significant body of research has contributed to our understanding of the material cues that effect bacterial adhesion, however, little is known of the material properties that impact the behavior preceding permanent adhesion, the surface-associated transport or dynamic engagement of bacteria. Knowing that hydrogel stiffness influences the static settling of microbes, we studied the effect of stiffness on bacterial surface-associated transport in a dynamic flow environment. To complete this objective, PEG hydrogels are synthesized at discrete stiffness and tested against a well-defined chemical control, PEG

brushes. A virulent strain of *S. aureus* is used to elucidate the mechanical sensitivity of surface-associated transport for a non-motile bacterial species. Anti-adhesive silica particles are prepared using a physioadsorbed layer of PEG to decouple the biological and colloidal components of dynamic bacterial surface interaction. Collaboration with Professor Maria Santore and Dr. Surachate Kalasin will be essential due to their expertise in colloidal interactions and polymer brush chemistry. The work corresponding to this objective is given in Chapter 6.

2.5 Objective 4: Synergistic Antifouling Chemistry

Chemical surface modifications to resist bacterial adhesion are highly effective, yet the chemistries used are frequently substrate-specific. Thus, another goal was to develop a universal fouling-resistant coating by harnessing the adherence of polydopamine (PDA) and the fouling-resistance of polymer zwitterion, in a simple one-step solution based process. To accomplish this objective, PDA and a model polymer zwitterion will be co-polymerized to create surface-adherent fouling resistant coatings on planar glass, cellulose nanofiber substrates, and hydrogels. The fouling resistance of the resulting adherent composite zwitterionic coatings will be tested using targeted biomacromolecule and bacterial challenges. Collaboration with Professor Todd Emrick and Dr. Chia-Chih Chang will be essential due to their expertise in polymer synthesis and characterization. The work corresponding to planar glass and cellulose nanofiber substrates are in Chapter 7.

2.6 Objective 5: Universal Fouling-Resistant Hydrogel Modification

Developing a fouling-resistant chemistry that can further reduce the adhesion of proteins and microorganisms to hydrogels would be a useful tool. The aim of this study is to demonstrate a universal platform for hydrogel modification that will maintain the permeability and mechanical properties of the hydrogel while enhancing its ability to resist protein adsorption and bacterial adhesion. To accomplish this objective, PEG and agar hydrogels will be synthesized at a range of polymer concentrations to create a library of chemically and mechanically diverse hydrogels. By introducing dopamine/zwitterion polymerization during hydrogel swelling, the mechanical properties of both PEG and agar hydrogel can be maintained while drastically improving the fouling resistance of the hydrogel against model protein and bacterial challenges. This modification platform offers a method for hydrogel modification with interchangeable substrates, negating the need for tailored designer chemistry to functionalize hydrogels. The work corresponding to this objective is described in Chapter 8.

2.7 Objective 6: Antifouling and Antibacterial Thin Film Surfaces

Many scientific breakthroughs occur due to interdisciplinary collaboration on seemingly unrelated disciplines. The aim of this objective was to develop methodologies to characterize the antifouling and antibacterial activity of a series of novel polymeric and crystalline films. By modifying established methodologies to accommodate the specific structural and chemical characteristics of each surfaces, the bacterial surface interactions of each system can be accurately captured. This work was made possible through a series of interdisciplinary collaborations with the research groups of Professors Alejandro

Briseno, Kenneth Carter, and James Watkins. The work corresponding to this objective is described in Chapter 9.

CHAPTER 3

SOFT HYDROGELS LIMIT BACTERIAL ADHESION

Adapted from: Kolewe, K.W.; Peyton, S. R.; Schiffman, J. D. Fewer Bacteria Adhere to Softer Hydrogels. *ACS Appl. Mater. Interfaces* **2015**, *7* (35), 19562–19569.

3.1 Summary

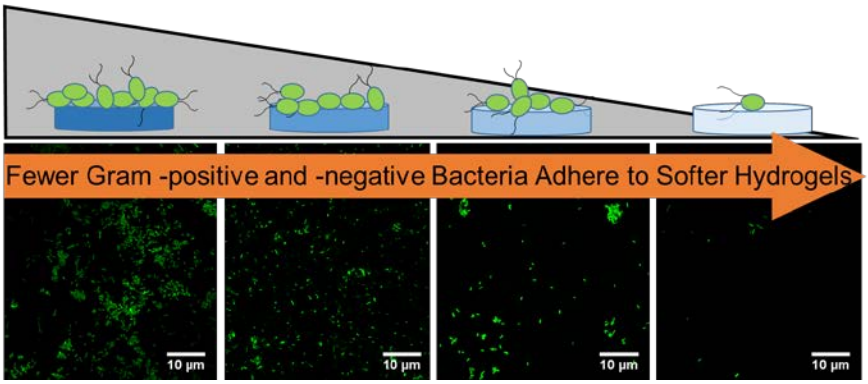

Figure 10: Fewer bacteria adhere to softer hydrogels independent of hydrogel chemistry.

Clinically, biofilm-associated infections commonly form on intravascular catheters and other hydrogel surfaces. The overuse of antibiotics to treat these infections has led to the spread of antibiotic resistance and underscores the importance of developing alternative strategies that delay the onset of biofilm formation. Previously, it has been reported that during surface contact, bacteria can detect surface stiffness through subtle changes in the function of their motors. However, how the stiffness of a thick polymer hydrogel influences bacteria attachment has not yet been demonstrated. Systematically, we investigated poly(ethylene glycol) dimethacrylate (PEG) and agar hydrogels that are twenty times thicker than the cumulative size of bacterial cell appendages, as a function of Young's moduli. Soft (44.05 - 308.5 kPa), intermediate (1,495 - 2,877 kPa), and stiff (5,152 - 6,489

kPa) hydrogels were synthesized. Microbial attachment and the development of early stage *Escherichia coli* and *Staphylococcus aureus* biofilms on the hydrogels were analyzed using confocal microscopy after 2 and 24 hr incubation periods, respectively. Independent of hydrogel chemistry and incubation time, *E. coli* and *S. aureus* attachment correlated positively to increasing hydrogel stiffness. For example, after a 24 hr incubation period, there was 52% and 42% less *E. coli* adhered to soft PEG and agar hydrogels, respectively, in comparison to stiff hydrogels. A reduction in area coverage of *S. aureus* (62% and 38% less) occurred when the Gram-positive microbe was incubated on stiffer PEG and agar hydrogels. We suggest that hydrogel stiffness is an easily tunable variable that potentially, could be used synergistically with traditional antimicrobial strategies to reduce the occurrence of biofilm-associated infections.

3.2 Introduction

Previously, it has been reported that bacteria have the ability to sense and differentiate between surfaces. Surface differentiation occurs through bacterial organelles, specific proteins, or biological complexes that detect signals from the environment and then respond with a transcriptional signal cascade.[24,84] While the dynamics of this "swim-or-stick" switch remain unclear, flagella seem central to determining if microbes are going to "stick" and colonize a surface. For motile bacterial species, the flagella drives both their swimming and swarming motility towards a surface; obstructing the motor rotation of motile bacteria induces them to switch to surface-associated behaviors.[85] Since biofilm formation is often a surface phenomenon, the influence of chemistry and structure-to-property relationships (i.e., nanotopographic patterning) on reducing bacterial adhesion

have been investigated and was the topic of several review papers.[75,76,86–90] For example, independent of feature dimensions (square, rectangular, or circular posts), Perera-Costa *et al.*[76] reported that organized topography significantly reduced bacterial attachment. Engineered roughness index was proposed as a possible explanation for the reduction of microbial adhesion, however, the general mechanism is poorly understood.[74]

A different materials approach to reduce bacterial adhesion on hydrogel surfaces could be to utilize a structure-to-property relationship, like stiffness. Lichter *et al.*[91] synthesized 50 nm thin polyelectrolyte multilayer (PEM) films from poly(allylamine hydrochloride) and poly(acrylic acid), whose Young's moduli ranged from 1000 to 100000 kPa. They reported a positive correlation between increasing film stiffness and the adhesion of *Escherichia coli* and *Staphylococcus epidermis*. After 1 hr of microbial growth, less bacteria attached to Saha *et al.*'s[92] 30 kPa non-crosslinked films than to their 150 kPa crosslinked films, which were comprised of poly($_L$-lysine) and hyaluronan modified with photoreactive vinylbenzyl groups. However, Saha *et al*. note that their limited range of elastic modulus ~120 kPa might have caused the relatively small difference in bacterial adhesion observed between their PEM films. Recently, Song and Ren[93] found that the stiffness of polydimethylsiloxane (PDMS) substrates, 100 kPa to 2600 kPa, affected the physiology of *E. coli* RP437 and *Pseudomonas aeruginosa* PAO1. Attachment and growth was promoted on softer surfaces, but antibiotic susceptibility was enhanced with increasing stiffness. The applicability of correlating biofilm formation on ultrathin charge-containing films and PDMS elastomers to biomedically relevant hydrogel coatings is limited. Crosslinked PDMS is a hydrophobic elastomer and polar solvents, such as water, struggle to wet PDMS;[94] whereas hydrogels are predominately water and easily wetted by water.[95]

The unique mechanical properties, elasticity, water content, and mesh size of PEMs, PDMS elastomers, and polymer hydrogels should be well-characterized[96,97] in order to gather structure-property relationships. Thus, the effect of a thick hydrogels tunable over a wide range of Young's moduli will expand our current understanding of how bulk materials properties affect bacterial adhesion and development.

To fill this critical gap, here we investigate the attachment of *Escherichia coli* K12 MG1655, a model Gram-negative bacteria and *Staphylococcus aureus* SH1000, a model Gram-positive bacteria[32,98] to hydrogels that are significantly thicker than the cumulative size of bacterial cell appendages. Model hydrogels were synthesized from the hydrophilic polymer, poly(ethylene glycol) (PEG), which is known to non-specifically reduce the initial attachment of proteins and bacterial adsorption/adhesion.[99] Chemistry control biopolymer agar hydrogels with mechanical properties analogous to the PEGDMA hydrogels were also investigated. Systematically, as a function of substrate stiffness, *E. coli* and *S. aureus* adhesion was assessed after 2 hr and 24 hr to capture both adhesion and early biofilm formation. *E. coli* is a motile microbe that uses its flagella and fimbriae to sense a surface and facilitate adhesion. Whereas the non-motile microbe, *S. aureus*, relies on surface protein adhesins to facilitate adhesion but lacks a clear mechanism for surface sensing.[21,98,100] Innovative catheter design, including hydrogel coatings, are routinely employed to improve the smoothness and lubrication of the catheter exterior while resisting infection.[41,101] From our findings, we suggest that improving the performance of hydrogel coatings through a basic design parameter that may not cause evolutionary pressure on pathogens, i.e. stiffness, would be a significant medical contribution.

3.3 Materials and Methods

3.3.1 Materials

All compounds were used as received. Poly(ethylene glycol) dimethacrylate, (PEGDMA, M_n = 750 Da), 3-(trimethoxysilyl)propyl methacrylate, ampicillin (BioReagent grade), M9 minimal salts (M9 media) , D-(+)-glucose, calcium chloride (anhydrous), phosphate buffered saline (PBS, 1× sterile biograde), bovine serum albumins (BSA), tryptic soy broth (TSB), Bradford reagent, and Luria-Bertani broth (LB) were purchased from Sigma-Aldrich (St. Louis, MO). Irgacure 2959 was obtained from BASF (Ludwigshafen, Germany). Magnesium sulfate anhydrous and molecular grade agar were obtained from Fisher Scientific (Fair Lawn, NJ). Deionized (DI) water was obtained from a Barnstead Nanopure Infinity water purification system (Thermo Fisher Scientific, Waltham, MA).

3.3.2 Fabrication of PEG Hydrogels

PEG hydrogels were prepared using previously established protocols.[102] Briefly, PEG solutions (7.5, 10, 15, 25, 40, and 50 vol% in 1 M PBS) were sterile filtered using a 0.2 μm syringe, then degassed using nitrogen gas. For UV-curing the radical photo initiator, 0.8 wt% Irgacure 2959 was added to the polymer precursor solution with induction under a long wave UV light, 365 nm for 10 min. PEG solution (75 μL) was sandwiched between two UV-sterilized coverslips (22-mm, Fisher Scientific) that were functionalized with 3-(trimethoxysilyl)propyl methacrylate during polymerization.[103] Fabricating the hydrogel between coverslips enabled all hydrogels to have a uniform thickness and limited the oxygen exposure. Following polymerization, the top coverslip

was removed with forceps and the hydrogels were swelled for 48 hr in 25 mL of M9 media. In this paper, the PEG hydrogels will be referred to as 7.5, 10, 15, 25, 40, and 50% PEG.

3.3.3 Agar Hydrogel Fabrication

Soft agar hydrogels were prepared by dissolving 3 wt% agar in sterile DI water for 30 min before uniformly heating the solution in a liquid autoclave cycle at 250 °C for 30 min. To achieve a higher weight percent of dissolved agar, hydrothermal preparation was used.[104] Here, 9 wt% agar in sterile water was heated for 2 hr in a 95 °C water bath, followed by a liquid autoclave cycle at 250 °C for 30 min. The hot solution was cast at a thickness of ~1-2 mm into glass petri dishes (Pyrex, Tewksbury MA) and allowed to gel. After the agar gels cooled, a flame sterilized 25.4 mm punch (Spearhead® 130 Power Punch MAXiset, Cincinnati, Ohio) was used to create circular hydrogels. In this paper, the agar hydrogels will be referred to as 3 and 9% agar.

3.3.4 Characterization of Agar and PEG Hydrogels

The thickness of PEG and agar hydrogels was determined using digital micrometer (Mitutoyo Corporation Kawaski Japan) by averaging 5 measurements taken on 5 different fully swollen hydrogels. Hydrogel stiffness was measured using a custom-built contact/adhesion test (CAT) test.[105] Hydrogels were prepared in 2 mm diameter cylindrical Teflon molds, then swollen for 48 hr in PBS before being mounted onto the stage of an inverted microscope to control uniform probe contact. A rigid flat cylindrical steel probe (1.50 mm diameter, High-Speed M2 Tool Steel Hardened Undersized Rod) was brought into contact with the hydrogel and the force (P), displacement (δ), and contact area (A)

were recorded via custom-developed National Instruments LabVIEW software. The test was carried out at a fixed displacement rate (25 μm/s) and a fixed displacement (250 μm). Force was monitored by a force transducer (Honeywell Sensotec, Columbus, OH) connected in series with a nanoposition manipulator (Burleigh Instruments Inchworm Model IW-820) that controlled the displacement. The interfacial contact area was captured using a CCD camera (Pixelfly, Kelheim Germany) mounted in-line with the inverted optical microscope (bright field, Zeiss Axiovert, Thornwood, NY). To calculate the Young's modulus, the hydrogel was assumed to reside in "elastic-half space" based on the probe to sample size ratio, which simplified the equation for Young's modulus with a flat cylindrical probe to:

Equation 1

$$E = \frac{P}{2aR}$$

Where E is the Young's modulus (N/m^2), P is the load (N), a is the measurement depth (m), and R is the radius (m).

Contact angle was determined using HPLC water on a Krüss DSA100 Drop Shape Analysis system (Hamburg, Germany) via a modified dynamic/static test averaged over 5 hydrogels. Hydrogels were fully swollen for 48 hr to determine the wet weight then were lyophilized at 90 °C for 72 hr to determine the amount of dry polymer mass. A modified version of the Flory theory,[106] which assumes that the solvent interaction of M9 media with PEG is the same as with PBS was then applied to determine mesh size (ξ):

Equation 2

$$\xi = v_{2,s}^{-1/3}(\bar{r}^2)^{1/2}$$

Where $v_{2,s}$is the swollen volume fraction of polymer and $(\bar{r}^2)^{1/2}$ is the average end-to-end distance of the crosslinked PEG. Four samples at every concentration were tested.

We quantified protein adsorption to the hydrogels using a fluorescent protein assay. Briefly, hydrogels were polymerized on 15 mm diameter coverslips that were adhered to the bottom of 24-well plates (Fisher Scientific). Samples were then swollen for 48 hr in PBS before being incubated for 48 hr at 23 °C in 1.0 and 10 μg/cm^2 of fluorescently tagged Fibronectin. During incubation, samples were gently rotated at 100 rpm. Samples were rinsed three times with PBS before the adsorption of Fibronectin was assessed using a Zeiss Axiovert Yokogawa Spinning Disk (10× magnification).

3.3.5 Evaluation of Bacterial Fouling

Escherichia coli K12 MG1655 *(E. coli*) (DSMZ, Leibniz-Institut, Germany) was transformed using the high copy green florescence plasmid pMF 230 (440 nm emission) and an ampicillin resistance marker to select for viable *E. coli*. *Staphylococcus aureus* SH1000 (*S. aureus*) and the high-efficiency pCM29 sGFP plasmid,[107] containing a chloramphenicol antibiotic was a generous donation from Dr. Alexander Horswill (Microbiology, University of Iowa). PEG and agar hydrogels (25 mm diameter) were placed at the base of 6-well plates (Fisher Scientific) to which 5 mL of M9 media with 100 μg/mL ampicillin or 10 μg/mL chloramphenicol were added for *E. coli* or *S. aureus*, respectively. The growth media in each well was inoculated with an overnight, 1.00 × 10^8 cells/mL culture of *E. coli* or *S. aureus* and then placed in an incubator at 37 °C for 2 or 24 hr. Hydrogels with attached bacteria were removed from the 6-well plates, dipped in M9 media to remove loosely adhered bacteria before being fixed on glass microscope slides

using 4% paraformaldehyde for 15 min. *E. coli* attachment was evaluated using a modified attachment assay via confocal microscopy (Nikon microscope D-Eclipse C1 80i, Nikon Corporation, Melville, NY, USA)[108] using a 63× objective wherein 10-15 randomly acquired images having an area of 3,894 μm^2 were taken with at least 3 parallel replicates at each hydrogel concentration. *E. coli* adhesion over the entire captured area, 3,894 μm^2, was quantified using *Image J 1.48* software (National Institutes of Health, Bethesda, MD) through direct cell counting.[109] *S. aureus* was imaged using a50× objective, and because staph forms grape-like colonies, the particle analysis function in *ImageJ* was used to calculate the colony area coverage over the acquired 58,716 μm^2 area.[72,110] Significant differences between samples were determined with an unpaired student *t*-test. Significance ($p \leq 0.05$) is denoted in graphs by an asterisk.

Table 1: Characteristics of PEG and agar hydrogels.

	Concentration [vol %]	Concentration [wt %]	Modulus [kPa]	Thickness [µm]	Contact Angle [°]	Mesh Size [Å]
PEG	7.5	8.325	44.1 ± 5.6	122.5 ± 5.9	72.3 ± 2.3	34.3 ± 1.5
	10	11.1	308.5 ± 31.1	153.3 ± 13.9	72.3 ± 3.4	27.2 ± 0.8
	15	16.65	1,495.3 ± 80.1	147.3 ± 22.9	69.9 ± 3.0	25.1 ± 0.7
	25	27.75	2,877.1 ± 904.8	164.9 ± 20.3	75.7 ± 2.5	19.3 ± 0.4
	40	44.4	5,152.5 ± 806.0	184.54 ± 15.1	66.6 ± 3.5	10.7 ± 0.5
	50	55.5	6,489.2 ± 116.5	219.7 ± 8.8	61.2 ± 4.0	10.0 ± 1.0
Agar	25	3	44.8 ± 1.63	1,574 ± 29	19.1 ± 4.0	–
	75	9	1336 ± 589	1,479 ± 39	15.8 ± 3.8	–

3.4 Results and Discussion

3.4.1 Characteristics of PEG and Agar Hydrogels

Six thick PEG and two thick agar hydrogels were successfully synthesized.[102] Table 1 summarizes the polymer concentration, thickness, Young's modulus, mesh size, and contact angle of all hydrogels used in this study.[97] Our PEG and agar hydrogels were all at least 100 μm, which is thicker than the diameter of the microbes used in this study. Unlike the thin polymer films used in previous studies,[91,92] thick hydrogels will ensure that the bacteria are only able to sense the stiffness of the hydrogel without confounding influence of the underlying "hard" glass coverslip mount. The Young's moduli of 7.5, 10, 15, 25, 40, and 50% PEG hydrogels spanned nearly 3 orders of magnitude. Based on this wide range, we categorized the PEG hydrogels into three regimes: soft (44.05-308.5 kPa), intermediate (1,495-2,877 kPa), and stiff (5,152-6,489 kPa). Prepared 3% and 9% agar hydrogels had soft (44.8 kPa) and intermediate (1,336 kPa) Young's moduli, respectively. Agar hydrogels cannot mimic the wide range of mechanical properties that can be achieved using PEG hydrogels;[111] agar solubility limited the synthesis of stiff agar hydrogels. For reader ease, we have rounded the Young's moduli data throughout the remainder of this document.

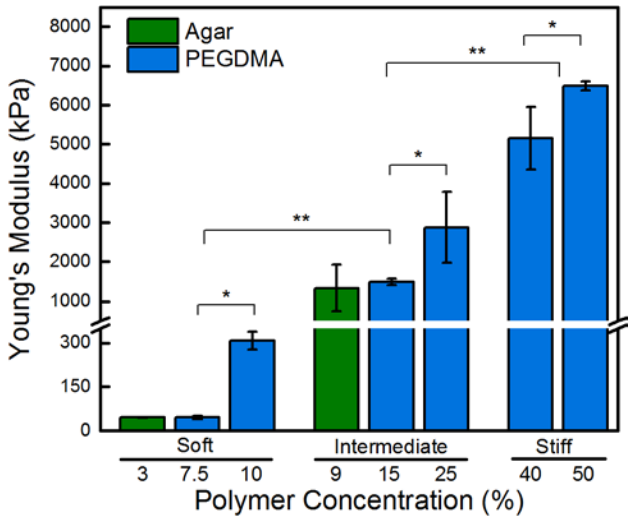

Figure 11: Young's moduli increases with increasing polymer concentration. Stiffness of PEG hydrogels matched with agar hydrogels to form 3 groups of statistically different hydrogels: soft (44 – 308), intermediate (1,340 – 2,880), and stiff (5,150 – 6,500). Stiffness of PEG hydrogels within each group are statically different (p value .01). Standard deviation is displayed.

The mesh size of the PEG hydrogels was inversely correlated to their Young's moduli, the softest hydrogel had a mesh size of 34.3 ± 1.5 Å, whereas the stiffest had a mesh size of 10.0 ± 1.0 Å. This is consistent with similar hydrogel systems found in literature,[106] is an order of magnitude smaller than *E. coli*, and is small enough to avoid adsorption of most proteins (1-100 nm) and molecules. Agar hydrogels were superhydrophilic with a contact angle below 20°. Thus, surface energy can be ruled out as a confounding variable. Confocal micrographs provided in Figure 12 display that no detectible Fibronectin protein adhered to the PEG hydrogels after 24 hr, consistent with previous reports for PEG-based materials. Agar hydrogels adsorbed significant Fibronectin, exceeding glass controls, which adsorbed significantly more protein than the PEG. Because most mechanisms of bacterial adhesion are protein-mediated, the presence of protein on the agar hydrogel surfaces serves as a positive control for the PEG hydrogels that resist protein adsorption over the time scale of this study, 24 hr.

3.4.2 Attachment of *E. coli* and *S. aureus* after 2 h Incubation on PEG and Agar Hydrogels

PEG hydrogels, agar hydrogels, and internal control glass coverslips were placed at the base of 6-well polystyrene plates to which *E. coli* in M9 media were incubated for 2 hr, Figure 13. Confocal microscopy paired with *ImageJ* software enabled the total cell attachment to be determined. The average attachment of *E. coli* was 21 ± 7 cells and 315 ± 67 cells for the soft 7.5% and stiff 50% PEG hydrogels, respectively. Attachment of *E. coli* onto the intermediate and stiff hydrogels was significantly greater than onto the soft hydrogels for both types of hydrogels. There is a strong linear correlation between PEG moduli and bacterial attachment ($R^2 = 0.90$). Soft agar hydrogels with statistically similar moduli (45 kPa) to PEG (44 kPa) had significantly more bacteria attached, 42 ± 8 cells. This may be an effect of the surface chemistry of the agar hydrogels or their larger mesh size.

Figure 12: A qualitative protein adsorption assay was conducted using (left to right column) PBS only (control) and florescently labelled Fibronectin at two concentrations: 1 µg/cm^2 and 10 µg/cm^2. No florescence was detected on PEG hydrogels, whereas protein readily adhered to glass and agar hydrogels. Representative confocal micrographs are presented.

Further evaluation if more microbes attached to stiffer hydrogels was conducted by challenging the Gram-positive bacteria, *S. aureus*, with soft and intermediate PEG and agar hydrogels. After a 2 hr incubation time, a small quantity of staph adhered to the soft and intermediate PEG hydrogel. There was only 0.16% *S. aureus* area colony coverage on the soft PEG hydrogels and a 0.27% area colony coverage on the intermediate PEG hydrogels then sharply increases to 1.8% on stiff PEG. Substantially more *S. aureus* adhered to agar hydrogels, the soft agar hydrogel had a 2.4% area colony coverage and the intermediate agar hydrogel had a 3.7% area colony coverage. This indicates that independent of hydrogel chemistry, increasing the hydrogel stiffness increases the amount of *E. coli* or *S. aureus* that adheres to a stiffer hydrogel after a 2 hr incubation period.

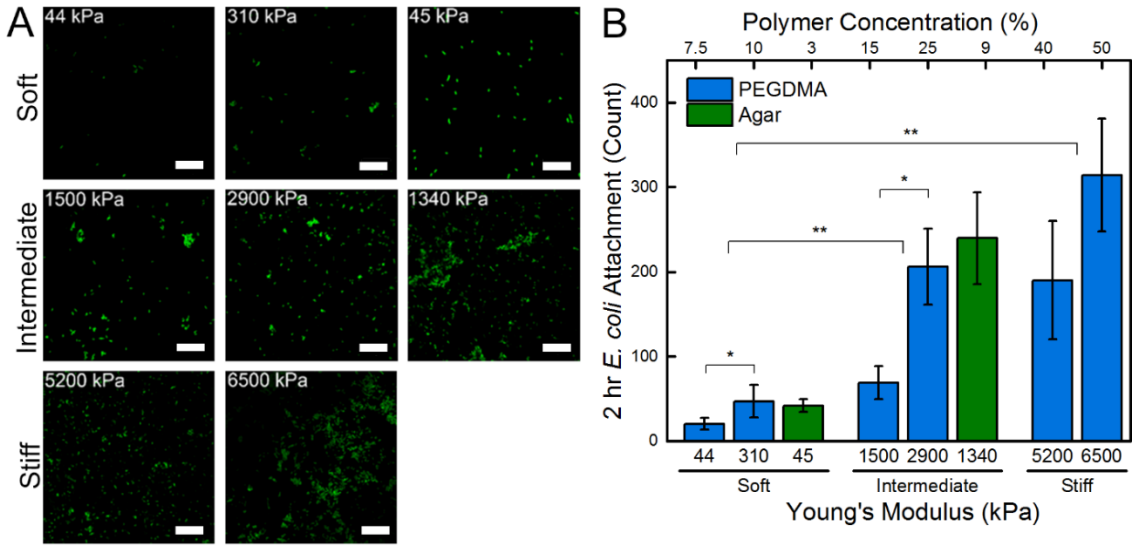

Figure 13: (A) Representative confocal micrographs (3894 μm^2) of *E. coli* attached after a 2 hr incubation period on soft (44 – 308 kPa), intermediate (1340 – 2880 kPa), and stiff (5150 – 6500 kPa) PEG and agar hydrogels. A 10 μm scale bar is displayed. (B) Total cell count quantified that there was a significant increase in *E. coli* attachment with increasing hydrogel stiffness. An asterisk denotes 95% significance between samples, whereas two asterisks denotes significance between stiffness regimes. Error bars denote standard error.

3.4.3 Attachment of *E. coli* and *S. aureus* after 24 hr Incubation on PEG and Agar Hydrogels

After a 24 hr incubation period, *E. coli* displayed early development into 3D microstructures, Figure 14A. The presence of microcolonies suggests that the signaling involved in the early stages of biofilm formation (limited quorum sensing, twitching motility) are active. Qualitatively, colony formation and proliferation was observed to be more robust on 9% agar hydrogels and all stiff regime PEG hydrogels. Stiff regime PEG hydrogels had significantly more attachment and growth than all other PEG hydrogels, Figure 14B. Attachment to the 3 and 9% agar hydrogels was more than twice that of PEG hydrogels that had a statistically equivalent Young's modulus, while attachment to glass substrates experienced a 4.5 fold increase, or an increase of ~600 *E. coli* cells. This data further suggests that the larger mesh size of agar hydrogels or their different surface chemistry may be promoting the attachment of *E. coli*.

After a 24 hr incubation period, *S. aureus* displayed characteristic grape-like colony formation on intermediate and stiff PEG hydrogels, as well as on soft and intermediate agar hydrogels, Figure 15A. Additionally, the same strong correlation observed for *E. coli* held true: bacterial adhesion increased with increasing hydrogel stiffness. Less than 1.0% of the soft 7.5% PEG hydrogels exhibited area colony coverage by *S. aureus*, whereas the stiff 50% PEG hydrogels had a statistically significant greater area colony coverage of 4.7%, Figure 15B. As reported with *E. coli*, substantially more *S. aureus* adhered to the agar hydrogels than to the PEG hydrogels. More than double the area colony coverage of *S. aureus* was present on agar hydrogels that had a Young's moduli that was statistically equivalent to the PEG hydrogels.

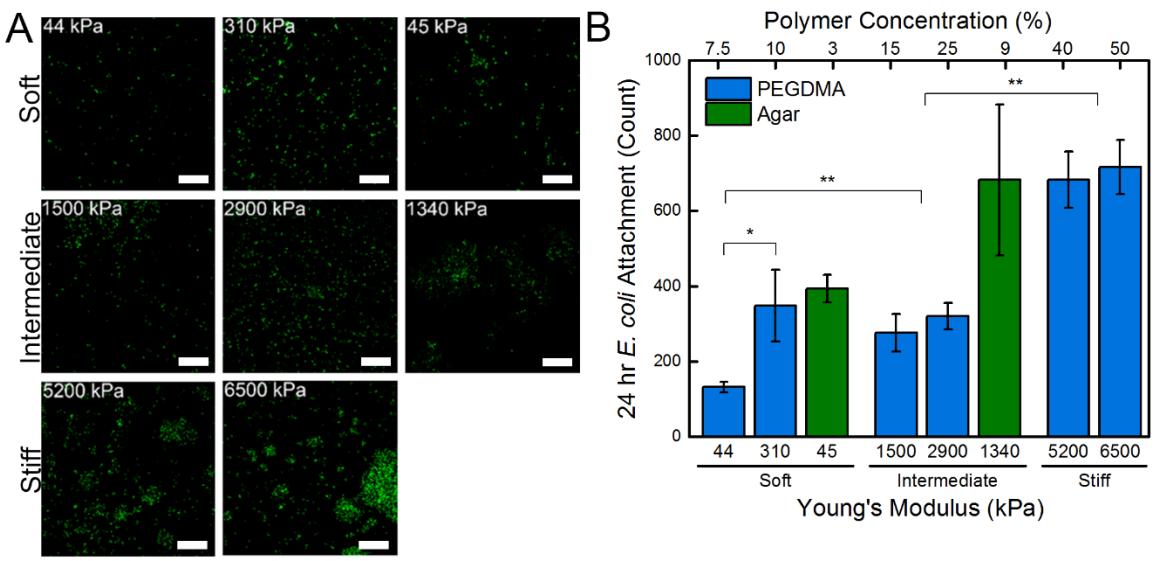

Figure 14: (A) Representative confocal micrographs (3894 μm^2) of *E. coli* attached after a 24 hr incubation period on soft (44 – 308 kPa), intermediate (1340 – 2880 kPa), and stiff (5150 – 6500 kPa) PEG and agar hydrogels. A 10 μm scale bar is displayed. (B) Total cell count quantified that there was a significant increase in *E. coli* attachment with increasing stiffness. An asterisk denotes 95% significance between samples, whereas two asterisks denotes significance between stiffness regimes. Error bars denote standard error.

The colonization of medical devices by bacteria is a problem of increasing concern. Poly(ethylene glycol)-based coatings are frequently used on medical implants to enhance their biocompatibility while mitigating fouling. If the hydrogel coatings were softer, potentially, fewer bacteria would initially adhere, thus delaying the onset of biofilms that are hard to combat using commercial antibiotics. After a 2 h incubation period, a 15-fold decrease or ~295 fewer *E. coli* attached to the softest PEG hydrogels as compared to stiffest PEG hydrogels. Our results suggest that this trend is independent of chemistry, and in our study, microbial adhesion mechanism. After a 24 hr incubation period 42% fewer *E. coli* attached to soft (45 kPa) versus intermediate (1336 kPa) agar hydrogels, whereas on PEG hydrogels, there was a 52% reduction of *E. coli* attachment over the same stiffness regimes, 44 kPa versus 1500 kPa. *S. aureus* displayed a strikingly similar trend; after the 24 hr incubation period, between the soft and intermediate hydrogels there was a 38 and

58% reduction in area colony coverage for the PEG and agar hydrogels, respectively. While we report the same observed trend for the Gram-negative and Gram-positive microbes, the full mechanism is beyond the scope of this study. Receptor specific binding through *E. coli* organelle, specifically type 1 fimbriae, auto transporter proteins, and aggregative fimbriae, can permanently bind bacteria to a surface,[33] but the ability of poly(ethylene glycol) to resist protein adhesion suggests that another mechanism is responsible. Whereas, *S. aureus* lack these extracellular organelle and instead rely on protein adhesions through microbial surface components recognizing adhesive matrix molecules (MSCRAMM).[20,112] As an inexpensive synergistic mode of modulating bacterial attachment, the stiffness of hydrogels can be tuned in combination with traditional nanoparticle or antibiotic loading to further delay the onset of biofilm formation in health care applications.

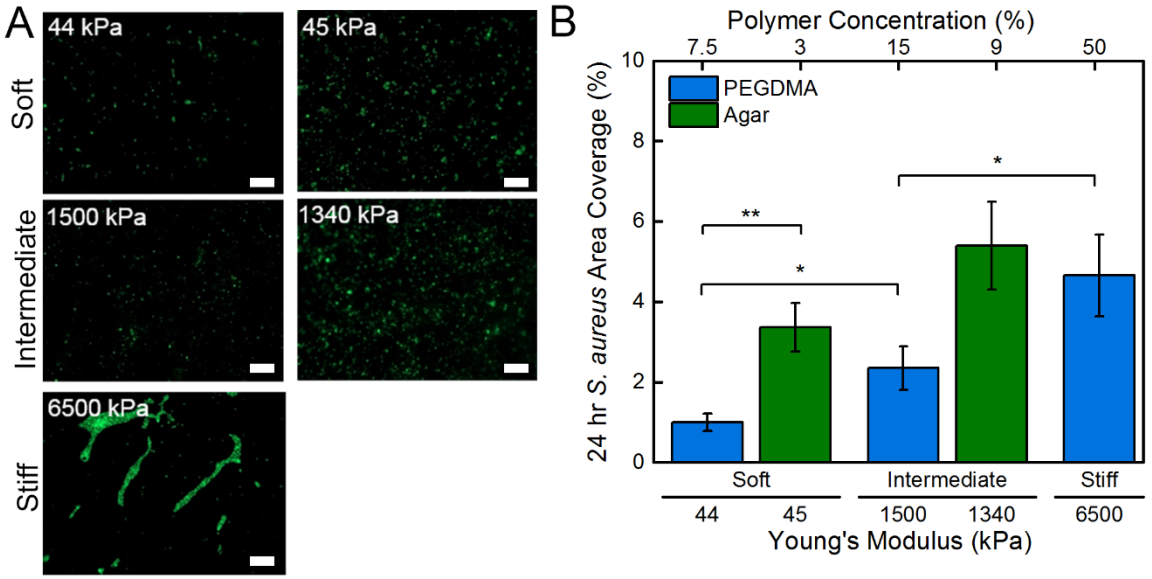

Figure 15: (A) Representative micrographs (58716 µm2) of *S. aureus* attached after a 24 hr incubation period on soft (44, 45 kPa), intermediate (1500, 1340 kPa), and stiff (6500 kPa) PEG and agar hydrogels. A 10 µm scale bar is displayed. (B) Area coverage quantified that there was a significant increase in *S. aureus* area coverage with increasing stiffness. An asterisk denotes 95% significance between samples, whereas two asterisks denotes significance between stiffness regimes. Error bars denote standard error.

3.4.4 Implications for the Future Design of Antifouling Materials

This work explored bacterial adhesion as a function of hydrogel stiffness by comparing the attachment of two different microbes onto PEG and agar hydrogels. The adhesion of both *E. coli* K12 MG1655 and *S. aureus* SH1000 was reduced for 24 hr on the softest surfaces we tested. This was surprising given the different modes of adhesion possessed by these two microbes and the very different surface chemistries of our two hydrogel platforms. We acknowledge that our findings cannot necessarily be extrapolated to form a sweeping statement about all microbial adhesion mechanisms, as other bacteria strains, changes to bacterial physiology, and various growth conditions should be tested. While it has yet to be determined if equivalent biofilms will eventually form on soft and stiff hydrogels, providing a clinician a longer time to identify and combat bacteria at the catheter implant site has implications on decreasing the amount of infections associated with mortality. We suggest that such fundamental insights could be used to define design principles for bacterial resistant surfaces because, surfaces that delay the onset of microbial attachment could transform a variety of industries, including, medical, marine, water treatment, and food processing.

3.5 Conclusions and Future Work

We have fabricated PEG and agar hydrogels over a wide range of Young's moduli. The adhesion of *E. coli* correlated positively with hydrogel stiffness over the investigated range of Young's moduli, 44–6500 kPa. This range exceeds previous stiffness ranges investigated and represents the first time that thick polymer hydrogels were used as a testing substrate. After a 24 hr incubation period, the soft 44 kPa PEG hydrogels had ~52%

fewer *E. coli* adhered to them than the intermediate 1500 kPa PEG hydrogels, and 82% fewer *E. coli* than the stiff 6500 kPa PEG hydrogels. Similarly, the adhesion of *E. coli* on soft 45 kPa agar hydrogels was reduced by 42% when compared to intermediate 1340 kPa agar hydrogels. After 24 hr, the adhesion of *S. aureus* was reduced by 62% on soft 44 kPa PEG compared to intermediate 1500 kPa PEG and by 79% when compared to the stiff 6500 kPa PEG hydrogels. The attachment of *S. aureus* onto soft 45 kPa agar hydrogels was reduced by 38% when compared to intermediate 1340 kPa agar hydrogels. For the first time, we have determined that more *E. coli* and *S. aureus* adhere to stiffer hydrogels and that this relationship occurs independent of hydrogel chemistry. We suggest that stiffness, a structure–property relationship, could potentially reduce the initial adhesion of bacteria on both synthetic and biopolymer hydrogels.

One future direction of research could investigate the long-term effects of hydrogel stiffness on bacterial proliferation and biofilm formation. Although it is accepted that the initial adhesion of bacteria to surfaces is influenced by the stiffness of the substrate, whether this phenomenon influences other intracellular processes has not been studied. Understanding whether stiffness effects the proliferation of bacteria already adhered to soft or stiff hydrogels would provide valuable insights into this structure–property relationship. The design of our previous work intentionally retarded the growth rate of bacteria by using a minimal growth media. However, the stiffness of a surface could also influence the growth rate of adhered cells in addition to the rate of initial attachment. Once developed into a biofilm, other quantification tools could be utilized to understand the influence of stiffness on bacterial behavior including profiling of the secreted EPS components within the biofilm matrix and released metabolic products.

A natural question arising from phenotypic approaches used here and in literature to assess bacterial adhesion, concerns the possible selection of a genetically distinct population. Do all bacteria of a given species display the same sensitivity to substrate stiffness or are the bacteria that adhere to soft substrates a genetically distinct subpopulation? This could be studied through genetic sequencing of the bacteria that adhere to soft vs stiff materials. This approach could provide information into the mechanical sensing mechanism or at least a general perspective of the genetic variation (if any) between adhered bacteria to any hydrogel and their planktonic brethren. This approach could be used to connect the observed phenotypic response of bacterial adhesion across species.

Connecting the bacterial response to substrate stiffness on different material platforms using comparable bacterial species and testing methods is essential. Currently it is difficult to draw comparisons in literature due to the variety of bacterial species and materials used for these studies. Porous substrates, elastomeric materials, and thin films are all vital materials in many applications so unifying the testing methodology by using the same bacterial strains and testing procedures would significantly improve the comparability of these studies. One specific challenge is that the chemistry and topography of a substrate may be altered when increasing the Young's modulus of the substrate. This change could give rise to confounding secondary influences in the observed behavior of bacterial adhesion. Using a two-material system, where the top layer displays the same surface chemistry and mechanical properties while the bottom material can be independently tuned, could provide insights into the specific influence that various material properties including, chemistry and topography, have on bacterial adhesion.

CHAPTER 4

BACTERIAL ADHESION IS AFFECTED BY THE THICKNESS AND STIFFNESS OF POLY(ETHYLENE GLYCOL) HYDROGELS

Adapted from: Kolewe, K. W.; Zhu, J.; Mako, N. R.; Nonnenmann, S. S.; Schiffman, J. D., Bacterial Adhesion is Effected by the Thickness and Stiffness of Poly(ethylene glycol) Hydrogels. *Under Revisions*

4.1 Summary

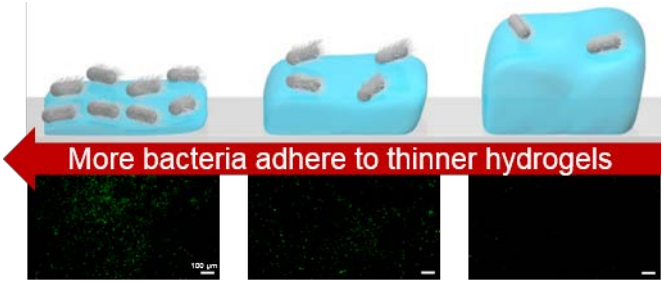

Figure 16: The mechanically sensitive adhesion of bacteria to PEG hydrogels is sensitive to the thickness of the hydrogel.

Despite lacking visual, auditory, and olfactory perception, bacteria sense and attach to surfaces. Many factors including, the chemistry, topography, and mechanical properties of a surface, are known to alter bacterial attachment, and in this study, using a library of nine protein-resistant poly(ethylene glycol) (PEG) hydrogels immobilized on glass slides, we demonstrate that the thickness or amount of polymer concentration also matters. Hydrated atomic force microscopy and rheological measurements corroborated that thin (15 μm), medium (40 μm), and thick (150 μm) PEG hydrogels possessed Young's moduli in three distinct regimes, soft (20 kPa), intermediate (300 kPa), and stiff (1000 kPa). The attachment of two diverse bacteria, flagellated gram-negative *Escherichia coli* and non-motile gram-positive *Staphylococcus aureus* was assessed after a 24 h incubation on the

nine PEG hydrogels. On the thickest PEG hydrogels (150 μm), *E. coli* and *S. aureus* attachment increased with increasing hydrogel stiffness. However, when hydrogel's thickness was reduced to 15 μm, a substantially greater adhesion of *E. coli* and *S. aureus* was observed. Twelve times fewer *S. aureus* and eight times fewer *E. coli* adhered to thin-soft hydrogels than to thick-soft hydrogels. Though a full mechanism to explain this behavior is beyond the scope of this paper, we suggest that because the Young's moduli of thin-soft and thick-soft hydrogels were statistically equivalent, potentially, the very stiff underlying glass slide was causing the thin-soft hydrogels to feel stiffer to the bacteria. These findings suggest a key takeaway design rule; to optimize fouling-resistance, hydrogel coatings should be thick and soft.

4.2 Introduction

Previous studies including our own work definitively show that bacteria respond to substrate stiffness and exhibit phenotypic changes in response to surface association;[113] however, the depths through which bacteria sense remains an open question. Here, for the first time, we systematically controlled the thickness and stiffness of hydrogels to decouple their effects on bacterial adhesion. We selected the antifouling polymer, poly(ethylene glycol) (PEG), as our model hydrogel system because of its excellent protein fouling resistance.[99,114] To ensure that PEG hydrogels of various thicknesses (15 μm, 40 μm, and 150 μm) were synthesized with three distinct, thickness-independent Young's moduli, ~20, ~300, and ~1000 kPa, we performed local nanomechanical characterization using atomic force microscopy (AFM) in an aqueous environment. Hydrated AFM is the optimal technique to study the local mechanical properties of fully hydrated soft hydrogels[115] since

it does not introduce artifacts typically observed with scanning electron microscopy or dry AFM.[116–120] Because of their unique surface sensing mechanisms,[84,121] bacteria adhesion studies were conducted using two model microbes, non-motile gram-positive *S. aureus* and flagellated gram-negative *E. coli*. By combining well-controlled PEG hydrogel design parameters (antifouling chemistry, thickness, stiffness) with two distinct model bacteria we have formed a powerful platform to systematically evaluate if bacteria adhesion is affected by the thickness or amount of PEG concentration in a hydrogel coating.

4.3 Methods

4.3.1 Materials

See Chapter 4.3.1 for details on the materials used in this study.

4.3.2 Fabrication of Hydrogels with Controlled Thickness

PEG solutions (10, 25, and 50 vol% in 162.7 mM PBS, corresponding to soft, intermediate and stiff hydrogels) were sterile filtered using a 0.2 µm syringe, then degassed using nitrogen gas. For UV-curing, 0.8 wt% Irgacure 2959 (a radical photo initiator) was added to the PEG solution with induction under a long wave UV light, 365 nm for 10 min. Hydrogels with three different thicknesses (thin, medium, and thick) were prepared by depositing 10, 40, and 85 µL aliquots of a PEG solution onto a glass coverslip (22-mm Fisher Scientific) that was functionalized with 3-(trimethoxysilyl)propyl methacylate.[103] A clean 22-mm coverslip was placed on top of the PEG solution to limit oxygen diffusion, facilitate polymerization, and to enable a uniform hydrogel thickness. Following polymerization, the top coverslip was removed using forceps and the PEG hydrogels were swollen for 48 hr in 162.7 mM PBS.

4.2.3 Hydrogel Characterization

The thickness of PEG hydrogels was determined using a digital micrometer (Mitutoyo Corporation, Kawaski, Japan) by averaging five measurements on at least three fully swollen hydrogels. Surface topographic images of hydrogels were acquired using a Cypher ES atomic force microscope (Asylum Research/Oxford Instruments; Goleta, CA). Dry hydrogels were imaged in AC mode in air using Tap300-G cantilevers (Budget Sensors) while hydrated hydrogels were imaged using a closed perfusion cell in water AC mode using Olympus TR800PSA (k = 183.54 pN/nm) cantilevers. The topographical profiles were analyzed using Igor Pro 6.37 (WaveMetrics, Inc., Lake Oswego, OR) to quantify the surface roughness of the hydrated hydrogels, including, their route mean square roughness (R_q), average roughness (R_a), skewness (R_{shw}), kurtosis (R_{kur}) minimum roughness (R_{min}), and maximum roughness (R_{max}).[122] The local stiffness of hydrogels was obtained using TR400PB cantilever through AFM nanoindentation in water at three distinct locations on each of nine fully swollen hydrogels. Thermal calibration in air was first performed to determine the probe's spring constant (k = 29.56 pN/nm). Subsequently, a calibration force curve on a hard surface (silicon) in water environment was obtained using the same probe to determine the lever sensitivity (Invols = 36.34 nm/V). Considering the cone shape of the chosen AFM tip, the Young's moduli was determined by data analysis in Igor Pro using the Sneddon's model:

Equation 3

$$F = \frac{\pi}{2} \times \frac{E}{1-\upsilon^2} \times \tan\alpha \times \delta^2$$

where $F, E, \upsilon, \alpha, \delta$ are the applied force, the reduced modulus, sample's Poisson ratio, half-opening angle of AFM tip and depth of indentation.

The bulk mechanical properties of PEG hydrogels were determined through small amplitude oscillatory shear measurements using a plate–plate geometry (Kinexus Pro rheometer (Malvern Instruments, UK), with a diameter of 20 mm and a gap of 1 mm. All hydrogels were prepared for rheology using 1 mm deep Teflon molds that had a 25-mm diameter; hydrogels were loaded into the rheometer and then trimmed to size using a razor blade. A strain amplitude sweep was performed to ensure that experiments were conducted within the linear viscoelastic region and a strain percent of 0.1% was selected. Oscillation frequency sweeps were conducted over an angular frequency domain, 1.0 and 100 rad/s at 23 ºC. As hydrogels are incompressible solids with a Poisson ratio of 0.5, the Young's modulus was calculated from the complex modulus using Equation 4:

Equation 4

$$E = 2G^*(1 - v)$$

where *E, G*,* and *v* are the Young's modulus, complex modulus, and the sample's Poisson ratio.

4.2.4 Evaluation of Bacterial Growth

E. coli K12 MG1655 was purchased from DSMZ (Leibniz-Institut, Germany) and transformed with pMF230, a high copy GFP plasmid. *S. aureus* SH1000 containing the high-efficiency sGFP was a generous donation of Dr. Alexander Horswill (University of Colorado Anschutz Medical Campus). Hydrogels were placed at the base of 6-well polystyrene plates (Fisher Scientific) to which 5 mL of M9 media containing 100 µg/mL ampicillin or 10 µg/mL chloramphenicol was added for *E. coli* or *S. aureus* (1.00×10^8 cells/mL), respectively. Internal controls (glass coverslips) were run in parallel (data not

shown). The growth media in each well was inoculated with an overnight culture of *E. coli* or *S. aureus*, which were washed and resuspended in M9 media,[123,124] before being placed in an incubator at 37 °C for 24 h. Hydrogels with attached bacteria were removed from the 6-well polystyrene plates and washed with PBS to remove loosely adhered bacteria. *E. coli* and *S. aureus* attachment was evaluated using an adhesion assay[72,110] that monitored the bacteria colony coverage within a 366,964 μm^2 area using a Zeiss Microscope Axio Imager A2M (20× magnification, Thornwood, NY). The particle analysis function in *ImageJ 1.48* software (National Institutes of Health, Bethesda, MD) was used to calculate the bacteria colony area coverage (%) by analyzing 10–15 randomly acquired images over three parallel replicates. Significant differences between samples were determined with an unpaired student *t*-test. Significance ($p \leq 0.05$) is denoted in graphs using asterisks.

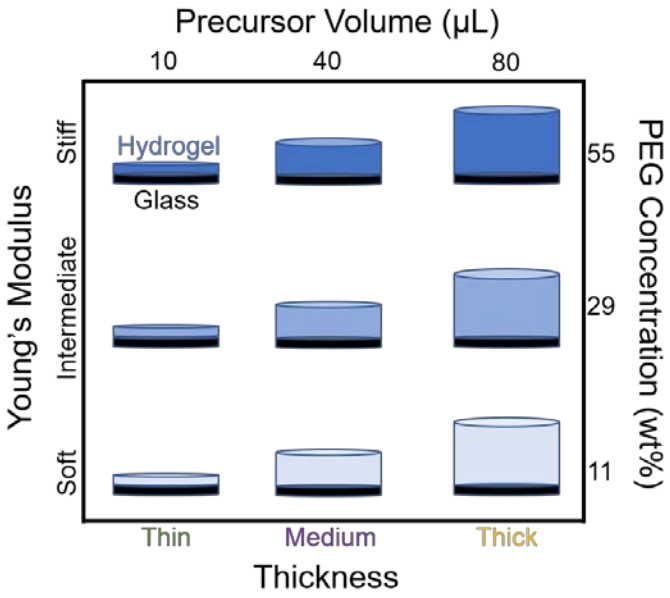

Figure 17: A schematic of the nine PEG hydrogels tested in this study. Throughout the results section, we will refer to a hydrogel sample by their thickness-stiffness (bottom and left axes), which was fabricated using the recipe noted on the top and right axes (precursor volume (µL) versus PEG concentration (wt%)). All PEG hydrogels were immobilized on glass slides.

4.4 Results and Discussion

4.4.1 Characteristics of PEG Hydrogels

By controlling the volume of poly(ethylene glycol) dimethacrylate (PEG) solution deposited onto glass slides, we have successfully synthesized hydrogels with three distinct thicknesses, Figure 17. A digital micrometer was used to determine that the average thickness of the thin hydrogels was 14 ± 2 μm, the medium hydrogels was 49 ± 4 μm, and the thick hydrogels was 155 ± 8 μm thick. Because all of the hydrogels are comprised of the same PEG chemistry, they displayed excellent resistivity to the adsorption of serum proteins, consistent with previous reports.[123]

The Young's modulus of the hydrogels was tuned by increasing the polymer concentration. While rheology is commonly used to characterize the mechanical properties of very thick hydrogels (1000 μm), we needed to confirm that decreasing the thickness of the hydrogels did not change their Young's moduli. Therefore, we characterized the mechanical properties of our hydrogels using hydrated atomic force microscopy (AFM). To validate our AFM approach, we acquired topographic images of PEG hydrogels that were dried at room temperature, Figure 18, and compared them to hydrogels that were maintained in an aqueous environment, Figure 19. While the dried hydrogels appeared wrinkled, collapsed, and decorated with salt precipitates,[116] by maintaining hydration during analysis, the surfaces were smooth and extensive analysis of the surface roughness demonstrated that there was no correlation between the surface roughness and thickness of hydrogels, Table 2.[122,125] Notably, there was no discernable trend between the thickness of the hydrogels and their route mean square roughness (R_q), average roughness (R_a), skewness (R_{shw}), kurtosis (R_{kur}) minimum roughness (R_{min}), or maximum roughness (R_{max}).

With an optimized method for keeping the hydrogels hydrated, we next confidently characterized the Young's moduli of the hydrogels.

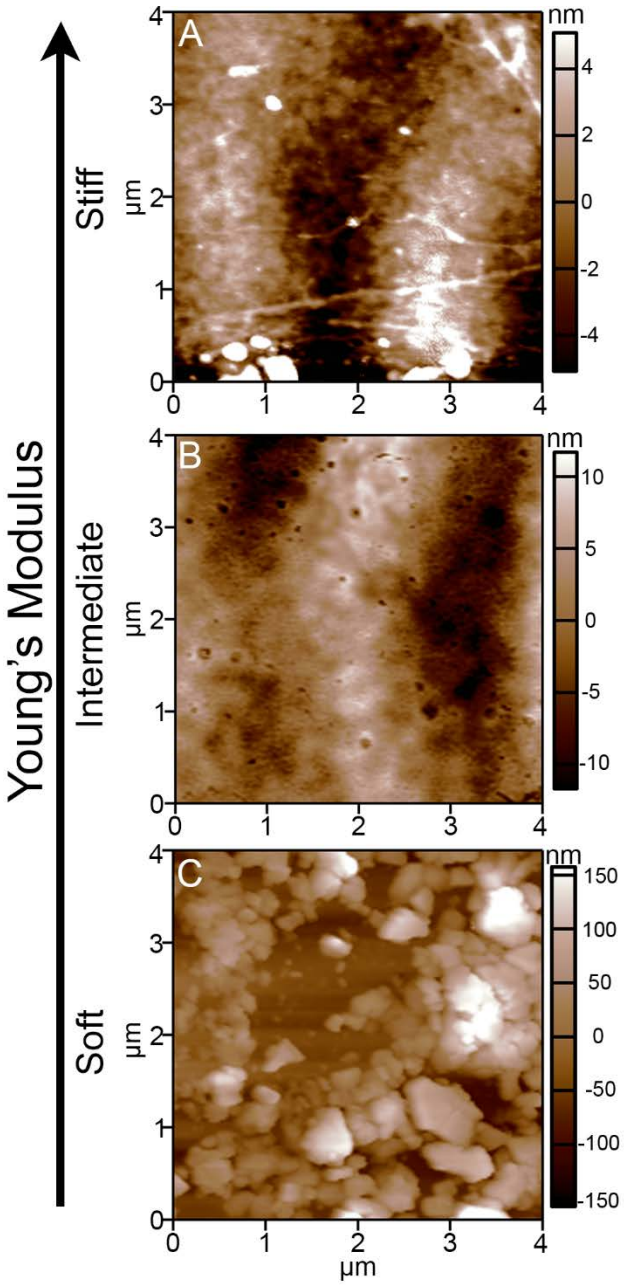

Figure 18: To demonstrate the need to acquire AFM scans on hydrated hydrogels, provided are representative surface topography AFM micrographs of (A) soft, (B) intermediate, and (C) stiff hydrogels that were dried slowly at room temperature. Hydrogels were 150 µm thick. A z-scale is provided alongside each image.

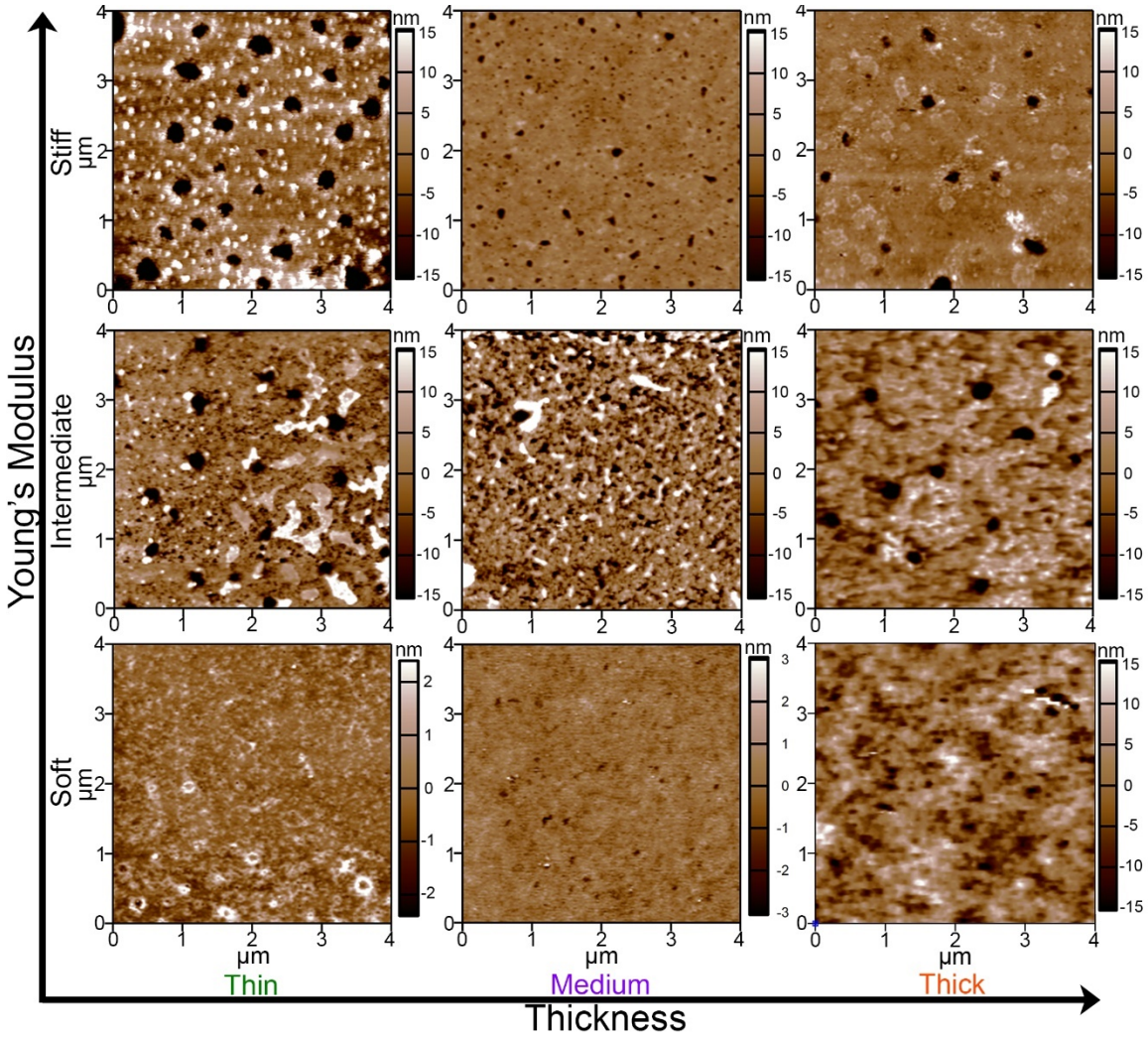

Figure 19: Representative AFM surface topography images of hydrated PEG hydrogels. Displayed is a grid of the hydrogels organized by Young's modulus and thickness. A z-scale is provided alongside each image.

Table 2: Surface roughness values for the PEG hydrogels, including, route mean square roughness (R_q), average roughness (R_a), skewness (R_{shw}), kurtosis (R_{kur}), and maximum roughness (R_{max}). Standard deviation is provided.

Hydrogel		R_q [nm]	R_a [nm]	R_{skw} [nm]	R_{kur} [nm]	R_{max} [nm]
Stiff	Thin	11.03±2.0	8.01±1.63	-0.75±1.10	3.53±4.25	37.99±5.78
	Medium	3.71±3.29	2.67±2.41	-0.82±1.14	5.88±4.81	18.01±12.64
	Thick	12.15±1.01	8.16±0.30	2.19±0.32	10.20±2.46	105.58±20.495
Int	Thin	7.27±0.50	4.89±0.58	-0.46±0.52	7.84±2.21	50.76±4.8
	Medium	11.98±2.60	8.25±1.86	-0.18±1.07	5.12±1.08	55.90±15.99
	Thick	17.43±1.00	12.03±0.53	2.22±0.21	7.45±1.20	166.91±36.85
Soft	Thin	0.71±0.09	0.51±0.06	2.05±0.49	15.34±9.85	12.11±6.36
	Medium	10.40±0.66	7.29±0.34	0.56±0.08	3.63±1.49	102.59±28.05
	Thick	9.36±3.18	7.141±2.5	0.54±0.48	4.39±4.33	75.70±14.23

Figure 20 and Table 3 contain the Young's modulus of thin, medium, thick hydrogels acquired using hydrated AFM, as well as the bulk rheological measurements acquired on very thick (1000 μm) hydrogels. AFM determined that the thin-stiff, medium-stiff, and thick-stiff hydrogels had a statistically equivalent Young's modulus values of 950 ± 90 kPa, 1000 ± 90 kPa, and 11000 ± 90 kPa, respectively, which were consistent with the literature.[115,126] There was no statistical differences between the two techniques; the Young's moduli of soft and intermediate hydrogels at all thicknesses (thin, medium, thick, and bulk) was the same. While the AFM measurements were consistent within the stiff hydrogels (thin, medium, and thick), their Young's moduli were lower than that acquired using rheology. This was likely because the lower water content of the stiff hydrogels exacerbated the differences between the compressive AFM measurements and shear rheological measurements, as previously reported.[127] The reasonable agreement between local and bulk measurements reaffirms that polymer concentration dictates mechanical properties of the PEG hydrogels and allows us to group the thin, medium, and thick hydrogels into three distinct regimes based on their Young's modulus: soft, intermediate and stiff.

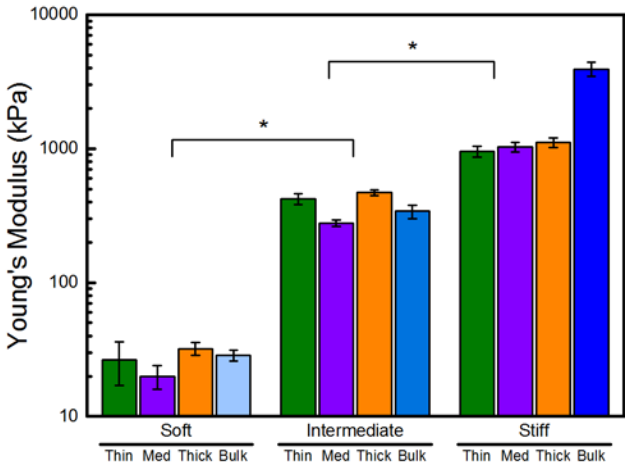

Figure 20: The Young's modulus of PEG hydrogels increased with increasing polymer concentration. AFM nanoindentation and bulk rheology were used to determine the Young's modulus of soft (11 wt% PEG), intermediate (29 wt% PEG), and stiff (55 wt% PEG) hydrogels. Error bars denote standard error. An asterisk (*) denotes 99% significance between stiffness regimes.

Table 3: Properties of PEG hydrogels, including Young's modulus and mesh size (ξ). Standard error is provided.

	Young's Modulus [kPa]				Mesh Size[3] [nm]
	Thin[1]	Medium[1]	Thick[1]	Bulk gel[2]	Bulk gel
Stiff	950±90	1000±90	1100±90	3900±700	1.0±0.1
Intermediate	420±40	280±20	470±20	330±120	1.9±0.04
Soft	27±10	20±11	32±4.0	29±8	2.7±0.3

[1]Measured using AFM nanoindentation. [2]Measured using oscillatory shear rheology. [3]Calculated using a modified version of the Flory theory Equation 2.

4.4.2 General Trends Regarding the Attachment of *S. aureus* and *E. coli* to PEG Hydrogels

Consistent with literature,[56,57] the presence of any hydrophilic PEG coating statistically reduced the amount of adhered bacteria compared to internal glass controls by ~95% for *S. aureus* and by ~93% for *E. coli*. Despite the reduction, it is notable that some microbes still attach and this study investigates how microbial attachment is affected by the thickness and stiffness of a PEG hydrogel layer. To decouple the effect that hydrogel

stiffness and thickness pose on bacterial adhesion, we conducted static bacterial adhesion experiments in minimal growth media on thin, medium, and thick PEG hydrogels (immobilized on glass slides), which were fabricated in each stiffness regime, Figure 17. Two general trends emerged following a 24 hr incubation: (1) fewer bacteria adhered to soft hydrogels than to stiff hydrogels and (2) more bacteria adhered to thin hydrogels than thick hydrogels at all stiffnesses. Due to the substantial differences in the data, which likely results from unique sensing and/or attachment mechanisms, the specific results for each bacterium will be discussed separately.

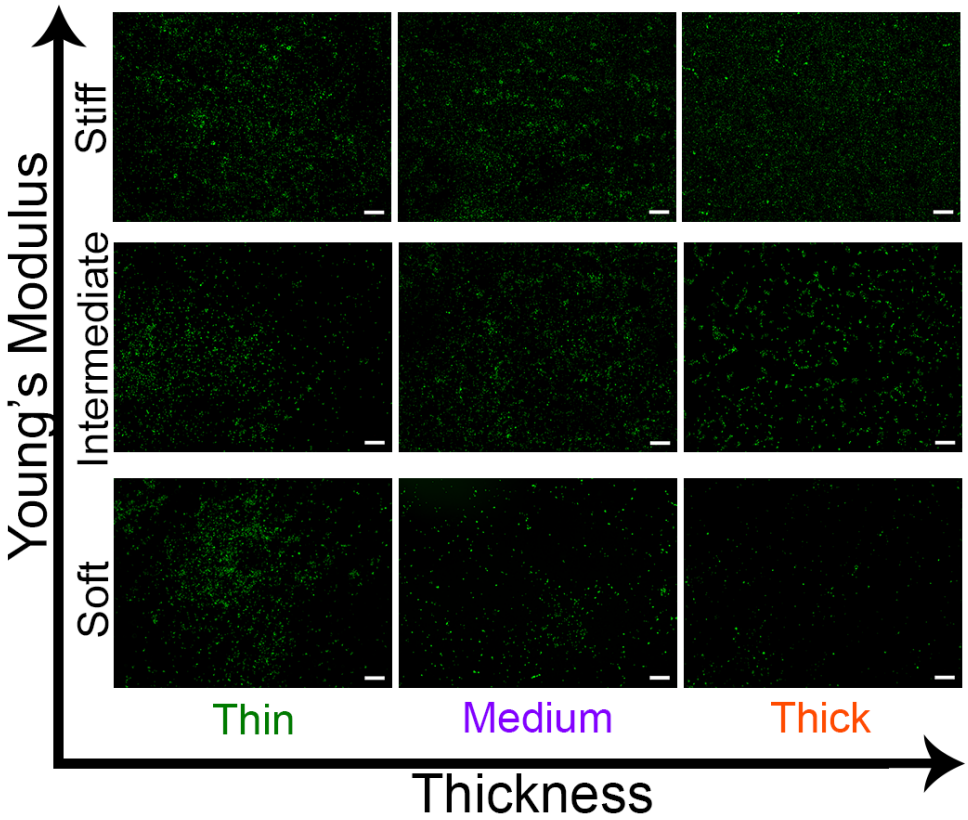

Figure 21: Representative fluorescent micrographs of *S. aureus* adhesion after a 24 h incubation period on thin (15 µm), medium (40 µm), and thick (150 µm) PEG hydrogels that were soft (30 kPa), intermediate (400 kPa), and stiff (1000 kPa). A 100 µm scale bar is displayed.

4.3.4 Attachment of *S. aureus* to PEG Hydrogels

Representative fluorescent micrographs of *S. aureus* incubated on PEG hydrogels are provided in Figure 21. Consistent with our previous study on thick PEG hydrogels,[123] *S. aureus* adhesion scaled with stiffness, as demonstrated by the statistically significant higher colony coverage on intermediate and stiff hydrogels (15 times and 25 times, respectively) than on the soft hydrogels, Figure 22. For the thin (15 μm) hydrogels, the effect of stiffness was significantly diminished, where the colony area coverage of *S. aureus* on thin-intermediate and thin-stiff hydrogels was 1.2 and 2 times greater than on the thin-soft hydrogels. Interestingly, the thickness of intermediate and stiff hydrogels had no impact on *S. aureus* adhesion, as the thin-intermediate, medium-intermediate, and thick-intermediate hydrogels induced statistically equivalent surface coverages of 2.5 ± 0.4%, 2.4 ± 0.3%, and 2.7 ± 0.2%, respectively. The thickness of soft hydrogels, however, displayed a profound effect on *S. aureus* adhesion. Significantly more bacteria adhered to thin-soft hydrogels than thick-soft hydrogels (99% confidence). There were statistically different area coverages of 1.9 ± 0.2%, 1.3 ± 0.5%, and 0.4 ± 0.2% on thin-soft, medium-soft, and thick-soft hydrogels, respectively. These results suggest that *S. aureus* surface attachment is sensitive to the thickness of soft hydrogels.

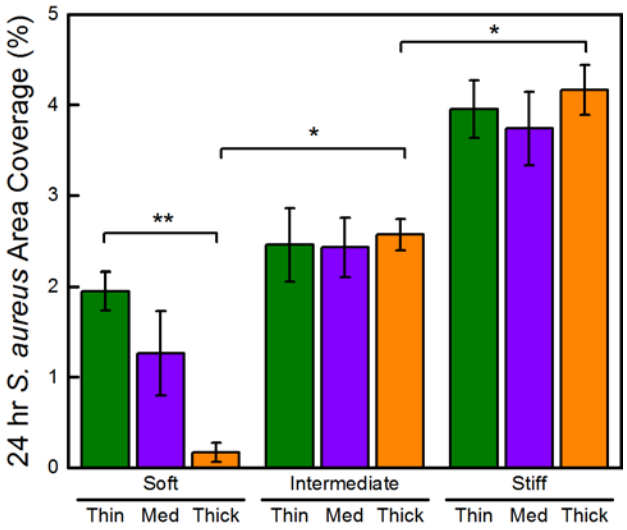

Figure 22: *S. aureus* attachment is influenced by the thickness of soft hydrogels. The total *S. aureus* area coverage after a 24 h incubation period on thin (15 µm), medium (40 µm), and thick (150 µm) PEG hydrogels that were soft (30 kPa), intermediate (400 kPa), and stiff (1000 kPa). One asterisk (*) denotes 95% significance between hydrogels in different stiffness regimes. Two asterisks (**) denote 95% significance between samples of the same stiffness.

4.3.5 Attachment of *E. coli* to PEG Hydrogels

Hydrogel thickness had a greater effect on *E. coli* adhesion than *S. aureus* adhesion. Consistent with our previous study,[123] more *E. coli* adhered to thick-stiff hydrogels than to thick-soft hydrogels, with 4 times and 7 times more colony coverage observed on the thick-intermediate and thick-stiff hydrogels than on the thick-soft hydrogels, respectively. Notably the area coverage of *E. coli* on the thick hydrogels was statistically lower than the *E. coli* coverage on thin and medium thickness hydrogels across all three stiffness regimes, Figure 23. Thin-stiff and medium-stiff hydrogels displayed a statistically equivalent *E. coli* coverage of 3.0 ± 0.4% and 2.9 ± 0.1%, respectively, but significantly less adhesion (95% confidence) than the thick-stiff hydrogels, 2.2 ± 0.2%. The *E. coli* adhesion on thin hydrogels occurred independent of stiffness, 1.9 ± 0.3%, 2.3 ± 0.5%, and 3.0 ± 0.4% for the thin-soft, thin-intermediate, and thin-stiff hydrogels, respectively.

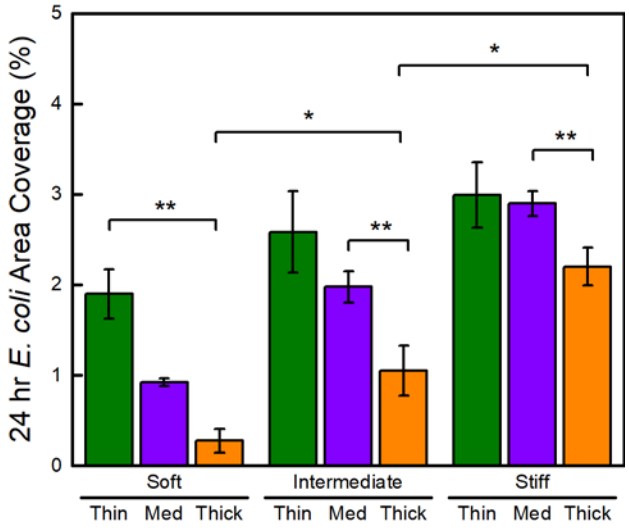

Figure 23: *E. coli* exhibits depth-sensitive adhesion to thin and medium thickness hydrogels at all three stiffnesses. Total *E. coli* area coverage after a 24 hr incubation period on thin (15 µm), medium (40 µm), and thick (> 150 µm) PEG hydrogels that were soft (30 kPa), intermediate (400 kPa), and stiff (1000 kPa). One asterisk (*) denotes 95% significance between hydrogels in different stiffness regimes. Two asterisks (**) denote 95% significance between samples of the same stiffness.

4.3.6 Discussion and Implications on Designing Antifouling Coatings

Our results demonstrate that two different bacteria, non-motile gram-positive *S. aureus* and flagellated gram-negative *E. coli,* adhered to PEG hydrogels in distinct manners, as evident by their different thickness and stiffness dependencies. The heat maps shown in Figure 24 displays the relative adhesion of *E. coli* and *S. aureus* as a function of hydrogel thickness and Young's modulus, thus facilitating a direct comparison of structure-property relationships between the two-microbial species. For example, the *E. coli* adhesion dependence observed on the intermediate hydrogels is noticeably absent from *S. aureus*, indicative of a species-specific phenotype. The remarkably similar increase in bacterial adhesion observed for both species on the soft hydrogels suggests that for soft hydrogels, the thickness of that hydrogel coating matters. We hypothesize that both

bacteria types feel through the thin hydrogels sensing the underlying very stiff glass substrate, thus instigating increased adhesion typical of a stiffer material. Notably, the hydrogels used in this study are comprised of the same protein-resistant PEG chemistry and consistent surface roughness. However, surface features arising from hydrogel formation including local polymer fluctuations or the release of air bubbles can create topographical features than may cause bacteria to view the hydrogels differently. Bacteria lack visual, auditory, and olfactory perception; surface sensing by bacteria is considered to occur as a combination of chemical signaling cues and physical appendage or membrane-based interactions.[121] After adhering to a surface, the membrane of a microbe deforms, which causes the bacteria to react to the membrane stress and change from a planktonic to a biofilm phenotype.[128] The mechanisms controlling the adhesion of bacteria to surfaces and the deformation of the cell membrane have been well studied on metal and polymeric materials.[129–131]

The extracellular organelle of *E. coli* are known to probe the stiffness of a surface in a manner similar to an AFM cantilever.[84,132] Unlike *E. coli*, *S. aureus* lacks extracellular appendages, thus an alternative surface sensing mechanism must dictate the statistically different adhesive behavior of *S. aureus*. While the mechanism remains unknown,[133] Li *et al.* reported that the kinetics of *S. aureus* adhesion was altered by shear stress, but does not alter *S. aureus'* expression of fibronectin-binding or collagen-binding proteins.[134] In this study, membrane deformation potentially plays a role due to the difference in Young's moduli between the peptidoglycan membrane of *S. aureus* and the hydrogel's stiffness. AFM force spectroscopy studies previously determined that the Young's modulus of the peptidoglycan membrane of *S. aureus* was ~ 47 kPa,[135] comparable to the soft hydrogels

used in this study, but significantly less than the intermediate and stiff hydrogels. Thus, soft hydrogels would deform more upon *S. aureus* contact, potentially enhancing the sensing mechanism and subsequently increasing the likelihood of adhesion. While the exact mechanism of how or why individual microbes display depth sensitivity is beyond the scope of this manuscript, we suggest that antifouling coatings should be designed with thickness in mind and that these results will spur further study in the burgeoning field of microbial response to substrate mechanics.

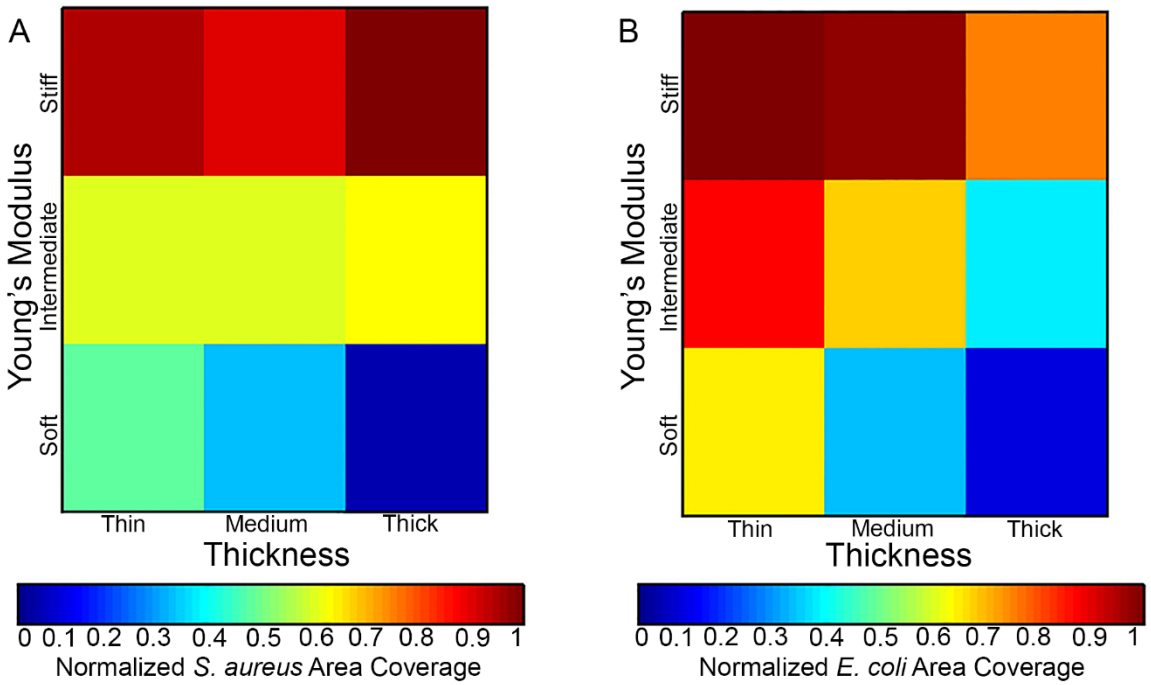

Figure 24: Heat map displays of the normalized (A) *S. aureus* and (B) *E. coli* area coverage on hydrogels after a 24 hr incubation period on thin (15 µm), medium (40 µm), and thick (> 150 µm) PEG hydrogels that were soft (30 kPa), intermediate (400 kPa), and stiff (1000 kPa). Data from Figures 22 and 23.

4.5 Conclusion and Future Work

To our knowledge, this is the first demonstration that bacterial attachment displays a depth-sensitivity through hydrogels to an underlying stiff substrate. Through systematic, *in situ* AFM mechanical and morphological characterization under aqueous environments, we decoupled hydrogel stiffness and thickness effects on the depth sensing of two diverse microbial species, *S. aureus* and *E. coli*. Decreasing the thickness of PEG hydrogels significantly increased bacterial adhesion, as 12 times more *S. aureus* and 8 times more *E. coli* adhered to the thin-soft hydrogels than to the thick-soft hydrogels. *S. aureus* adhesion was strongly influenced by the thickness of soft hydrogels, but displayed only minimal variation in bacterial adhesion on thinner intermediate and stiff hydrogels. *E. coli* displayed greater thickness-dependence; a higher colony coverage occurred on medium than on thick hydrogels of all Young's moduli. The substantial differences in bacterial adhesion observed between thin and thick hydrogels suggests that the underlying stiff substrate may have influenced the perceived mechanical properties of the hydrogel by the adherent bacteria. These findings suggest that bacteria are sensitive to the thickness of soft hydrogels.

Future work could investigate the depth-sensitivity of bacterial adhesion to other types of materials, both organic and inorganic. For example, a similar studying using elastomeric materials would help determine how much of the bacteria's thickness sensitivity can be attributed to the high-water content of hydrogels. Furthermore, integrating the two systems together would provide an additional experimental tool to decouple the influence of each material. If a thin hydrogel could be polymerized onto a tunable PDMS platform or a thin layer of PDMS could be deposited onto a tunable

hydrogel surface, the chemical, mechanical, and morphological properties of the interface would remain constant while the bulk stiffness could be modified. Although characterization of the stiffness for the composite system would be challenging, this could directly answer questions surrounding what the bacterial actually "feels" from the surface and how far this sensing mechanism extends. The use of support layers of different chemical composition yet comparable Young's modulus while maintaining the same hydrogel top-layer would enhance our knowledge regarding the specific properties of an underlying substrate that influence bacterial interactions.

Determining the mechanism of depth-sensitive mechanical sensing displayed by each bacterial species would be another interesting study. As with the mechanical sensitivity of bacteria, investigating the genetic information of multiple bacterial species following adhesion experiments on thin vs thick surfaces using a "competition experiment" could lead to valuable insights by creating an environment where the bacteria has the opportunity to sample multiple surfaces before selecting its preferred conditions. The mechanically sensitive surface sensing mechanisms used by gram-negative bacteria could serve as a starting point to identify the mechanism(s) that gram-positive bacteria use to detect surface properties.

From a materials characterization perspective, hydrated AFM is a powerful tool that could be for numerous studies concerning the characterization of hydrogels. For example, monitoring hydrogel morphology induced by the intrinsic network swelling of a hydrogel when immersed in different liquids could provide an interesting perspective on whether there is a dependence of hydrogel surface morphology on the type of swelling

liquid. By using a flow cell, one could investigate the mechanical and morphological response of stimuli responsive hydrogels, for example, pH sensitive swelling.

Alternatively, studying the location and morphology of adhered bacteria on a copolymer system with alternating soft and stiff regions would provide insights into the ability of bacteria to differentiate stiffness at controllable length scales. This type of competition study could directly compare patterns of different chemical compositions with equivalent stiffness, or comparable chemical compositions with differing mechanical properties. Furthermore, the high-resolution enabled by AFM could provide insights into the location of bacterial appendages between specific regions. Quantifying the expression of these appendages on regions with specific chemical or mechanical properties would improve our understanding of how specific material properties influence bacterial behavior.

CHAPTER 5

MECHANICALLY SENSITIVE SURFACE TRANSPORT OF *STAPHYLOCOCCUS AUREUS* MW2

Adapted from: Kolewe, K. W.; Kalasin, S.; Santore, M. M.; Schiffman, J. D., Mechanically Sensitive Surface Transport of *Staphylococcus aureus* MW2 on Poly(ethylene glycol) Brushes and Hydrogels

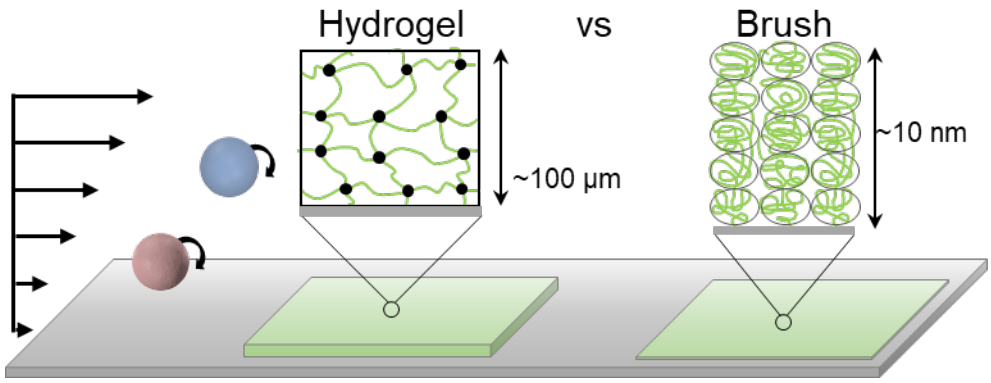

Figure 25: Hydrogel stiffness increases the frequency and duration of dynamic adhesion, a mode of surface-associated transport of bacteria.

5.1 Summary

Surface-associated transport of flowing bacteria is a mechanism for otherwise immobile bacteria to migrate on surfaces and could be associated with biofilm formation or spread of infection. This study establishes that *S. aureus* bacteria exhibit materials-dependent surface-associated transport on PEG surfaces in flow. In this study, a series of well-controlled protein and bacterial-adhesion resistant PEG hydrogels and two PEG brushes were studied. *S. aureus* was found to dynamically adhere in gentle flow to these biocompatible surfaces, without permanent attachment, without the influence of gravity. *S. aureus* demonstrated a propensity for repeated surface-engagement on stiff hydrogels

(1300 kPA) and brush surfaces (450-1800 kPa). Control studies with similarly sized poly(ethylene oxide) (PEO)-coated rigid silica microspheres, established that the observed engagement behavior of *S. aureus* was biologically-specific and not simply diffusion controlled. *S. aureus* displayed a tendency for longer and more frequent surface encounters on stiff hydrogels and brushes compared to soft hydrogels (1-15 kPa). This mechanically sensitive surface-engagement was not observed with silica particles, as the duration, length, and frequency of surface engagements was comparable for soft and stiff surfaces. This is the first report of mechanically sensitive surface-transport of bacteria which could have implications for the initiation of biofilms on polymeric medical devise.

5.2 Introduction

5.2.1 Effect of Fluid Flow on Bacterial Interactions

Fluid flow is a critical element of virtually all real environments.[136] The effect of flow on HAIs can be profound, as secondary tissue infections and deadly systemic infections (sepsis) can result from the transport of bacteria away from the original or primary infection site. Figure 25 highlights the most common locations of secondary infections resulting from device-associated HAIs. Yet flow is often neglected in laboratory research in favor of higher throughput static experiments.[137] There are numerous examples of specific bacterial adhesion mechanisms that arise as a result of shearing fluid flow. For example, the most common adhesive protein in *E. coli*, FimH, forms shear dependent catch-bonds.[138,139] Located at the tip of extracellular fimbriae, bonds formed through this protein adhesin have been shown to form on protein treated and abiotic surfaces.[140] The strength of the bonds formed through FimH are highly shear-dependent. At low shear,

bonds are typically reversible and induce close surface associated through periodic adhesion and arrest; however, the strength of the bond increases at high shear inducing irrepressible adhesion.[141] Further, similar behavior has been shown by other bacterial species including *S. aureus* and *Pseudomonas aeruginosa*,[25,142,143] indicating that this is not a localized phenomenon of one bacterial species, rather an evolutionarily developed trait to cope with fluid flow.

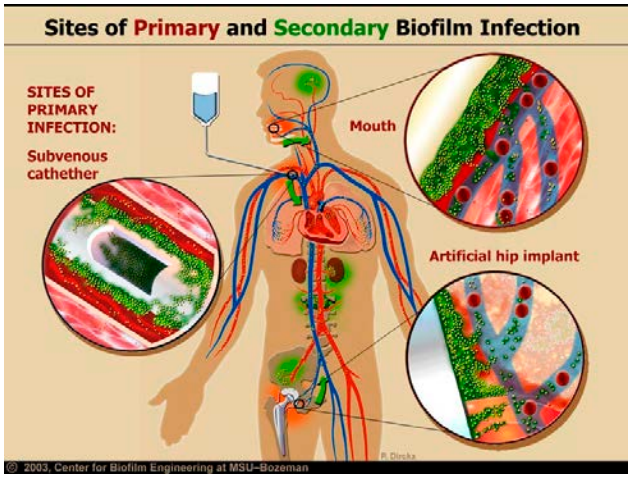

Figure 26: Common locations of secondary biofilm infections that occur once bacteria reach the bloodstream from primary sources. Figure courtesy of the Montana State University Center for Biofilm Engineering.

5.2.2 Surface-Associated Bacterial Motility

Initially, it was hypothesized that upon surface contact bacteria will either adhere or disengage and remain in solution. However, this is an overly simplified view of bacterial surface interactions. Beginning with the pioneering work of *Henrichsen*, who classified the surface motility of hundreds of strain variants of over 40 species of bacteria;[144] surface-motility is now accepted as a key component in bacterial colonization of abiotic and biotic surfaces. The most studied and best characterized modes of surface motility, swimming and swarming, are driven by the rotation of flagella.[145,146] Further, bacteria that express pili

or fimbriae display unique twitching motility to direct surface transport.[147] However, not all bacteria express extracellular appendages, yet all bacteria display the ability to travel across a surface. In particular, immobile bacterial species that express no extracellular appendages including *S. aureus* and *Staphylococcus epidermis* have demonstrated the ability to move from a primary infection site to a secondary location within the human body when in the presence of shear. Therefore, immobile bacteria that lack a direct mechanism of active transport likely harness shear flow as an alternative mode of surface-associate motility or transport.

5.2.3 Polymer Brushes

Polymer brushes are a well-studied type of monolayer film that consist of polymers anchored at one end to the substrate yet not crosslinked between neighboring polymers. Although a variety of deposition methods have been developed, the most effective of which is chemical grafting. The increased control of grafted brushes are advantageous due to the surface density, localization of polymer chains, and stability of grafted polymers.[148] Brushes can be formed on surface through either a top-down, "grafted-to" approach, or a bottom-up, "grafted-from" approach. End-functionalized polymers are "grafted-to" a surface by binding or anchoring to complementary surface-functionalities.[149] Alternatively, surface-initiated polymerization can be used to "graft-from" a surface by building layers of polymer than diffuse to the surface. In either case, polymer brushes are a versatile approach to chemical surface modification and can be achieved using a variety of polymers depending on the solvent used for polymerization. Fouling-resistant PEG brushes are a well-characterized and benchmark protein resistant film.[150,151] For this study, PEG brushes

are used a well-defined chemically controlled analog to PEG hydrogels. The brush monolayer has a certain degree of compressibility that can be tuned to mirror the bulk compressibility of hydrogels. However, brushes are effectively thin enough for mechanical contributions of the bound substrate to influence bulk mechanical measurements, and therefore will be considered a "stiff" surface for bacterial-surface interactions.

Table 4: Fabrication parameters of PEG hydrogels.

Name	PEG Content [wt %]		Dynamic Moduli [kPa]		Swelling Ratio
	M_N:750	M_N:20000	G'	G''	
Soft-2*	5	10	1.8	0.38	15 ± 0.40
Soft-1	11	NA	9.5	0.24	8.6 ± 1.0
Stiff-1	55	NA	1300	190	2.2 ± 0.05

5.3 Methods

5.3.1 Hydrogel Fabrication

Details on homopolymer PEG hydrogel fabrication are provided in Chapter 4.2.1 and outlined in Table 4. Co-polymerized PEG was prepared with 5 wt% M_N:750 PEG and 10 wt% M_N: 20000 in PBS. The hydrogel precursor solution was then pipetted onto a glass slide (Fisher Scientific) functionalized with 3-(trimethoxysilyl)propyl methacylate,[103] then sandwiched with a 24 × 40 mm glass coverslip to ensure uniform hydrogel thickness and inhibit oxygen diffusion. Following polymerization, the coverslip was removed with forceps and the hydrogels were swelled for 48 hr in 25 mL of PBS with a Debye length of 1nm (0.008 M Na_2HPO_4, 0.002 M KH_2PO_4, and 0.1M NaCl). Prior to flow experiments, hydrogels were cut with a sterile razor to fit the rubber gasket used to seal the flow chamber.

5.3.2 Hydrogel Characterization

Details on PEG hydrogel characterization are provided in Chapter 5.2.2

5.3.3 PEG Brushes

Glass substrates were prepared by immersing FisherFinest microscope slides overnight in concentrated sulfuric acid and rinsing thoroughly in DI water to produce a clean silica surface. The slides were immediately sealed in a laminar flow chamber and contacted with flowing pH 7.4 phosphate buffer (0.008 M Na_2HPO_4 and 0.002 M KH_2PO_4). Poly-L-lysine-g-PEG copolymers were synthesized and characterized as previously described. [150,152]A 100 ppm copolymer solution in phosphate buffer was flowed over the surface for 10 minutes at a wall shear rate of 5.0 s^{-1}. The flowing phosphate buffer was subsequently replenished for ~10 minutes to wash any excess PLL-PEG from the flow cell. The buffer was then changed to phosphate buffer saline buffer with a Debye length of 1 nm and then the bacteria experiment commenced. The copolymer adsorption traces were frequently monitored by near-Brewster reflectivity to confirm the copolymer adsorption: ~1.1 mg/m^2 (containing 0.95 mg/mg^2 of PEG for the 2K Brush and 1.0 mg/m^2 of PEG for the 5K Brush, based on the compositions of the two copolymers).[153] Knowing the total adsorbed amounts and PEG contents in the layers allowed us to describe the brushes, in the results section, in terms of parameters from established models for brushes.

5.3.4 Fibrinogen Adsorption

Fluorescently labeled fibrinogen was made by reacting fluorescein isothiocyanate (FITC isomer I, F2502 from Aldrich) as previously described.[154] The reaction product was

purified by passing the protein solution through a P-6 gel column (Biorad). Fluorescent labeling density was determined by fluorescence spectroscopy to be 4-5 fluorescein tags per fibrinogen molecule. Protein adsorption was measured in a steady laminar flow chamber via total internal reflectance fluorescence (TIRF) with a detection limit of ~0.03 mg/m^2 at a working concentration of 25 ppm for 30-40 min.[154]

5.3.5 Bacteria Preparation

Staphylococcus aureus MW12 (*S. aureus)* was a generous gift from Prof. Neil Forbes at the University of Massachusetts Amherst. *S. aureus* was grown overnight in Tryptic Soy Broth at 37 ºC then washed and re-suspended in 1 nm Debye length PBS at a working concentration of 1×10^8 cells/mL.

5.3.6 Engineered Particle Preparation

Control studies employed monodisperse 1-um silica spheres from Gel Tech (Orlando), coated with ~ 0.1 mg/m^2 of adsorbed 10 kDa polyethylene oxide, prepared by mixing the particles and the polymer solution in appropriate amounts. These particles possessed a zeta potential of -15 mV, similar to that reported for *S. aureus*. Dynamic light scattering revealed hydrodynamic particle diameter that was indistinguishable from that of bare silica, indicating that the PEO adsorbed in a flat nanometer-scale layer dominated by trains (segments in contact with the surface) with few little tails or loops. In this way the PEO, with its adsorption by hydrogen bonding to the non-dissociated surface silanols on the silica microspheres, blocked hydrogen bonding sites that would otherwise cause bare silica particles to adsorb to PEG brushes.

5.3.7 Methodology of Dynamic Engagements

Bacteria rolling studies were performed in a flow cell mounted in custom-built lateral microscope system with 20x Nixon objective. The slit flow chamber (260 x 178 μm) was illuminated from behind and oriented perpendicular to the floor to eliminate the contribution of gravity to bacteria surface-interactions as previously described.[155,156] A syringe pump was used to maintain a constant wall shear rate of 22 s^{-1} throughout this study. Data was recorded and stored on DVDs and instances of dynamic engagement were analyzed using the manual particle tracking feature in *FIJI* (*FIJI* is just *ImageJ*).[157] Particle tracking directly provides the distance traveled over the time step (0.2 s) and the associated instantaneous of the colloid throughout its path across the viewing window. A cell/particle was considered dynamically engaged if the instantaneous velocity average less than 5 μm/s yet traveled a minimum of 5 μm in length. To acquire a complete population of dynamically engaged colloids, 25-30 bacteria and particles were acquired per surface testing that exhibited at least one instance of sustained dynamic engagement.

5.4 Results and Discussion

5.4.1 Characteristics of PEG Hydrogels and PLL-PEG Brushes

Hydrogels were polymerized as a function of polymer concentration to tune the mechanical properties of the hydrogel, Figure 26. Table 5 summarizes the material characteristics of homo and copolymer PEG hydrogels including equilibrated polymer concentration, storage moduli, mesh size, and thickness as well as the hydrogels resistance to Fibrinogen adsorption. Comparable storage moduli of 9.5 and 1.8 kPa were determined through SAOS measurements for 11 wt% M_N:750 PEG and 5 wt% M_N:750/10 wt% M_N:

20000, respectively. As their storage moduli is comparable, these hydrogels will be further referred to as Soft-1 and Soft-2 to denote the number of polymers used in fabrication. The high polymer concentration 55 wt% M_N:750 hydrogel displayed a significantly larger storage modulus, 1300 kPA, and will be referred to as Stiff-1.

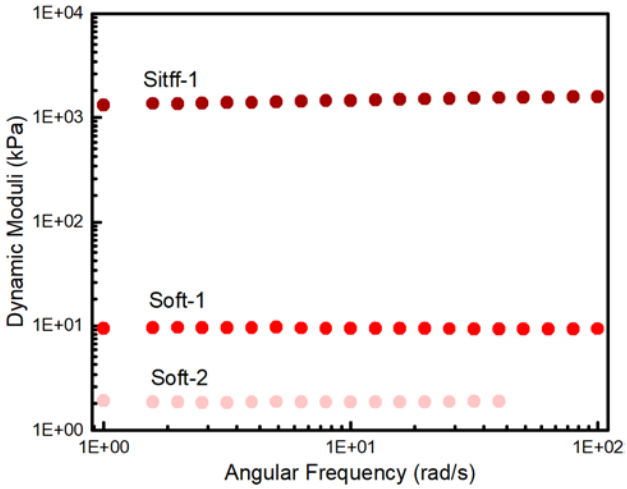

Figure 27: Dynamic moduli of PEG hydrogels acquired through SAOS measurements.

Table 5: Characteristics of PEG hydrogels as a function of polymer concentration

Name	PEG Content [wt %]	G' [kPa]	Mesh Size [nm]	Thickness [m]	Fibrinogen Adsorption [mg/m^2]
Soft-2	7 ± 0.1	1.8	4.1 ± 0.4	100 ± 5	< 0.01
Soft-1	8.6 ± 2	9.5	2.7 ± 0.1	110 ± 5	< 0.01
Stiff-1	46 ± 1	1300	1.0 ± 0.1	105 ± 5	< 0.01

To facilitate comparison of PEG hydrogels and brushes, the concentration of PEG was determined at equilibrium to be 7, 9, and 46 wt% PEG for Soft-2, Soft-1, and Stiff-1, respectively. Further, the theoretical mesh sizes of Soft-2, Soft-1, and Stiff-1 were determined to be 4.1 ± 0.4, 2.7 ± 0.1, and 1.0 ± 0.1, respectively, an inverse correlation

with storage modulus. By controlling the volume of precursor used in each hydrogel formulation, the thickness of hydrogels was independently determined to be 105 μm.

Table 6: Characteristics of PEG brushes.

Name	Equilibrated PEG Content [wt%]*	G [kPa[**	Mesh Size [nm]+,1	Thickness [nm]+	Fibrinogen Adsorption [mg/m2]
2K Brush	11	1800	1.9 ± 0.1	8-9	< 0.01
5K Brush	6	450	2.9 ± 0.2	15-17	< 0.01

* calculated via Flory brush model in which all segments form a uniform solution in the region of the layer, from the surface out to the thickness value in the table. The mass of PEG in the 2K brush was 0.95mg/m^2, and in the 5K brush was 1.0 mg/m^2 to facilitate this calculation.

** Set equal to the osmotic pressure of the brush, because the leading term in the brush compression is the squeezing out of solvent. Calculations osmotic pressure employ a chi parameter of 0.4 for PEG in water.

+ Values from Gon, Fang, Santore Macromolecules 2011.

1. taken as average distance between tethering points. Requires only knowledge of tether molecular weight and adsorbed amount, and employs the finding that the PLL tethers the PEG but does not require further models of brush structure.

5.4.2 Surface-Associated Motion Signature Analysis

Dynamic bacteria and particle adhesion studies were conducted in a laminar flow cell at a wall shear rate of 5 s^{-1}. Orienting the chamber perpendicular to the floor eliminated the impact of gravity on particle- or cell-coating interactions. A suspension containing ~10^8 cells or microparticles/mL was used in each experiment, a sufficiently dilute concentration to eliminate the effect of cell-cell and particle-particle interactions. In each run, data from at least 20-25 surface-engaged cells or particles over 10 min of video was analyzed. We found no significant differences between multiple runs, so data for 3 runs of each bacteria/particle-surface combination were combined to produce a larger, more meaningful statistical population.

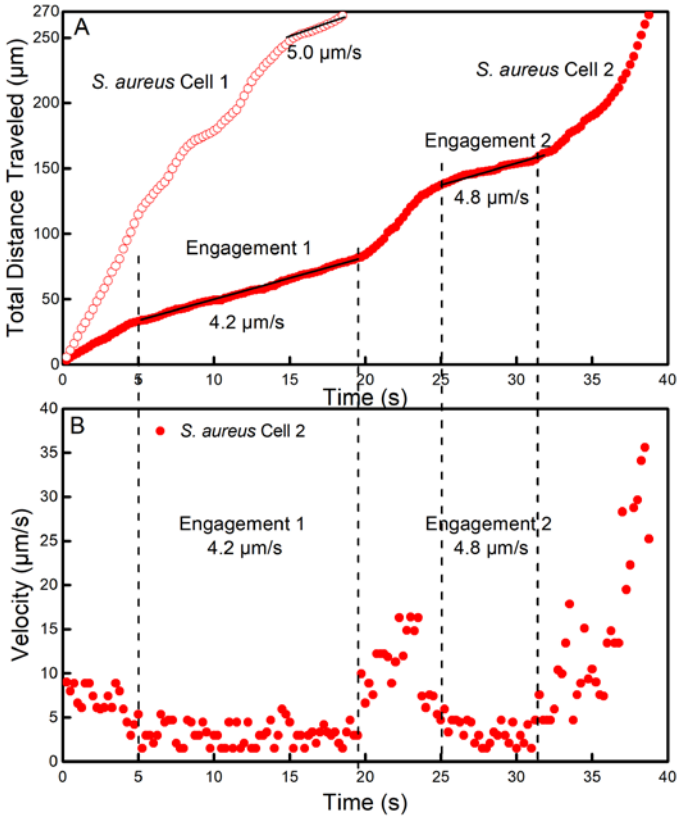

Figure 28: (A) Example trajectories of two representative *S. aureus* cells flowing near a 2K brush. (B) Instantaneous velocities, for Cell 2 from part A (solid circles), acquired at 30 frames/s and the cell-wall separation on the right axis calculated according to Goldman et al.[158] Two periods of engagement with rolling-like behavior are highlighted.

Of the hundreds of thousands of bacteria and particles to flow past the PEG surfaces, a fraction of surface-engaged colloids can be differentiated by their translational velocity. Passive diffusion drives initial surface engagement as both *S. aureus* and silica particles are immobile, therefore rendering surface engagement a statistical probability. Following surface contact bacteria and particles can become dynamically engaged, displaying periods of sustained surface engagement, where engaged colloids display substantially decreased translational velocity. Tracking the translational velocity of near-surface bacteria and particle, provides a quantifiable metric to separate incidental contact

from true dynamic engagement, Figure 27. The criteria for surface-associated transport is a continuous period of at least 1 s where the translational velocity is no larger than 5 μm/s.

5.4.3 Single Surface Encounter: Engagement Length

The length of each surface encounter provides an easily quantifiable metric to differentiate the relative degree of attraction for each colloid-surface combination. Essentially, the more of a surface a single bacteria cell is able to sample, the more likely a defect or other adhesion point can be found that enables permanent attachment and colonization. As previously stated, the minimum length of an individual rolling encounter is 5 μmto differentitate sustained engagement from incidental contact. The distribution of engagement distances of single surface encounters is provided in Figure 28, where the top window corresponds to *S. aurues* surface encounters while the bottom corresponds to silica particles.

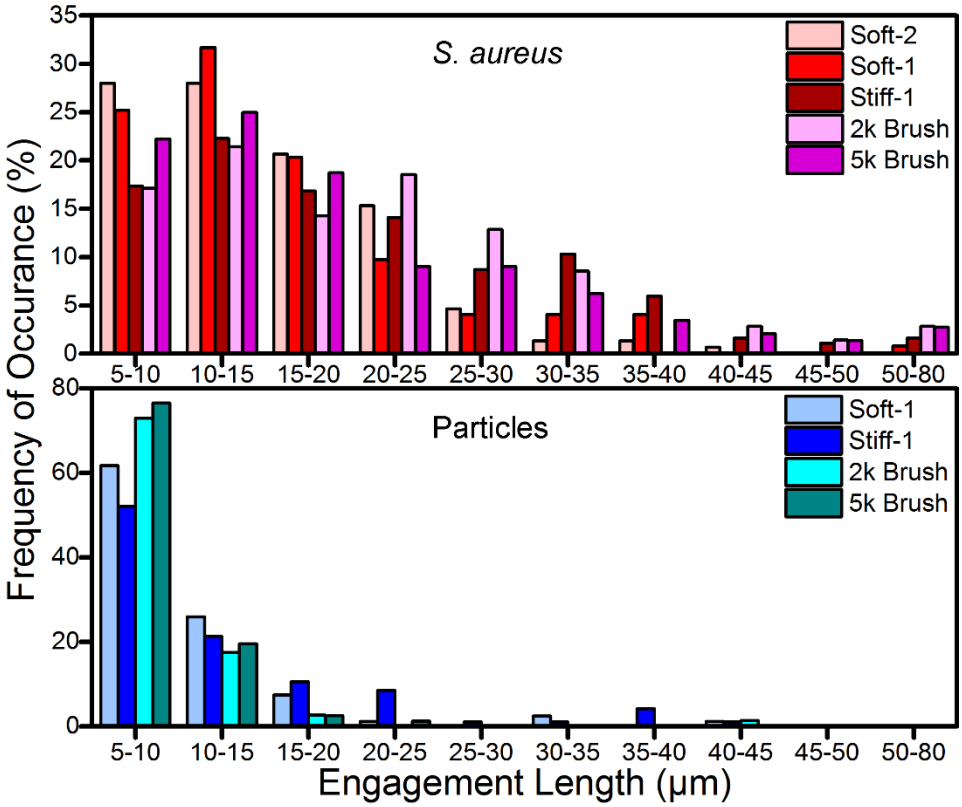

Figure 29: The encounter engagement length distribution of *S. aureus* (red) and PEGylated silica particles (blue) for each PEG surface. The frequency of occurrence for each distance segment was determined as the percentage of the total number of surface encounters that traveled a minimum distance of 5 µm specific to each colloid/surface combination.

There are a number of readily apparent and key differences between the bioloigcal and synthetic collodial systems. As expected, the additional physio-chemcial interactions arising from the living *S. aureus* cells displayed enhanced surface engagement on every hydrogel and brush surface. When viewing the distribution as a whole, *S. aureus* surface encounters exhibited a wide range engagement lengths on each of the 5 PEG surfaces (5-80 µm), whereas the range of silica engagement lengths was only (5-45 µm). Additionally, the median engagement length of *S. aureus* was longer than silica on every hydrogel and brush surface, Table 7.

Table 7: The median encounter length for the overall distribution of S. aureus and functionalized silica microparticles on PEG hydrogels and brushes.

Encounter Length	Soft-2 [μm]	Soft-1 [μm]	Stiff-1 [μm]	2k [μm]	5k [μm]
Bacteria	13.4	13.9	17.8	18.6	17.5
Particles		8.9	9.6	6.8	7.1

Although *S. aureus* exhibited greater surface engagement than silica particles, there were substantial differences arising between the distributions of each tested surfaces. Hydrogel stiffness had a clear influence on the engagement length of *S. aureus* as cells on average had shorter encounters on Soft-2 and Soft-1 hydrogels than on Stiff-1. For example, ~90% of *S. aureus* encounters on Soft-2 and Soft-1 hydrogels travel 25 μm or less in length compared to ~70% on Stiff-1 hydrogels. Further, the median engagement length of *S. aureus* on Stiff-1 hydrogels, 17.8 μm, was ~4 μm or one additional full rotation longer than the median engagement length on Soft-2 or Soft-1 hydrogels, 13.4 and 13.9 μm respectively. Interestingly, the median length of *S. aureus* encounters Stiff-1 hydrogels was comparable to the stiff 2k and 5k brush controls, 18.6 and 17.5 μm respectively. As silica particles demonstrated no difference in engagement length between Soft-1 and Stiff-1 hydrogels, 8.9 and 9.6 μm respectively, the observed behavior of *S. aureus* on stiff surfaces is not universal to all colloids. Rather, a biological phenomenon arising from the ability of *S. aureus* to sense the stiffness of a surface through a biological mechanism.

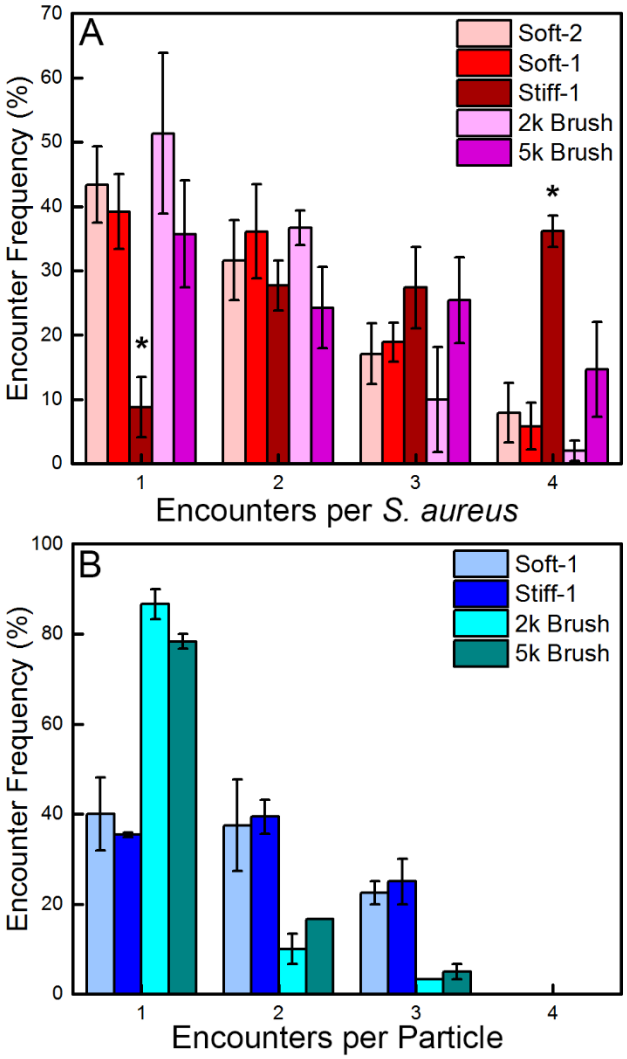

Figure 30: Distribution of the frequency of occurrence of multiple surface encounters for (A) *S. aureus* cells **(B)** or PEG-coated microparticles. At least 50 cells/particles were analyzed per coating. The x axis refers to the total number of observed encounters of each cell/microsphere within the viewing area. An asterisk (*) denotes statistical significance (p=.01).

5.4.4 Repeat Surface Engagements

After a surface-engaged colloid releases from the surface, one of two outcomes can occur: 1) the colloid escapes to bulk flow and doesn't encounter the surface again within the viewing window or 2) the colloid returns to the surface for an additional encounter(s). The propensity of a single *S. aureus* and silica particles to have multiple surface encounters

is depicted in Figure 29 by the frequency of a single (1), or repeated (2, 3, or 4+) surface encounters for an individual colloid.

The number of *S. aureus* that exhibited multiple encounters is roughly equivalent on both soft hydrogels and control brush surfaces with ~40% of cells displaying only a single encounter. However, *S. aureus* displayed significantly different behavior on Stiff-1 hydrogels, likely due to the mechanical sensitivity of *S. aureus*. If a single *S. aureus* experienced a sustained surface encounter on Stiff-1 hydrogels, then over 90% experienced at least 1 more surface encounter. The propensity of *S. aureus* to experience multiple surface encounters is 30% greater on Stiff-1 hydrogels than on any other surface. Further, almost 40% of cells experienced 4 or more surface encounters within the viewing window. A large deviation in encounter frequency between Stiff-1 hydrogels and Soft-2 and Soft-1 hydrogels is not unexpected considering the differences in the engagement length of single encounters; however, the substantial difference between *S. aureus* encounter frequency on Stiff-1 hydrogels compared to 2k and 5k brushes is striking due to the similar effective stiffness of these surfaces. Although the effective moduli of 2k and 5k brushes, 450 and 1800 kPa respectively, is comparable to G' of Stiff-1 hydrogels, 1300 kPa, the bacteria may detect stiffness cues from the underlying glass surface below the nm thick PEG brush monolayer.

Silica particles, interestingly, displayed similar rates of single encounters on Soft-1 and Stiff-1 hydrogels. This finding provides further evidence that the mechanically driven behavior exhibited by *S. aureus* is a biological sensing phenomenon and not a natural result occurring for any colloid interacting with hydrogels of different stiffness. There is a notable divergence between the number of silica particle surface encounters on hydrogels and

brush controls. The well-controlled architecture of the PEG brush may provide a better steric barrier to silica particle engagement than hydrogels, or the presence of methacrylate end-groups of the PEG used in hydrogel fabrication may provide adhesive points that increase silica particle interaction.

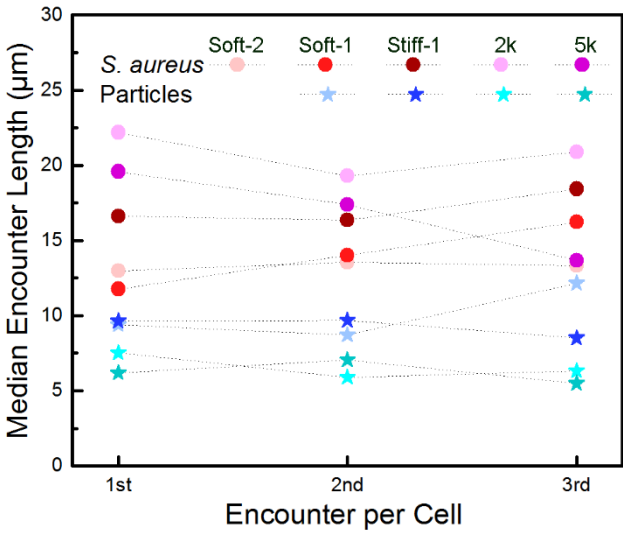

Figure 31: Median length as a function of encounter number (1st, 2nd, and 3rd) encounter for *S. aureus* (Red circles) and silica particles (Blue stars). This analysis does not include any solo encounters where the bacteria or particle had only one surface encounter during the observable period within the viewing window.

5.4.5 Encounter-by-Encounter Analysis of Encounter Engagement Length

To determine whether there was any "memory" or influence of previous surface encounters for engagement length and duration, we analyzed the engagement lengths for each colloid-surface combination encounter-by-encounter. Any bacteria that experienced only a single encounter were eliminated from the analyzed population, then the lengths of the 1st, 2nd, 3rd, etc encounters were grouped together. Statistical analysis on the resulting 1st, 2nd, and 3rd encounter groups determined the median length for each colloid-surface combination for each encounter, Figure 30.

Interestingly, there was not a statistically significant increase in encounter length with successive encounters on any surface. Further, the median engagement lengths of *S. aureus* on Soft-2 and Soft-1 hydrogels were less than the stiff surfaces for the 1st and 2nd encounters. The population of 3rd encounters was too small to accurately draw conclusions, but are provided to show the lack of an overall trend in the data. Analysis of the overall distribution of the engagement lengths of each encounter supported this conclusion. For *S. aureus*, there was little difference between the overall engagement length distribution (Figure 28) and the corresponding engagement length distribution of the 1st and 2nd encounter on each PEG surface. As expected from our previous results, the bacteria exhibited longer encounter lengths on every surface than silica particles.

5.4.6 Characterization of the Separation Between Surface Encounters

Knowing that the mechanical properties of a surface influence the frequency of a colloid re-engaging the surface, the natural question concerns the behavior of the colloid during the separation between encounters. To answer this question, the distance, time, and velocity of the periods between surface encounters for individual bacteria and particles were analyzed, Figure 31. Both the mean and median were calculated for each parameter, however the mean was heavily influenced by outliers, so the median proved to be the better statistical fit to describe the data for all three parameters. Due to the small population of particles that exhibited multiple surface encounters, it was difficult to draw firm conclusions on the separation behavior of silica particles on PEG brushes; however, silica particles are provided in the figure analysis for completeness.

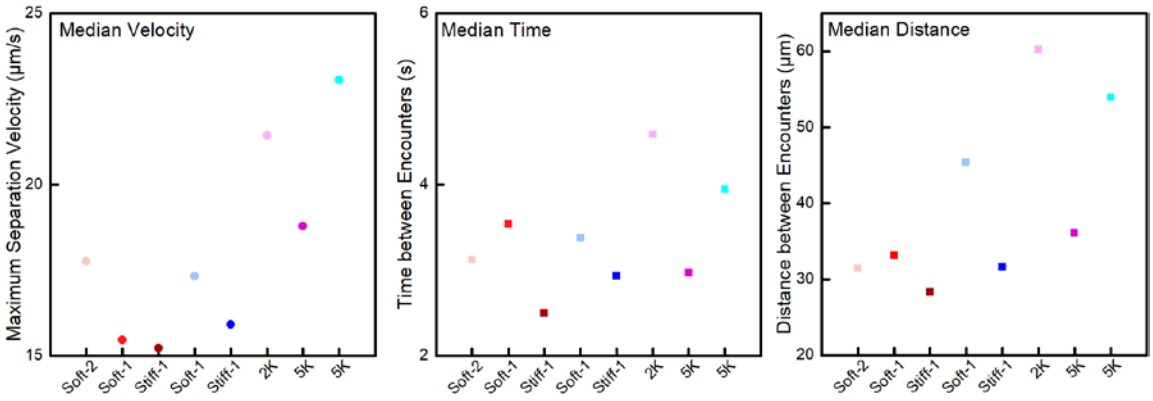

Figure 32: The separation of *S. aureus* (Red) and silica particles (Blue) between surface encounters for each type of surface tested. The maximum velocity achieved between encounter (left panel), time between encounter (center panel), and total distance traveled (right panel) were quantified for each bacteria or particle that exhibited multiple surface encounters within the viewing window.

In general, the separation behavior of each colloid was similar on every surface; however, one qualitative trend emerged for *S.* aureus. For each of the analyzed parameters, *S. aureus* demonstrated the smallest encounter separation on Stiff-1 hydrogels. For example, dynamically engaged *S. aureus* spent half a second (0.5 s) less between surface encounters on Stiff-1 hydrogels than any other hydrogel or brush surface. Although the maximum velocity between encounters and distance traveled between encounters were within statistical error for each surface, the lowest velocity and shortest distance traveled between encounters were both observed for *S. aureus* on Stiff-1 hydrogels.

5.4.7 Cumulative Surface Interaction: Influence of Colloid and Surface Properties

There is no statistical difference between the first or the 5th encounter of a single bacteria or particle with a surface. Therefore, the total residence time of surface engagement was calculated to account for all the surface encounters of each colloidal population, Figure 32. This metric enables direct comparison of the strength of colloidal

physio-chemical interactions between different surfaces in a dynamic flow environment. Longer residence times corresponds to a larger colloidal strength of interaction. Notably, residence time results are consistent with all previous metrics of dynamic surface-engagement, only simplified into a single universal metric. If the residence time of a colloid on a surface was short, then there is a lower probability of permanent adhesion or arrest downstream. In a biological sense, reduced residence times are indicative of fouling resistant surfaces as there is a lower chance of bacterial adhesion and colonization.

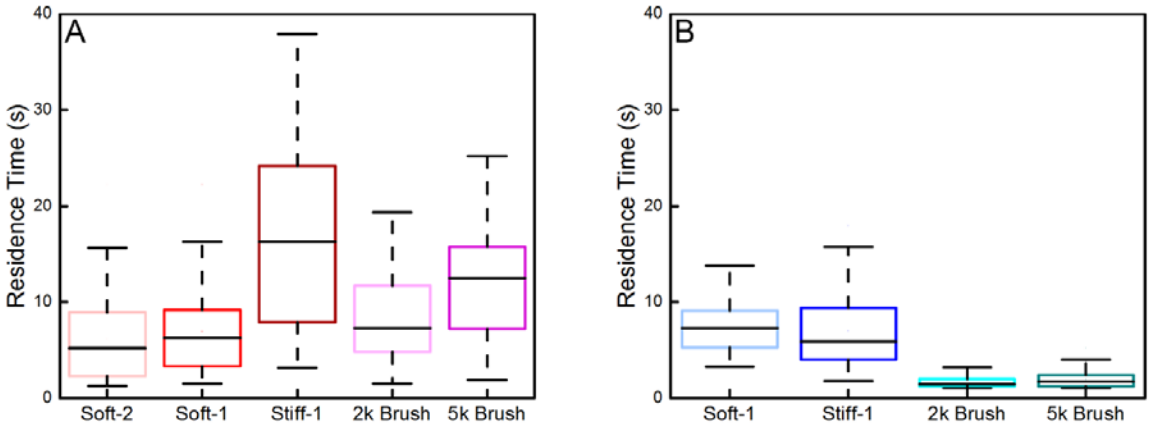

Figure 33: The total residence time of a single *S. aureus* cell (Red, A) and silica particle (Blue, B) on PEG surfaces. The residence time for each cell/particle is the sum of all surface encounters for each colloid resulting in the total surface engagement. The solid black line in each box represents the median residence time while the top and bottom of each box represent the 25th and 75th quartile each specific distribution, respectively.

The residence time of *S. aureus* on Stiff-1 hydrogels, 16.3 s, was significantly longer than on any other surface. This is approximately ~3 times longer than the residence time on Soft-2 or Soft-1 hydrogels, 5.2 and 6.2 s respectively. Reinforcing the conclusion that *S. aureus* have stronger interaction with stiff than soft hydrogels of the same chemistry. Interestingly, PEG brushes did not show this same correlation as the residence time of *S. aureus* on 5k brushes, 12 s, was significantly greater than the stiffer 2k brush, 7.2 s.

However, PEG brushes are an elastic monolayer attached to a rigid glass surface, so uncharacterized stiffness effects arising from the underlying glass may contribute to bacterial-surface interactions with the brush controls. Silica particle residence time was statistically equivalent for Soft-1 and Stiff-1 hydrogels, 4.5 and 5.7 s respectively, further emphasizing the biological specificity of the mechanical surface sensitivity of *S. aureus*. The short ~1.5 s residence time of silica particles on both 2k and 5k brushes indicates the weak surface interaction of the colloid and the robust resistance of silica adhesion to PEG brushes. It is important to note that our results in this dynamic study are consistent with static bacterial studies performed by our group and others.[91,123,159]

5.5 Conclusion and Future Work

The probability of a colloid initially encountering a surface is probabilistic in nature, independent of the type of colloid and the material properties of the surface. However, we have shown that once engaged, the type of colloid (living vs synthetic) and the mechanical properties of the surface, influence the frequency of repeated surface encounters by a single colloid. Surface-engaged *S. aureus* exhibited engagement lengths a full cell-rotation longer on stiff surfaces (stiff hydrogels and brush surfaces) than on soft hydrogels. This sensitivity was not demonstrated by silica particles on these same surfaces, indicating that the mechanical sensitivity of *S. aureus* is biologically based and likely associated with a surface-sensing pathway. Although the specific mechanism used by *S. aureus* to detect substrate stiffness is beyond the scope of this work, the short time-scales of surface interaction in this study may be a clue towards understanding the specific mechanism.

This is the first demonstration of mechanical sensitivity in a gram-positive bacterial species in flow. The increased frequency of surface encounters for *S. aureus* on stiff surfaces and the significant increase in the overall surface residence time on stiff hydrogels indicates a preference to stiffer materials. This behavior could have direct implications in the colonization of stiff polymeric medical devices, like catheters. Alternatively, insights into the strength of non-specific bacteria-surface interactions can be used as a design parameter in microfluidic device applications including cell sorting.

One avenue of future work concerns the separation of bacteria populations without the use of expensive targeted antibodies. The work conducted thus far has shown a marked increase in surface interaction for a gram-positive bacterium, *S. aureus*. Further study into the dynamic interaction of gram-negative bacteria and other microbes (yeast, fungi, etc) could unlock a new mechanism for microbial separation. For example, understanding how other clinically relevant bacterial species responds to hydrogel stiffness could enable the design of non-adhesive point-of-care devices that could detect pathogens by their affinity to surfaces with differences stiffness. Once bacteria adhere to the surface of a device, the functionality of the surface is comprised. Thus, point-of-care devices are designed for single use applications. However, with a sufficient residence time and complementary signaling system, a device could be designed that could respond to dynamically engaged bacteria without the need for permanent retention. This potentially creates an opportunity for a cost-saving reusable point-of-care device.

One such mechanism to separate bacterial populations is motility. Preliminary work from an ongoing collaboration between the Schiffman and Santore research groups, demonstrates that highly motile bacteria experience increased surface interaction that non-

motile. Additionally, motile bacteria display a tendency to swim against the direction of flow. This behavioral characteristic could be utilized in the channel design of a microfluidic device, in which periphery low-shear channels could be designed to extend from a central region of greater shear flow. With the correct orientation of these periphery channels, surface-engaged motile bacteria could be selectively drawn away from a mixed population of cells. Understanding the role that surface motility has on surface engagement could help design devices that separate out currently undetected non-motile bacterial pathogens involved in medical device infections.

Another avenue of research harnessing the macro-fluidic dynamic adhesion methodology used in this study, would be to investigate alternative anti-adhesive substrates. Residence time is a robust parameter that encompasses the surface interactions of any colloid to a surface, not just bacteria. Thus, information regarding the antifouling behavior of surfaces with other species of interest could be performed alone or in sequence. In this manner promising fouling-resistant material platforms, such as zwitterionic polymers, can be first challenged with serum proteins before exposure to bacteria to more accurately simulate the fluidized conditions within the human body. Our current work has established standards for the dynamic interaction of *S. aureus* and silica particles on two well understood material platforms, PEG hydrogels and brushes. PEG remains the gold-standard biomaterial for many applications, thus PEG must serve as a benchmark for future studies into antifouling materials both against biological and synthetic foulants.

CHAPTER 6

ANTIFOULING POLYMER ZWITTERION COATINGS

Adapted from:

(1). Chang, C.-C.; Kolewe, K. W.; Li, Y.; Kosif, I.; Freeman, B. D.; Carter, K. R.; Schiffman, J. D.; Emrick, T. Underwater Superoleophobic Surfaces Prepared from Polymer Zwitterion/Dopamine Composite Coatings. *Adv. Mater. Interfaces* **2016**, *3*, 1500521.

(2). Kolewe, K. W.[‡]; Dobosz, K. M.[‡]; Rieger K. A.; Chang, C.-C.; Emrick T.; Schiffman, J. D. Antifouling Electrospun Nanofiber Mats Functionalized with Polymer Zwitterions. *ACS Appl. Mater. Interfaces* **2016**, *8* (41), 27585-27593.

6.1 Summary

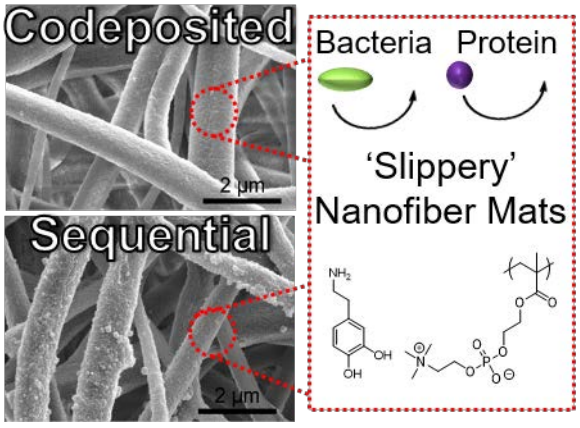

Figure 34: Composite coatings of pMPC/PDA are a scalable antifouling coating platform.

Surface hydration is a key component to the design of antifouling surfaces. The incorporation of hydrophilic polymers on surfaces promotes the retention of water and subsequently reduces the interaction of fouling species through the formation of a

hydration barrier. Although there are numerous mechanism to graft hydrophilic polymers to surfaces, these approaches are material specific and require tailored chemistry for use on different surfaces. Mussel-inspired adhesives based on dopamine can coat a multitude of surfaces, thus hold potential as a universal solution to surface-modification. Here, a novel composite coating is described that harnesses the adhesive versatility of mussel adhesion, polydopamine (PDA), and the fouling resistance of polymer zwitterions, poly(methcaryloyloxylethyl phosphorylcholine) (pMPC). Two scalable methods yielded conformal coatings on planar surfaces and cellulose nanofibers i) a two-step sequential deposition featuring dopamine polymerization followed by the physioadsorption of pMPC, and (ii) a one-step codeposition of PDA with pMPC. The resulting super-hydrophilic coatings of sequential and codeposited pMPC/PDA demonstrated excellent fouling resistance when challenged with proteins; however significant differences in resistance to *E. coli* and *S. aureus* adhesion. This chapter highlights two coatings with comparable chemical composition and demonstrates

6.2 Introduction

6.2.1 Zwitterion Immobilization

The fouling-resistance of zwitterionic polymers was previously discussed in Chapter 1.2.2.1.2. Due to the growing interest in these polymers for antifouling applications, a variety techniques have been used to immobilize zwitterions on surfaces including; layer-by-layer assembly,[160] surface-initiated polymerization,[161–163] solution casting,[164,165] self-assembled monolayers,[166] and brushes.[62] Although the resulting surface for each technique results in fouling-resistant surfaces, these approaches are either

substrate specific or require pretreatment to facilitate zwitterion retention. Therefore, a platform that can immobilize zwitterions with substrate interchangeability, would be highly desirable for antifouling and any other application using zwitterionic polymers.

6.2.2 Polydopamine

Drawing inspiration from the incredible adhesive versatility of mussels to virtually all organic and inorganic surfaces, Messersmith *et al*.[167] developed a universal surface modification, polydopamine (PDA). Mussels adhere to surfaces through a combination of secreted proteins, catechol containing 3,4-dihydroxy-L-phenylalanine (DOPA) and amine containing lysine amino acids. Dopamine (3,4-dihydroxyphenylethylamine), (Figure 34A) contains both functionalities and in a basic aqueous environment auto-oxides to form thin polymer film known as polydopamine. Although there are conflicting proposed structures of PDA, an extensive study by Liebscher *et al*. elucidated a structure composed of indole moieties covalently linked through C-C bonds between their benzene rings, Figure 34B.[168] The catechol and quinone groups in PDA enable a host of secondary chemical reactions, facilitating the formation of functional coatings on any surface.[169,170]

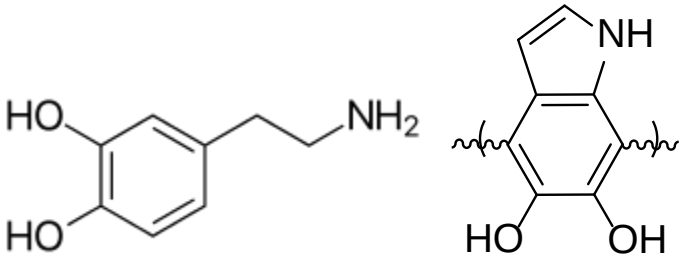

Figure 35: Structure of (A) dopamine and (B) polydopamine, the product of dopamine oxidation polymerization.

Since its discovery PDA coatings have been applied to a wide variety of materials consisting of various chemical compositions and physical structures. Due to the oxidative

mechanism of dopamine polymerization, PDA films are decorated with spherical aggregates, the size of which are sensitive to standard processing variables including: dopamine concentration, pH, temperature, and buffer composition.[170,171] Additionally, the melanin-like structure of PDA presents a brown color that starkly contrasts the white powder of unreacted dopamine, providing a simple indicator for successful coating deposition. Due to its ability to polymerize on any surface, the antifouling performance of PDA has been investigated in a variety of settings. On membranes for example, PDA coated surfaces display excellent resistance to protein adsorption following short exposure to protein solutions.[172] However, given sufficient time microbes readily colonize polydopamine likely due to lower surface hydration than what is typically associated antifouling hydrophilic polymers.[173]

6.2.3 Electrospinning Zwitterionic Nanofibers

Electrospinning is a scalable and versatile technique for producing highly porous materials that exhibit outstanding structure-property relationships.[174,175] The produced mats are comprised of nano- and macroscale diameter fibers, which have microscale interstitial spacing, a large surface-to-volume ratio, high specific surface area, and porosity values greater than >80%.[176,177] By coupling their unique structural characteristics with an optimized surface chemistry, electrospun fiber mats are promising for applications ranging from tissue engineering,[178,179] to wearable electronics,[180] to water purification technologies.[181,182] Unfortunately, these materials are susceptible to biofouling, which can cause detrimental complications, such as, reduced efficiency and selectivity of membranes[183] and infections from contaminated medical devices.[13]

Electrospinning with zwitterions has been limited to sulfobetaine derivatives and the as-spun fibers were observed to lack chemical and/or mechanical integrity.[184] Brown *et al*.[185] demonstrated that zwitterionic copolymers containing sulfobetaine methacrylate in a poly(*n*-butyl acrylate) matrix could be electrospun into fibers of ~100 nm diameter. Due to the low solution concentration and viscosity, fiber spinning was hypothesized to result from zwitterion aggregation rather than chain entanglement. In contrast, it was demonstrated that a high solution concentration of high molecular weight poly(sulfobetaine methacrylate) favored smooth fiber formation with diameters ranging from 200 to 800 nm.[186,187] In a subsequent report, Lalani and Liu[188] used a three-step process, namely, polymerization, electrospinning, and photo-crosslinking, to form water-stable Ag^+ impregnated poly(sulfobetaine methacrylate) nanofiber mats that were antifouling and antibacterial. An additional study incorporated sulfobetaine groups into small diameter tissue engineered vascular grafts by spinning biodegradable, elastic polyurethanes containing sulfobetaine from a polycaprolactone-diol:sulfobetaine-diol mixture reacted with diisocyanatobutane and chain-extended with putrescine.[189] Cyanoacrylate monomers (i.e., super glue), have been electrospun alone[190] and in combination with other acrylic polymers via air-flow assistance[191] and via the rapid polymerization of the ethyl-2-cyanoacrylate monomer in the presence of moisture.[192] While preliminary success at spinning zwitterion-containing solutions has been demonstrated, the solution and apparatus requirements, i.e., polymer concentration, solvent system, applied voltage, etc., must be re-optimized in each case. Additionally, after optimization, there is no guarantee that the zwitterion are present at the surface of the nanofiber mats for maximizing non-fouling effects. We suggest that a facile, effective nanofiber mat surface modification, which

potentially could be employed for any polymer zwitterion, would represent a cost-effective approach towards controlling fouling while retaining the chemical stability and mechanical properties of the underlying nanofiber mat.[193–195]

6.3 Methods

6.3.1 Materials

All compounds were used as received. Cellulose acetate (M_w = 30 kDa), dopamine hydrochloride, M9 minimal salts (M9 media), D-(+)-glucose, calcium chloride (anhydrous), phosphate buffered saline (PBS, 1 × sterile biograde), Luria-Bertani broth (LB) tryptic soy broth (TSB), bovine serum albumin (BSA, M_w = ~66 kDa), and sodium chloride (NaCl) were obtained from Sigma-Aldrich (St. Louis, MO). Tris(hydroxymethyl)aminomethane (Tris), ethanol, and sodium hydroxide (NaOH) were obtained from Fisher Scientific (Fair Lawn, NJ). Deionized (DI) water was obtained from a Barnstead Nanopure Infinity water purification system (Thermo Fisher Scientific, Waltham, MA).

6.3.2 Cellulose Fiber Mat Fabrication

A 15 w/v% solution of cellulose acetate in acetone was mixed for 24 hr at 20 rpm using an Arma-Rotator A-1 (Bethesda, MA).[196] The solution was loaded into a 5 mL Luer-Lock tip syringe capped with a Precision Glide 18-gauge needle (Becton, Dickinson & Co. Franklin Lakes, NJ), which was secured to a PHD Ultra syringe pump (Harvard Apparatus, Plymouth Meeting, PA). Alligator clips were used to connect the positive anode of a high-voltage supply (Gamma High Voltage Research Inc., Ormond Beach, FL) to the needle

and the negative anode to a copper plate wrapped in aluminum foil. A constant feed rate of 3 mL/hr, an applied voltage of 25 kV, and a separation distance of 10 cm were used to spin cellulose acetate. The assembled electrospinning apparatus was housed in an environmental chamber (CleaTech, Santa Ana, CA) with a desiccant unit (Drierite, Xenia, OH) to maintain a temperature of 22 ± 1 ºC and a relative humidity of 55%. All nanofiber mats used in this study were electrospun for 1 hr. To convert the cellulose acetate nanofibers to cellulose nanofibers, the mats were sandwiched between sheets of Teflon and thermally treated at 208 °C for 1 hr before being submerged in a 0.1 M NaOH 4:1 v/v of water/ethanol solution for 24 hr. The cellulose nanofiber mats were placed in a desiccator for 24 hr at room temperature (23 °C) before functionalization.

6.3.3 Preparation of pMPC/PDA Functionalized Planar Films and Nanofiber Mats

PMPC, Mn: 30 kDa, was prepared according to a previously published method.[173,197] The fabricated cellulose nanofiber mats and cleaned planar surfaces were surface-functionalized using one of three following techniques: (i) only polydopamine (PDA), (ii) a sequential process using PDA then polyPMC, or (iii) a simultaneous codeposition of PDA and PMPC. First, the base platform cellulose nanofiber mats were punched into circles with 2.54 cm (1 inch) diameters using a Spearhead® 130 Power Punch MAXiset (Fluid Sealing Services, Wausau, WI) and placed in a 6-well plate with 5 mL of the desired functionalization solution. For PDA functionalization, the cellulose nanofiber mats were submerged in a freshly prepared Tris buffer (10 mM, pH 8.5) containing 2 mg/mL PDA for 6 hr.[167] For the sequentially functionalized nanofibers, the mats were submerged in the described PDA solution, then submerged in Tris buffer containing 2

mg/mL pMPC for 24 hr.[173] Codeposition of PDA/pMPC onto the nanofiber mats was achieved by submerging the mats in Tris buffer containing 2 mg/mL of PDA and 2 mg/mL pMPC for 6 hr.[173] After each treatment, the mats were rinsed 3× with DI water. Throughout this manuscript, we will refer to the three sample types as PDA, pMPC/PDA sequential, and pMPC/PDA codeposited.

6.3.4 Characterization of pMPC/PDA Functionalized Planar Films and Nanofiber Mats

Micrographs of cellulose nanofiber mats with and without functionalization (PDA, sequential, and codeposited) were acquired using an FEI-Magellan 400 scanning electron microscope (SEM, Hillsboro, OR). A Cressington 208 HR sputter coater (Cressigton Scientific Instruments, Watford, England) was used to coat samples with ~5 nm of platinum. The fiber diameter and particle diameter distribution were determined by measuring 50 random fibers or 100 random particles from 5 micrographs using *Image J1.45* software (National Institutes of Health, Bethesda, MD). A PerkinElmer Spectrum 100 Fourier transform infrared spectrometer (FTIR, Waltham, MA) confirmed the regeneration of cellulose acetate nanofiber mats to cellulose after the alkaline treatment. High resolution x-ray photoelectron spectroscopy (XPS, Physical Electronics Quantum 2000 Microprobe, Physical Electronics Inc., Chanhassen, MN) scans were obtained to determine the chemical composition using the known sensitivity factors. A monochromatic Al X-rays at 50 W was used with a spot area of 200 μm and the take-off angle was set to 45˚. Contact angle measurements were acquired using a home-built apparatus equipped with a Nikon D5100 digital camera with a 60 mm lens and 68 mm extension tube (Nikon, Melville, NY).[198] Data represents the average of five drops of glycerol (4 μL) measured on

two different cellulose, PDA, pMPC/PDA sequential, and pMPC/PDA codeposited nanofiber mats.

6.3.5 Bacterial Fouling of pMPC/PDA Functionalized Planar Films and Nanofiber Mats

The model gram-negative and gram-positive microorganisms were *Escherichia coli K12* MG1655 (*E. coli*) and *Staphylococcus aureus* SH1000 (*S. aureus*), respectively. *E. coli* purchased from DSMZ (Leibniz-Institut, Germany) contained a GFP plasmid while the *S. aureus* contained a high-efficiency pCM29 sGFP plasmid.[107] Free-standing cellulose nanofiber mats with and without functionalization (PDA, sequential, and codeposition), were punched into circles with 2.54 cm diameters and placed at the base of 6-well plates (Fisher Scientific) to which 5 mL of M9 media with 100 μg/mL ampicillin or 10 μg/mL chloramphenicol was added for *E. coli* or *S. aureus* (1.00×10^8 cells/mL), respectively. Planar films of pMPC/PDA and PDA were run in parallel with glass controls. The growth media in each well was inoculated with an overnight culture of *E. coli* or *S. aureus*, which were washed and resuspended in M9 media,[123,124] then placed in an incubator at 37 °C for 24 hr. Nanofiber mats and planar films with attached bacteria were removed from the 6-well plates and washed with PBS to remove loosely adherent bacteria. *E. coli* and *S. aureus* attachment was evaluated using an adhesion assay[72,110] that monitored the bacteria colony coverage within a 366,964 μm^2 area using a Zeiss Microscope Axio Imager A2M (20× magnification, Thornwood, NY). The particle analysis function in *ImageJ* was used to calculate the bacteria colony area coverage (%) by analyzing 10–15 randomly acquired images over three parallel replicates. Significant differences between samples were

determined with an unpaired student *t*-test. Significance ($p \leq 0.001$) is denoted in graphs by two (**) asterisks.

6.4 Results and Discussion

6.4.1 Morphological Characteristics of pMPC/PDA Functionalized Nanofiber Mats.

Cellulose nanofiber mats were successfully prepared by alkaline treatment of the electrospun cellulose acetate nanofiber mats, Figure 35. FTIR spectra spectra of the as-spun cellulose acetate and the regenerated cellulose nanofiber mats confirm the disappearance of the 1750 cm^{-1} peak indicates that the acetate groups have been replaced with hydroxyl groups supporting the regeneration of cellulose. Predominantly, the cellulose nanofiber mats displayed a cylindrical morphology[199,200] with an average fiber diameter of 1.08 ± 0.46 μm. The cellulose nanofiber mats served as the base substrate for the three surface functionalizations examined. Previous reports concluded that the thickness of PDA coatings can be reliably controlled by adjusting dopamine concentration, pH, temperature, buffer, and reaction time.[170,171,173,201] Since this study aims to explore the presentation of the zwitterionic moieties, we chose to use a consistent PDA coating condition that previously resulted in thin (~25 nm) underwater superoleophobic and antifouling coatings on silicon wafers.[173] As expected, stable coatings did not form on the cellulose nanofibers with pMPC alone.

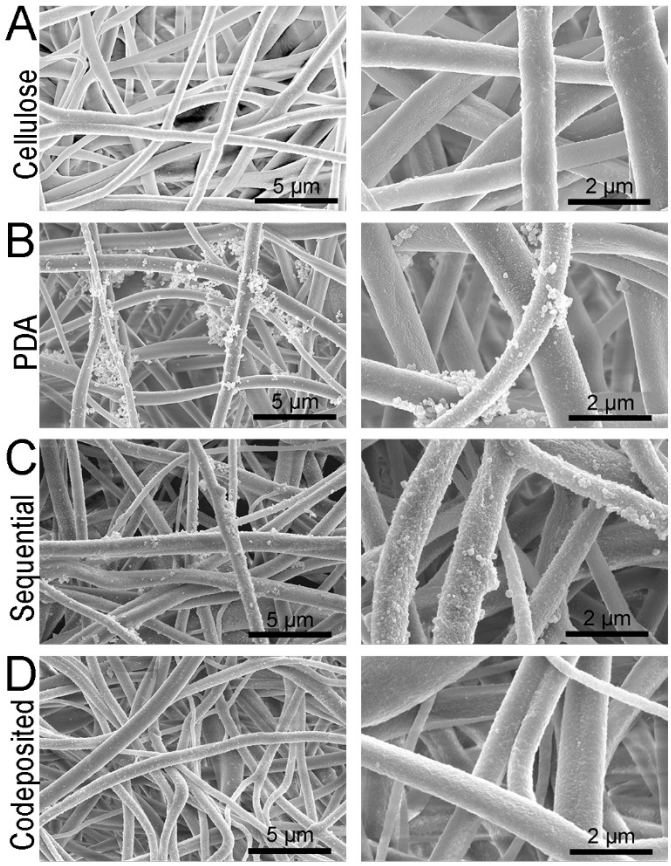

Figure 36: (A) SEM micrographs of the cellulose nanofiber mats used as the base materials for this study. The morphology of (B) PDA and (C, D) pMPC/PDA (sequential and codeposited) functionalized nanofiber mats are also displayed.

Visually, the as-prepared white cellulose nanofiber mats changed to brown after functionalization with PDA, pMPC/PDA sequential, and pMPC/PDA codeposition, consistent with previous reports.[202] Cellulose nanofiber mats that were coated with PDA exhibited particulate aggregates throughout the nanofiber matrix consistent with previous reports of PDA coatings on smooth surfaces.[170,171] The PDA particles within the aggregates had an average diameter of 0.73 ± 0.9 µm, Figure 36. Inspection of the SEM micrographs (Figure 1) showed that the pMPC/PDA sequential deposition resulted in fewer large aggregates and decreased average particle size on the fiber surface (0.32 ± 0.3 µm). Notably, particle aggregation was nearly eliminated on the cellulose nanofiber mats that

were functionalized using the one-step pMPC/PDA codeposition method. Here, the surface of the individual nanofibers largely appeared smooth with average particle diameter of 0.14 ± 0.08 μm. Sundaram *et al.*[203] previously reported a similar finding, in the presence of a hydrophilic polymer, catechol-terminated poly(carboxybetaine methacrylate), reduced PDA aggregate size on microporous membranes from 3 μm to <100 nm. Overall, the average fiber diameter of the cellulose nanofiber mats functionalized with PDA, pMPC/PDA sequential, and pMPC/PDA codeposition, remained equivalent to the base cellulose nanofiber mats.

The effect of this surface functionalization on the hydrophilicity of the nanofiber mat was determined by static contact angle measurements using glycerol. Contact angles were determined to be statistically equivalent for all mats: 36.8 ± 6.7° for the unmodified cellulose nanofiber mats, 36.5 ± 6.2° for PDA, 34.0 ± 6.8° for pMPC/PDA sequential, and 31.1 ± 5.3° for pMPC/PDA codeposition. As expected, a hydrophilic contact angle was acquired on all nanofiber mats.

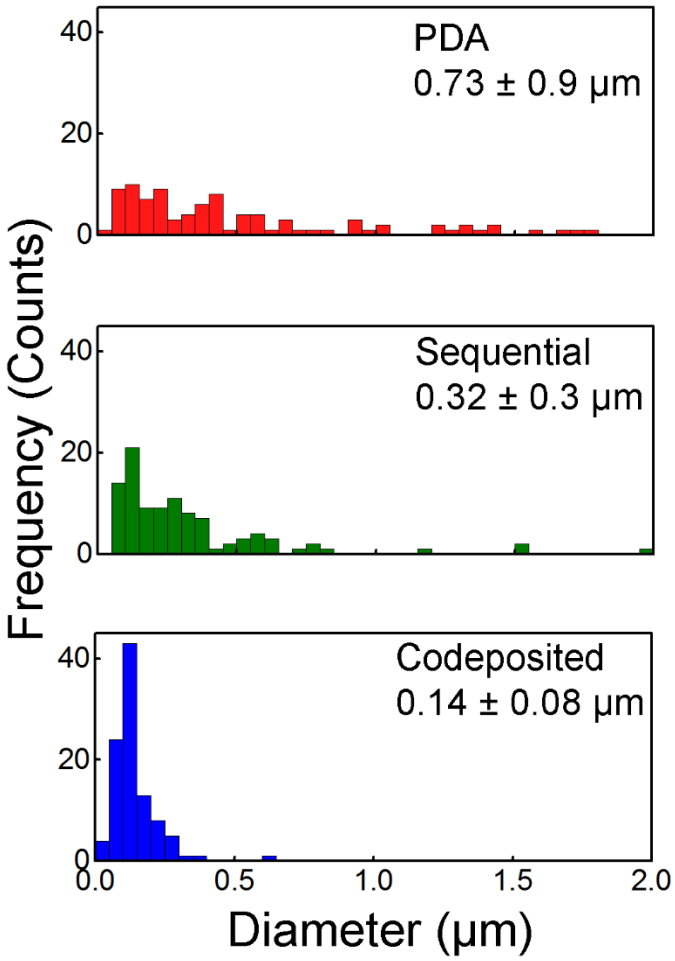

Figure 37: Distribution of particle aggregate size on the PDA and pMPC/PDA (sequential and codeposited) functionalized nanofiber surface are displayed along with their average size and standard deviation (n = 100).

6.4.2 Chemical Characteristics of pMPC/PDA Functionalized Nanofiber Mats.

Representative survey scans and high-resolution XPS spectra were acquired to determine the surface chemical composition of the cellulose, PDA and pMPC/PDA nanofiber mats, Figure 37 Nitrogen signals were expectedly absent from the base cellulose nanofiber mats, while the PDA functionalized fibers exhibited a nitrogen signal at 399 eV, confirming successful PDA deposition.[170] Cellulose nanofiber mats functionalized with both PDA and pMPC, either by sequential or codeposition method, were found to have a nearly identical surface composition of P_{2p} and N_{1s}, thus confirming the presence of pMPC

after their treatments (Figure 37 (B, C)). Sequential and codeposited nanofiber mats displayed a characteristic phosphorus P_{2p} signal at 132.4 eV due to the presence of pMPC, which was absent from the PDA functionalized materials. The phosphorus-to-carbon (P/C) ratio of the sequential and codeposited mats were 0.016 and 0.013, respectively, corresponding to 6.4 and 8.2 dopamine molecules for every PC group. The nitrogen N_{1s} region of the XPS spectra revealed a peak at 399 eV within the PDA functionalized nanofiber mats, indicative of primary amines. With the addition of pMPC, a peak appears at 401 eV indicating the presence of quaternary amine that is unique to pMPC. The spectra of the pMPC/PDA sequential and codeposition nanofiber mats presented a 0.32 ± 0.1 and 0.36 ± 0.1 ratio of the quaternary amine to primary amine nitrogens.

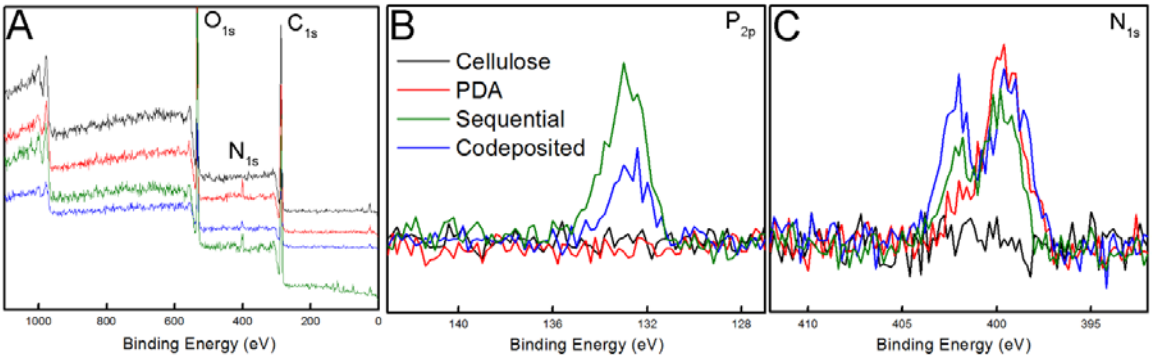

Figure 38: XPS spectra of cellulose, PDA, and pMPC/PDA (sequential and codeposited) functionalized nanofiber mats including (A) survey scans and (B) high resolution scans of P2p and (C) N1s as a function of electron binding energy.

6.4.3 Bacterial Adhesion on Planar Films

PDA and pMPC/PDA coated glass slides were evaluated for their ability to resist the adhesion of *E. coli*. Samples were incubated for short (2 hr) and long (24 hr) durations in M9 minimal growth media to evaluate the kinetics of *E. coli* adhesion. As shown in Figure 38, both PDA and pMPC/PDA coated surfaces, after 2 hr incubation, showed significantly lower bacteria attachment relative to the glass control. *E. coli* attachment was

reduced by 65% for PDA coated surfaces, and 87% for pMPC/PDA modified surfaces. While surfaces modified with PDA only exhibited short-term resistance against *E. coli* adhesion, significant bacterial fouling was seen after 24 hr exposure, consistent with literature reports.[204] Additional reports showed PDA-modified membranes to cause a 75% reduction in *Pseudomonas aeruginosa* biofouling over a 2 hr period; nonetheless, significant fouling was observed over longer time frames when using non-disinfected bacteria-containing water.[205,206] In our case, *E. coli* attachment was not reduced by a statistically significant amount (~13%) for PDA modified surfaces relative to the glass control after 24 hr. However, pMPC/PDA modified surfaces exhibited large reductions, >85%, in *E. coli* attachment relative to PDA-modified surfaces and glass controls, a remarkable improvement in bacterial fouling resistance.

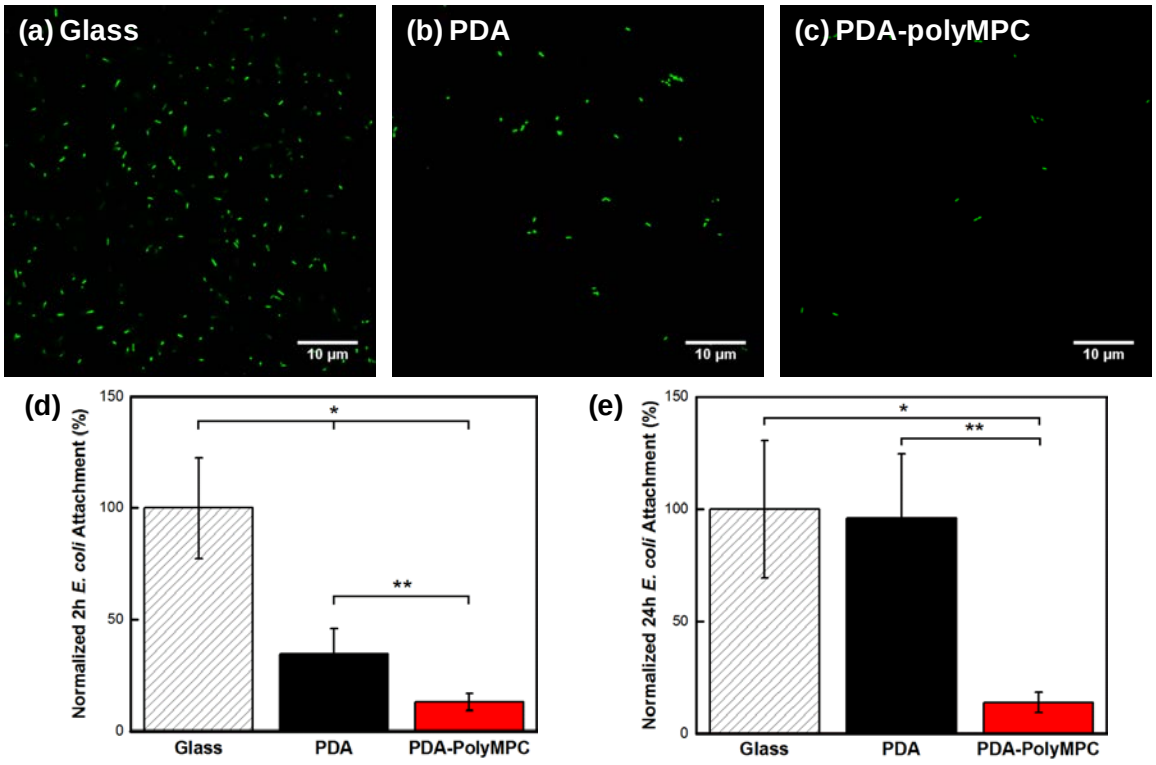

Figure 39: Micrographs of *E. coli* incubated for 2 hr on (a) glass control, (b) PDA (2 mg/mL dopamine) coated glass, and (c) PMPC/PDA (2 mg/mL dopamine and 5 mg/mL pMPC) coated glass. Normalized *E. coli* attachment after (d) 2 hr and (e) 24 hr on unmodified glass, PDA- and pMPC-PDA-modified glass slides. Values were normalized to percent coverage on the unmodified glass control. Statistical significance was evaluated by one-way analysis of variance (ANOVA) and the Bonferroni post test. */** denotes statistically significant p-value of 0.001 with respect to unmodified glass

The enhancement in antifouling properties is due to an enhancement in surface hydration, which is anticipated to reduce non-specific adsorption of proteins secreted by bacteria, thus providing longer-term anti-fouling properties than seen with PDA-only modified surfaces. This effect presumably renders pMPC/PDA coated surfaces too 'slippery' for *E. coli* adherence. Of the few reports on pMPC resistance to bacterial fouling, Ishihara and coworkers noted a large reduction in *E. coli* attachment on pMPC grafted poly(ether ether ketone) after 1 hr, though longer incubation times would have provided a more comprehensive analysis.[207] Significantly, the pMPC/PDA coating maintained its

effectiveness against *E. coli* adhesion even after 24 hr incubation, thus opening opportunities for this composite coating approach in practical applications and systems.

6.4.4 Bacterial Antifouling Activity of pMPC/PDA Functionalized Nanofiber Mats

The bacterial antifouling capability of the cellulose and pMPC/PDA functionalized nanofiber mats was evaluated after 24 hr using two model microbes, the Gram-negative *E. coli* and the Gram-positive *S. aureus*. The extent of fouling from both microbes used in this study is observed visually by the representative florescence micrographs provided in Figure 39. Quantitatively, the colony area coverage of both bacterial species on cellulose nanofiber mats were statistically the same, 6.1 ± 0.5% and 6.3 ± 0.4% for *S. aureus* and *E. coli*, respectively. When cellulose nanofiber mats were functionalized with PDA, the amount of fouling by *S. aureus* increased to 7.5 ± 1.6% over the control cellulose nanofiber mats, while *E. coli* was unchanged, 6.3 ± 0.2%. Although PDA resists protein adsorption over short time periods, prolonged exposure leads to surface conditioning and ultimately bacterial fouling.[205] As demonstrated here, antifouling performance is improved markedly by incorporation of zwitterionic polymer.

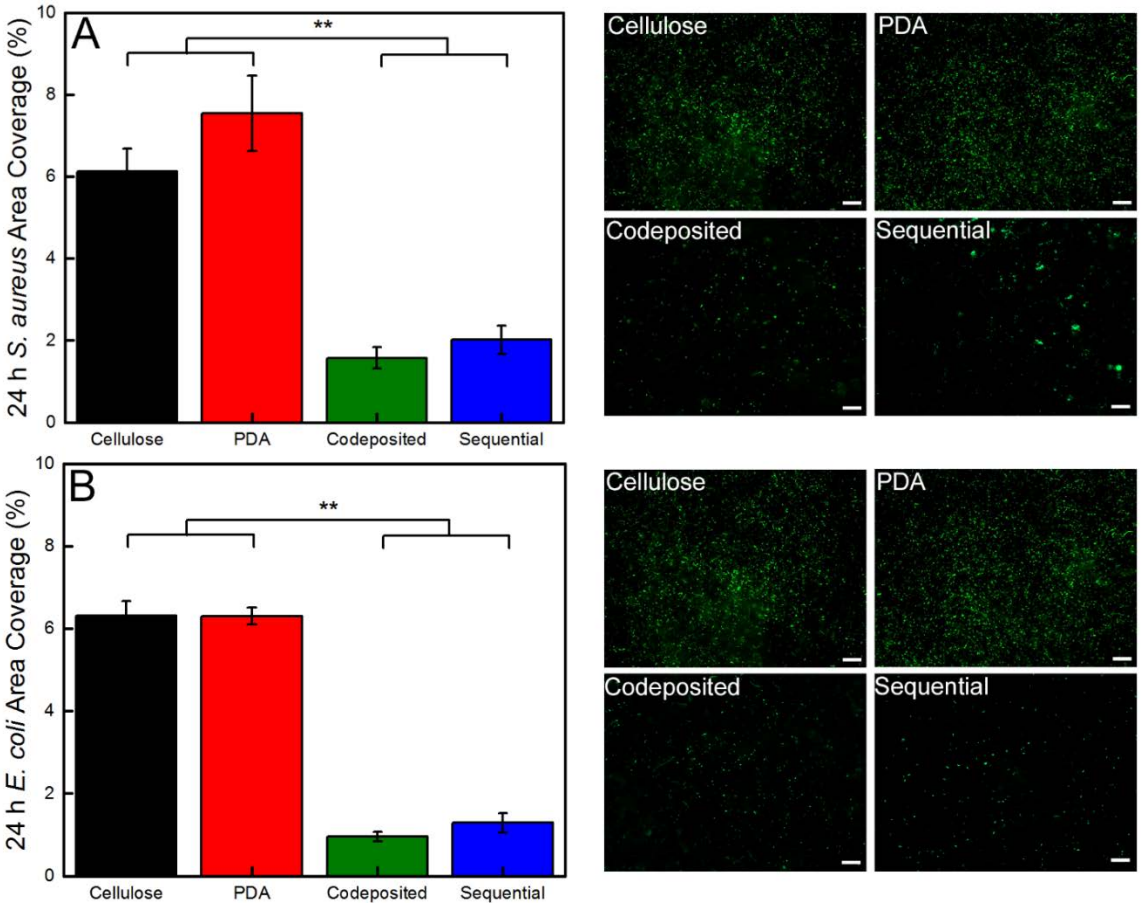

Figure 40: Quantification of the area coverage of (A) S. aureus and (B) E. coli on the cellulose, PDA, and pMPC/PDA (sequential and codeposited) functionalized nanofiber mats. Representative florescent micrographs (366964 µm2) are also provided and a 50 µm scale bar is displayed. Error bars denote standard error, and two asterisks (**) denote $P \leq 0.001$ significance between samples.

The pMPC/PDA sequential and codeposited coatings significantly reduced bacterial fouling of the nanofiber mats compared to PDA and cellulose controls. Sequential nanofiber mats reduced *S. aureus* fouling by 73% (2.0 ± 0.3%) relative to PDA and a statistically significant, 80% reduction in *E. coli* fouling (1.3 ± 0.2%**)**. Codeposition generates a uniform coating that improved biofouling resistance by 79% and 85% compared to PDA, for *S. aureus (*1.6 ± 0.3%) and *E. coli* (1.0 ± 0.1%), respectively. The 85% fouling reduction achieved with the pMPC/PDA coatings on high surface area nanofiber mats, is notably consistent to our previous demonstration on glass surfaces,[173]

which is especially impressive considering the documented ability of 3D-scaffolds to readily adsorb bacteria.[196] These results indicate the presence of pMPC on the surface of nanofibers significantly improves resistance to both protein and bacterial fouling, with some dependence on the deposition method. The adhesion of both bacterial species was ~25% greater on the pMPC/PDA sequential nanofiber mats indicating the influence of a secondary effect, likely, surface morphology. The larger aggregates on the sequential nanofiber mats either promoted bacterial adhesion and/or the smoother surface of the codeposited coating prevented adhesion.

6.5 Conclusion and Future Work

In these studies, we have described the use of pMPC as an antifouling coating on planar glass substrates and electrospun cellulose nanofiber mats using both a sequential and codeposited method featuring PDA. The codeposition of pMPC and PDA harnesses non-covalent interactions of the between catechol containing polymers and PC groups. Further, physioadsorption of pMPC onto PDA surfaces through sequential polymerization, emphasized the versatility of zwitterion immobilization through non-covalent interactions. Composite pMPC/PDA coatings demonstrated increased stability in solutions with pH values ranging from 4-10 compared to PDA-only coatings. The thickness of codeposited composite coatings was tuned by the polymer concentration of pMPC while the thickness of sequential coatings was dependent on the thickness of the original PDA coating.

We further investigated the ability of these mats to resist biofouling by challenging the planar glass surfaces with *E. coli* for 2 and 24 hr and the cellulose fiber mats with *E. coli* and *S. aureus* for 24 hr. The pMPC/PDA composite coatings are much more

hydrophilic than PDA coatings, and thus less prone to bacterial fouling; exhibiting a nearly 10× reduction in *E. coli* attachment relative to PDA coated surfaces after 24 hr, whereas PDA coated surfaces exhibited significant bacterial fouling that was statistically equivalent to the glass control. Both functionalization methods showed significant improvement in bacteria fouling resistance on nanofiber mats, yet codeposition performed noticeably better against both bacterial species (85% for *E. coli* and 79% for *S. aureus*). This may be due, at least in part to the morphology of the coating. Larger aggregates on the sequential coatings could provide adhesion points for bacterial attachment, but the exact mechanism is not yet understood. Nonetheless, this work indicates the utility of PDA as a robust bioinspired "glue" to maximize the efficiency of codeposited antifouling zwitterions, which we anticipate will be broadly applicable to efficiently limiting fouling on biomedical implants and membranes used for separations.

There are a variety of possibilities for future work stemming from this work. If additional pMPC can be physioadsorbed to a composite surface formed through codeposition of pMPC/PDA, the antifouling performance of the surface could be further improved. Although leeching would have a larger impact on physioadorbed coatings due to the nature of this interaction, regeneration would help alleviate any loss in performance. This duel-action approach towards surface modification could increase the performance of pMPC/PDA surfaces for long term usage.

The use of PDA as a platform for non-covalent interactions could be useful for applications that utilize hydrophobic materials yet require an adherent hydrophilic surface, such as solar cell fabrication, battery design, or protein crystallography.[208,209] Incorporation of pMPC would further increase the hydrophilicity of the modified surface; however,

secondary effects of the zwitterion could influence the overall performance. Further studies to elucidate the non-specific mechanism of pMPC inclusions would provide valuable insights into the critical functional groups that can be manipulated to widen the number of polymers that can be incorporated. This information could be used to tailor next generation fouling-resistant zwitterionic polymers without sacrificing the performance of the desired application. Other phosphocholine-based zwitterions would be a starting point, but alternative zwitterionic chemistry (sulfobetaine and carboxybetaine) or functionalized PEG molecules would substantially broaden the impact of composite PDA-mediated surface modification. Additionally, PDA coatings with zwitterionic polymers could be designed for use as sensors. As the most important features of PDA-mediated zwitterion immobilization are the ability to coat any surface and the non-specific mechanism of zwitterion incorporation, these features could be exploited to develop surface-based sensors by manipulating the end groups of the zwitterion. Although modifying the structure of the zwitterion could reduce overall fouling-resistance of the composite coating, resisting any non-specific biomacromolecule adsorption or microbial adhesion would enhance the sensitivity of the device.

CHAPTER 7

INTEGRATION OF POLYDOPAMINE INTO FOULING-RESISTANT HYDROGELS

Adapted from: Kolewe, K. W.; Emrick, T.; Nonnenmann, S. S.; Schiffman, S. D. Integration of Polydopamine into Fouling-resistant Hydrogels. In preparation

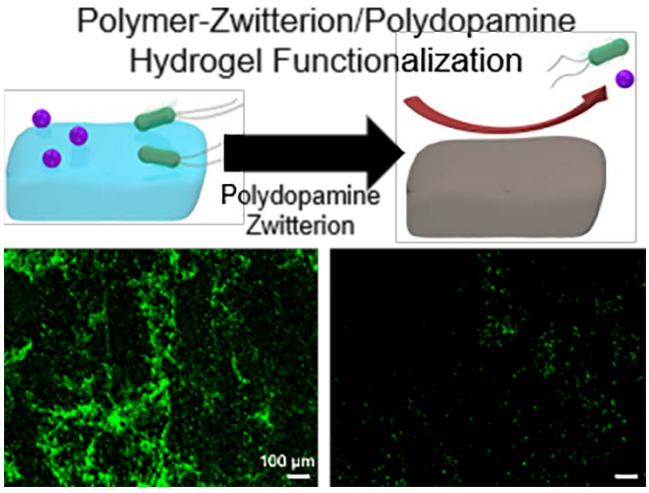

Figure 41: The resistance of hydrogels to protein adsorption and bacterial adhesion can be significantly improved through modification with pMPC/PDA.

7.1 Summary

Biofilm-associated infections stemming from medical devices are increasingly challenging to treat due to the spread of antibiotic resistance. In this study, we present a platform to synergistically enhance the antifouling performance of covalently crosslinked poly(ethylene glycol) (PEG) and physically crosslinked agar hydrogels by incorporation of the fouling-resistant polymer zwitterion, poly(2-methacryloyloxyethyl phosphorylcholine) (pMPC). Dopamine polymerization was initiated while swelling the hydrogels, which provided dopamine and pMPC an osmotic driving force into the hydrogel interior. PEG and agar hydrogels were synthesized over a broad range of storage moduli (1.7-1300 kPa), which remained statistically equivalent after being functionalized with pMPC and

polydopamine (PDA). When challenged with fibrinogen, a model blood-clotting protein, pMPC/PDA PEG and agar hydrogels displayed a >90% reduction in protein adsorption compared to hydrogel controls. Further, a greater than order-of-magnitude reduction in *Escherichia coli* and *Staphylococcus aureus* adherence to the pMPC/PDA PEG and agar hydrogels, was observed relative to the control hydrogels. This study demonstrates a versatile platform to enhance the fouling resistance of hydrogels through a pMPC/PDA incorporation strategy that is independent of the chemical composition and network structure of the original hydrogel.

7.2 Introduction

As the work in previous chapter demonstrated, the incorporation of polymer zwitterions can significantly improve the fouling-resistance of a surface in a one- or two-step composite coating with PDA. However, the materials we used to optimize this coating, glass, silicon, and cellulose fibers are all non-porous, thus dopamine polymerizes as a thin surface coating that is unable to diffuse into the targeted surface. Hydrogels however, are highly porous and primarily composed of water. This enables diffusion of small molecules and some network structures allow diffusion of larger biomacromolecules like proteins. The inherent high-water content and permeability of hydrogels is highly desirable for many applications, but this makes functionalization more difficult. Thus, hydrogel modification is typically accomplished by modifying the properties of the polymer network prior to polymerization. This designer chemistry can be advantageous, but must be customized for each hydrogel formulation. Although a one-step modification platform would not be suitable for all hydrogel applications, it could be a useful tool to optimize the fouling-resistance of existing hydrogel chemistries for medical applications.

7.3 Materials and Methods

7.3.1 Materials

See Chapter 4.3.1 and Chapter 6.3.1 for details on the materials used in this study.

7.3.2 Fabrication of pMPC/PDA PEG and Agar Hydrogels

Unmodified PEG and agar hydrogels were prepared as described in Chapter 4.2.1. PMPC was synthesized as previously described.[173,197] The unmodified PEG and agar hydrogels were placed into 6-well polystyrene plates (Fisher Scientific) and immersed in 5 mL of Tris buffer (10 mM, pH 8.5) containing only PDA (2 mg/mL) or solutions containing both PDA (2 mg/mL) and pMPC (2 mg/mL) for 6 hr. All hydrogels were removed from the reaction solution and washed 3 times with DI water before being placed in a new 6-well plate at 23 °C with DI water until further testing. Throughout the results section, hydrogels are referred to as PEG and agar (if unmodified), PDA, or pMPC/PDA hydrogels.

7.3.3 Characterization PDA Diffusion in PEG Hydrogels

To develop a diffusion profile, hydrogels were fabricated in cylindryical molds to be 2 mm thick and 22 mm in diameter at polymer concentrations of 8.3 and 55 wt% PEG and 1 and 8.3 wt% agar. Following polymerization, hydrogels were swollen in 5 mL of Tris buffer containing 2 mg/mL dopamine. Following 1, 6, and 24 h of incubation, hydrogels were removed from solution and gentely rinsed with DI water and cut with a razor. The hydrogel's surface and cross-sections were photographed using a digital single lens reflex (DSLR, Nikon D5200) camera with an AF-S NIKKOR 18-35mm 1:3.5-5.6G

lens. The Red-Green-Blue (RGB) color values at the surface and center of hydrogel cross-sections was quantified using Adobe Photoshop CC. Representative images of 55 wt% PEG hydrogels are presented in Figure 42.

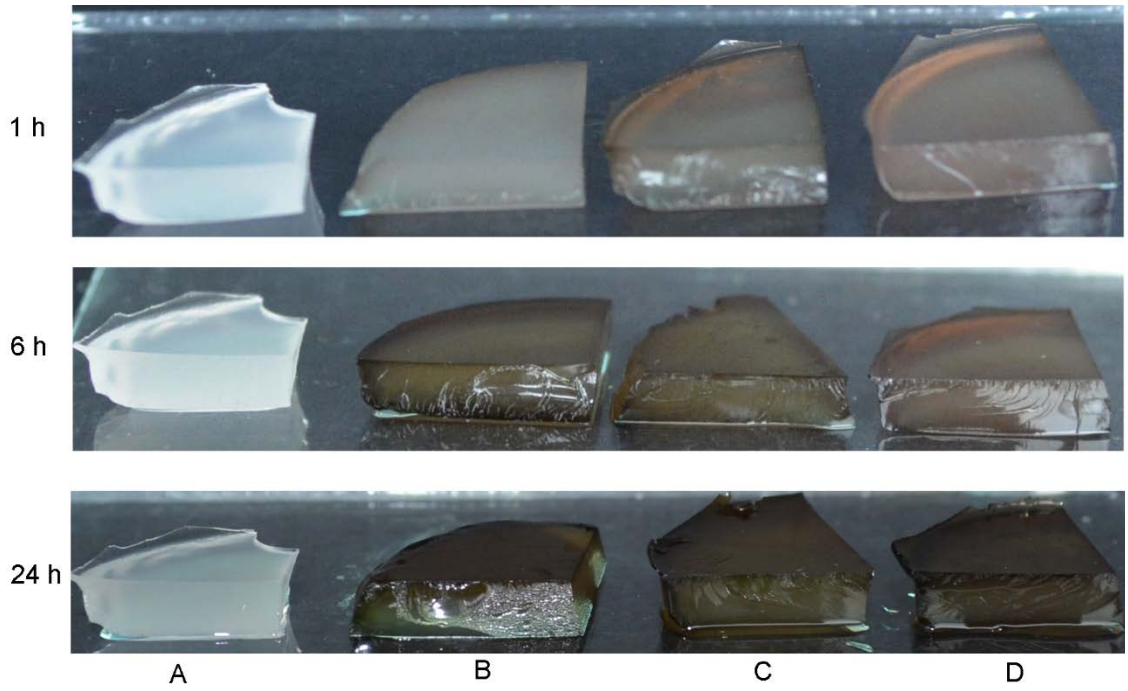

Figure 42: Representative images of the cross-sections 55 wt% PEG hydrogels are provided for unmodified controls (A) and following polymerization of PDA after 1, 6, and 24 hr. PDA was introduced at three distinct stages of hydrogel synthesis: (B) hydrogels swollen to thermodynamic equilibrium, (C) directly following UV polymerization, and (D) prior to hydrogel synthesis resulting in simultaneous hydrogel and PDA polymerization

7.3.4 Chemical Characterization of pMPC/PDA PEG and Agar Hydrogels

The chemical composition of unmodified, PDA, and pMPC/PDA PEG and agar hydrogels was determined using a Perkin-Elmer Spectrum 100 Fourier transform infrared spectrometer (FTIR, Waltham, MA). All spectra were taken in the spectral range of 4000−500 cm^{-1} by accumulation of 32 scans and with a resolution of 4 cm^{-1}. Scans were performed in duplicate on three replicates for each hydrogel. Equilibrium swelling experiments were performed to determine the volumetric swelling ratio, *Q*, of unmodified,

PDA, and pMPC/PDA PEG hydrogels. Unmodified PEG hydrogels were swollen in PBS for 24 hr at 23 °C until equilibrium swelling was achieved, then weighed to obtain their equilibrium swelling mass, M_S. These hydrogels were lyophilized (Labconco, FreeZone Plus 2.5 Liter Cascade Console Freeze-Dry System, Kansas City, MO) for 72 h then weighed to determine their dry mass, M_D. To quantify Q for PDA and pMPC/PDA hydrogels, the unmodified PEG hydrogels were weighed directly following polymerization to obtain the weight of the base PEG hydrogel. Following the 6 hr IPN polymerization, hydrogels were washed 3 times with DI water to remove unincorporated polymer and immersed in PBS for 48 hr then weighed to determine M_S. Hydrogels were then lyophilized and weighed to determine M_D. Four replicates were tested for each hydrogel. Q was calculated using the following equation:

Equation 5

$$Q = \frac{M_S}{M_D}$$

7.3.5 Mechanical and Morphological Characterization of pMPC/PDA PEG and Agar Hydrogels

Small amplitude oscillatory shear (SAOS) measurements were acquired on the PEG and agar hydrogels using a plate–plate geometry with a diameter of 20 mm and a gap of 1 mm (Kinexus Pro rheometer, Malvern Instruments, UK). Prepared hydrogels (circular 25 mm diameter × 1 mm deep) were loaded into the rheometer and trimmed to size using a razor blade. A strain amplitude sweep was performed to ensure that experiments were conducted within the linear viscoelastic region and a strain percent of 0.1% was selected. Oscillation frequency sweeps were conducted over an angular frequency domain 1.0 and 100 rad/s at 23 ºC.

The size of PDA aggregates on the surface of hydrogels was measured using atomic force microscopy (Cypher ES AFM, Asylum Research, Santa Barbara CA) equipped with a PerFusion attachment for complete sample immersion. Imaging in DI water at room temperature (~23 °C) was performed using TR800PSA tips (Olympus, Tokyo, Japan). Hydrogels were prepared on 15 mm glass coverslips and care was taken to ensure that the hydrogels remained hydrated throughout the entire AFM preparation and testing process.

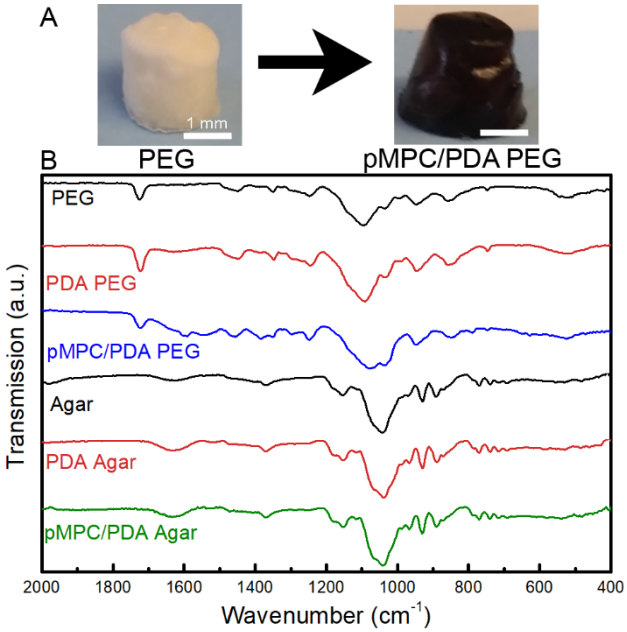

Figure 43: (A) Digital image displaying the color transition of PEG hydrogels following PDA or pMPC/PDA polymerization. Scales bars are 1 mm in length. (B) FTIR spectra of PEG and agar hydrogels with and without PDA and pMPC/PDA functionalization.

7.4 Results and Discussion

7.4.1 Characteristics of pMPC/PDA PEG and Agar Hydrogels

PEG dimethacrylate (8.3, 28, and 55 wt%) hydrogels were synthesized at consistent dimensions of 22 mm diameter and 150 µm thickness and agar (1.0, 3.0, and 9.0 wt%) hydrogels were synthesized at consistent dimensions of 22 mm diameter and 1 mm thickness. Chemical functionalization of these platform hydrogels was achieved through a

process coined "swelling-assisted“ polymerization. By immersing the hydrogels in Tris buffer containing 2 mg/mL of dopamine and pMPC during the swelling phase of hydrogel synthesis, the resulting concentration gradient induces an osmotic driving force into the hydrogel that facilitates pMPC/PDA formation throughout the polymer network.

Qualitatively, the successful polymerization of PDA throughout the PEG and agar hydrogels was observed by the appearance off the brown color characteristic of the melanin-like structure of PDA**,** Figure 43A. The inclusion of PDA and pMPC within the bulk of the hydrogels was confirmed using Fourier transform infrared spectrometer (FTIR), Figure 43B. Evidence of PDA includes the characteristic C=C stretches and N-H bending vibrations at 1604 and 1608 cm^{-1}, respectively, while pMPC adsorption displays characteristic signals of C-O and P-O at 1082 cm^{-1}.[173] Peaks for both PDA and pMPC remained present in FTIR scans acquired after rinsing the samples 3 times with DI water and after weeks of storage in DI water. This simple one-step process yielded robust pMPC/PDA-functionalized PEG and agar hydrogels that exhibit stability at physiologically relevant pH values.

The diffusion and subsequent polymerization of dopamine on the surface and interior of PEG and agar hydrogels was monitored as a function of time, Figure 44. The Red-Green-Blue (RGB) color values of the surface and center of hydrogels was quantified through photographs of the hydrogel’s cross-section, where increased RGB color values, darker colors, directly corresponded to PDA formation. RGB analysis determined that PDA formation occurred rapidly at the hydrogel surface (within 1 h). After a reaction time of 6 h, a uniform brown color was observed indicating successful PDA formation was acheived throughout the entire cross-section of all hydrogels independent of chemistry. Other

methods of PDA incorporation are highlighted in Figure 44 and found to provide similar results after a reaction time of 6 h; however, "swelling-assisted“ PDA formation was found to be the most consistent and were used in the remainder of this study.

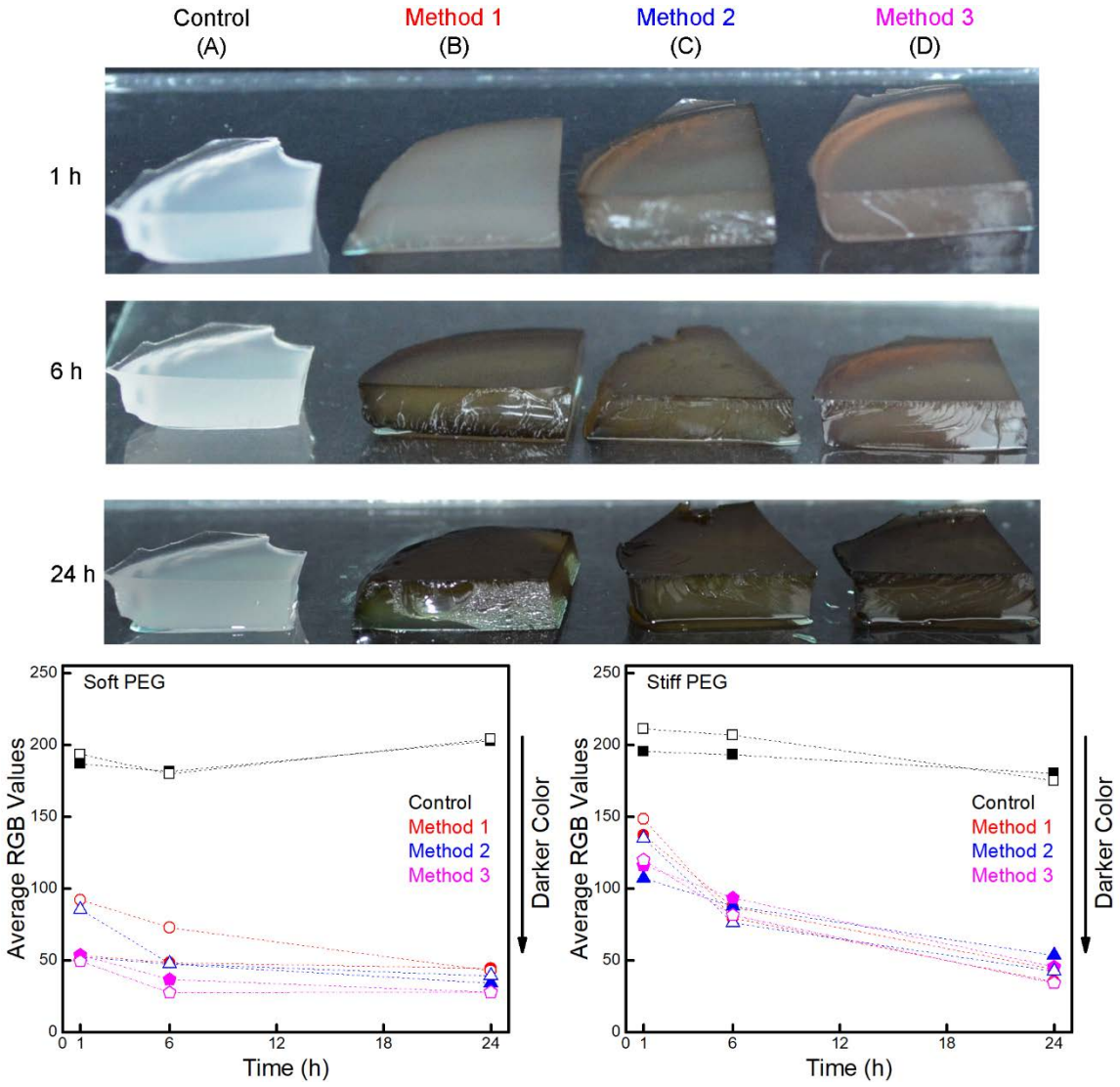

Figure 44: (A) Cross-sectional digital images of 55 wt% PEG hydrogels following 1, 6, and 24 h of PDA polymerization. Column (a) contains control PEG hydrogels. Three different methods of functionalization were tested. Column (b) shows hydrogels that were swollen to thermodynamic equilibrium before dopamine polymerization, (c) shows dopamine polymerization that was initiated following hydrogel formation but before swelling, and (d) shows the results of adding dopamine prior to synthesizing the hydrogel, which resulted in the simultaneous dopamine polymerization and hydrogel formation. Throughout this paper hydrogels were prepared using Method 2 (column c). Average color analysis on the exterior surface (solid symbols) and center cross-section (open symbols) for soft 8.3 wt% PEG and stiff 55 wt% PEG hydrogels.

The surfaces of 55 wt% PEG hydrogels were imaged using atomic force microscopy (AFM) in a hydrated enviroment after 6 h of swelling-assisted pMPC/PDA formation, Figure 45. Following pMPC/PDA formation and thorough rinsing in deionized (DI) water, the hydrogel surface was decorated with small PDA aggregates, characteristic of the mechanism of dopamine polymerization[170,210] PDA formation in the presence of pMPC significantly reduce the aggregate size from approximately 3 µm to less than 200 nm.[173] On the surface of the pMPC/PDA PEG hydrogels the aggregates ranged in size from 5 nm to 150 nm.

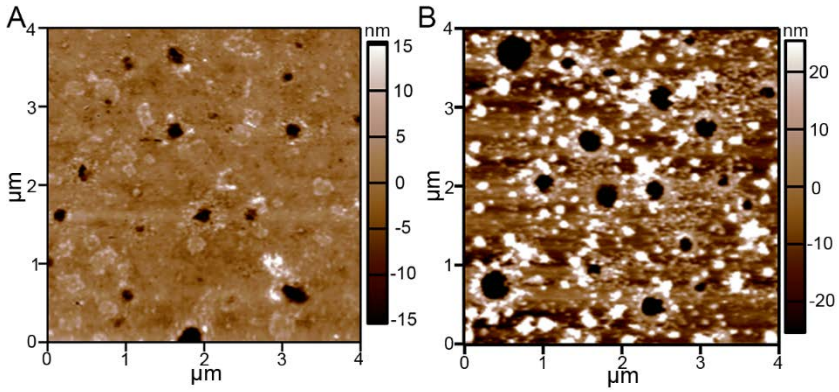

Figure 45: Representative surface topography AFM micrographs of a (A) control and (B) pMPC/PDA PEG hydrogel. Micrographs were acquired on hydrated 55.0 wt% PEG hydrogels, in DI water. A z-scale is provided alongside each image.

The equilibrium swelling ratios (Q) were statistically equivalent for the control and pMPC/PDA PEG hydrogels synthesized at all polymer concentrations, Table 8. This finding is interesting as PDA has previously been shown to inhibit hydrogel swelling. Therefore, the strong interaction with water of the zwitterionic polymer likely overcame any swelling inhibition of PDA.[62] The PEG hydrogels used in this study were covalently crosslinked through methacrylate moieties; their approximate mesh size (ξ) was calculated using the Peppas modification of Flory theory.[106] The mesh size was determined to be 3.4 ± 0.2 nm, 1.9 ± 0.1 nm, and 1.0 ± 0.1 nm for 8.3 wt%, 28 wt%, and 55 wt% PEG hydrogels,

respectively. Agar hydrogels are physically crosslinked networks with large pores. The equilibrium swelling of other biopolymer hydrogels has been reported to range from 400 - 6600% with large deviations.[211] Thus, the effect of pMPC/PDA on the equilibrium swelling of agar hydrogels could not be determined reliably. Cyro-scanning electron microscopy has been used to approximate the pores of 1% agar hydrogels to range from 370 to 800 nm in diameter.[212] In general, the smallest pore size of agar hydrogels is much larger than that of the PEG hydrogels and therefore provided no barrier for pMPC/PDA diffusion. Therefore, pMPC/PDA was successfully incorporated into both PEG and agar hydrogels despite substantial differences in their crosslinking chemistry, architecture, and network construction.

Table 8: Storage (G') modulus, loss (G'') modulus, volumetric swelling ratio (Q), and mesh size (ξ) of PEG and agar hydrogels with and without PDA and pMPC/PDA incorporation.

PEG [wt %]	G' [kPa]	G'' [kPa]	Q [%]	G' [kPa]	G'' [kPa]	Q [%]	ξ [nm]
8.3	1.7 ± 0.1	0.02 ± 0.01	13 ± 1.6	2.0 ± 0.2	0.04 ± 0.01	11 ± 0.8	3.4 ± 0.2
28	77 ± 3	3 ± 0.3	3.8 ± 0.4	94 ± 18	3.8 ± 0.4	3.4 ± 0.1	1.9 ± 0.04
55	1300 ± 200	190 ± 5	2.2 ± 0.05	1300 ± 60	60 ± 10	2.2 ± 0.1	1.0 ± 0.1

Agar [wt %]	G' [kPa]	G'' [kPa]	Q [%]	G' [kPa]	G'' [kPa]	Q [%]	ξ [nm]
1.0	2.5 ± 0.4	0.06 ± 0.01	-	2.1 ± 0.1	0.06 ± 0.01	-	~
2.9	30 ± 4	2.9 ± 1.3	-	37 ± 1.0	1.5 ± 1.8	-	~
8.3	370 ± 50	52 ± 11	-	240 ±	60 ± 30	-	~

7.4.2 Mechanical Characteristics of pMPC/PDA PEG and Agar Hydrogels

Hydrogel stiffness is intrinsically tied to the concentration of polymer, thus, increasing polymer concentration effectively increases the crosslink density and subsequently the stiffness of the hydrogel.[213] Small amplitude oscillatory shear (SAOS) measurements indicated that the elastic component dominated the complex modulus throughout and G' displays frequency independence for the PEG (8.3, 28, and 55 wt%) and

agar (1.0, 2.9, and 8.3 wt%) hydrogels, (Data not shown). Based on their dynamic moduli, we categorized the hydrogels into three regimes: soft (1.7 ± 0.1 kPa PEG and 2.5 ± 0.4 kPa agar), intermediate (110 ± 40 kPa PEG and 30 ± 4.0 kPa agar), and stiff (1300 ± 200 PEG and 370 ± 50 kPa agar).

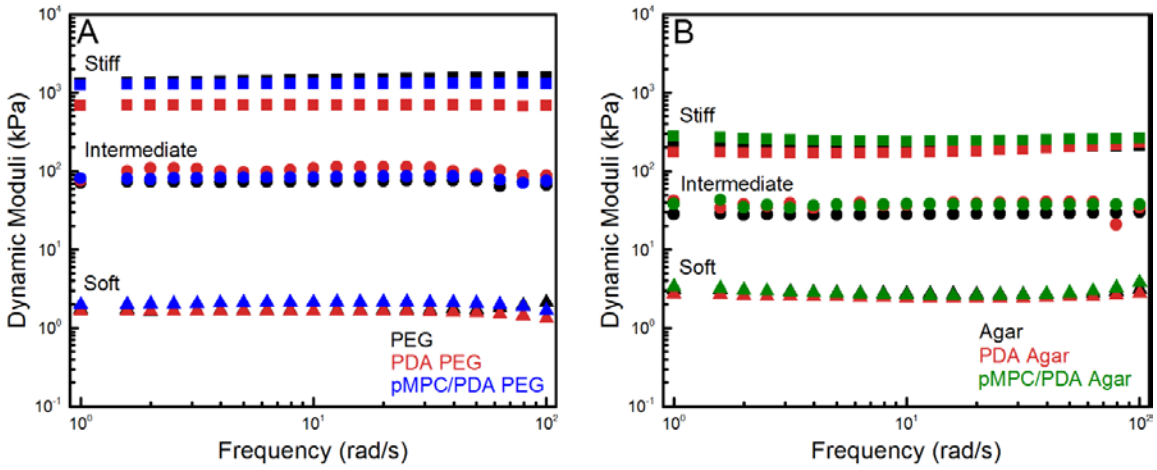

Figure 46 Representative frequency sweeps of (A) PEG and (B) agar hydrogels with and without PDA and pMPC/PDA functionalization. PEG hydrogels (8.3, 28, and 55 wt% PEG) and agar hydrogels (1.0, 2.9, and 8.3 wt% agar) are labeled as soft, intermediate, and stiff, respectively.

Ideally, introducing a second polymer network, such as pMPC/PDA, would not disrupt the original hydrogel network, and would either improve or maintain mechanical strength without sacrificing stability.[214] Following PDA or pMPC/PDA polymerization, the mechanical properties of the PEG and agar hydrogels displayed minimal variation from the control hydrogels, Figures 44 and Table 8. For example, intermediate PEG hydrogels had statistically equivalent G' values of 110 ± 40 kPa, 100 ± 6.0 kPa, and 94.0 ± 18 kPa for control, PDA, and pMPC/PDA PEG hydrogels, respectively.

After PDA incorporation, the stiff PDA PEG hydrogels displayed a significant loss in mechanical strength: G' decreased from 1300 ± 230 kPa to 710 ± 20 kPa and the G'' decreased from 190 ± 5.0 to 20 ± 1.0 kPa. Interestingly, stiff pMPC/PDA PEG hydrogels

displayed a comparable G' to the control PEG hydrogels, 1300 ± 6.0 kPa, but a smaller G'' of 63 ± 13 kPa. Agar hydrogels displayed no difference in G' or G'' following PDA or pMPC/PDA polymerization for soft, intermediate, and stiff hydrogels, Figure 46B. The changes in the mechanical properties of PEG hydrogels following PDA polymerization are likely linked to the mesh size of the PEG network. The 1.0 – 3.4 nm mesh size of the PEG hydrogels generally excluded PDA aggregate diffusion into the hydrogel interior. However, the large 3 μm aggregates arising from PDA-only polymerization, potentially disrupted the network structure of the stiff PEG hydrogels contributing to the reduction in G'; whereas the hydrogel's network structure was unaffected the smaller <150 nm pMPC/PDA aggregates. The similar mechanical properties of the agar hydrogels, before and after PDA and pMPC/PDA polymerization, is likely due to their large pore structure, reducing the effect of PDA aggregates on the mechanical properties.

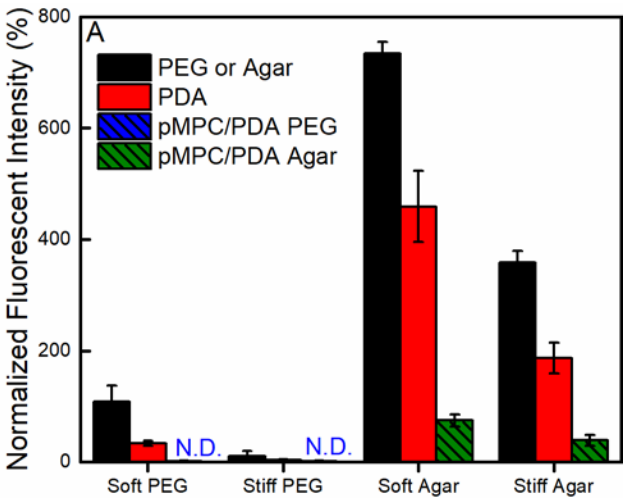

Figure 47: Protein adsorption to PEG and agar hydrogels with and without PDA and pMPC/PDA functionalization following incubation with fibrinogen. The fluorescent intensity of irreversibly adsorbed fibrinogen was quantified and normalized against protein-free controls. Adsorption below the detector limit labeled as not-detected (N.D.).

7.4.3 Protein Resistance of pMPC/PDA PEG and Agar Hydrogels

The fouling resistance of PEG and agar hydrogels with and without PDA and pMPC/PDA was evaluated by a fluorescent protein assay using fibrinogen, a model serum protein. After 24 h exposure to a solution of 100 μg/cm^2 fibrinogen, minimal protein adsorption was detected via fluorescence microscopy on the PEG hydrogels whereas a significant amount of fibrinogen adsorbed to the agar hydrogels, Figure 47 and Table 9. Compared to unmodified hydrogel controls, a statistically significant improvement was observed for both PEG and agar hydrogels following PDA polymerization.[215] The pMPC/PDA PEG hydrogels demonstrated further improvement in protein fouling resistance and achieved "ultralow-fouling" by adsorbing a non-detectible amount of fibrinogen.[62,216] Resistance to protein adsorption is the hallmark of PEG surfaces, so the 99% improvement in antifouling performance following pMPC/PDA incorporation indicates a complementary relationship between PEG and pMPC in response to protein exposure. Compared to the protein-resistant PEG hydrogels, agar hydrogels are high-fouling and well-known to readily adsorb protein when challenged.[217] The improvement in resistance to fibrinogen adsorption on agar hydrogels was even more pronounced; pMPC/PDA agar hydrogels adsorbed 10 times less fibrinogen (70 ± 10 units) in comparison to control agar hydrogels (730 ± 20 units). The inclusion of pMPC/PDA enabled agar hydrogels to resist protein fouling almost as effectively as PEG.

Table 9: Quantification of the Fibrinogen adsorption to unmodified, PDA, and pMPC/PDA PEG and agar hydrogels. Additionally, the relative reduction in fibrinogen adsorption compared to unmodified controls for PDA and pMPC/PDA PEG and agar hydrogels is given.

	Fibrinogen Adsorption [EGFP unit count]			Reduction in Fibrinogen [%]	
Hydrogel	Control	+ PDA	+pMPC/PDA	+ PDA	+pMPC/PDA
Soft PEG	110 ± 30	30 ± 4	N.D.	69	99
Stiff PEG	10 ± 10	4 ± 1	N.D.	64	99
Soft Agar	730 ± 20	460 ± 60	70 ± 10	38	90
Stiff Agar	360 ± 20	190 ± 30	40 ± 10	48	89

7.4.4 Bacterial Resistance of pMPC/PDA PEG and Agar Hydrogels.

PEG and agar hydrogels, with and without pMPC/PDA, were challenged for 24 h with two model bacterial species, Gram-positive *S. aureus* and Gram-negative *E. coli*. Glass coverslips, PDA, and pMPC/PDA thin films (on glass) served as control samples. Despite their resistance to fibrinogen adsorption, *S. aureus* and *E. coli* adhesion occurred on PEG hydrogels. As expected by the prevalence of protein adsorption to agar hydrogels and previous reports,[217] both bacteria adhered more readily to the agar hydrogels than to the PEG hydrogels. Qualitative indications of early biofilm development were observed on the stiffest control PEG and agar hydrogels by the clustering of *S. aureus* into microcolonies, Figure 48. Consistent with our previous work[123] on the control PEG and agar hydrogels, the coverage of bacteria colonies increased with stiffness. Although PDA surface modification was shown to slightly reduce bacterial adhesion, consistent with previous literature, PDA functionalization alone is insufficient to substantially resist adhesion of either bacterial species.[204,218] For example, although PDA reduced *S. aureus* colony coverage from 6.2 ± 1.0% to 3.6 ± 1.0% compared to unmodified glass, pMPC/PDA functionalized surfaces significantly reduced surface coverage by an additional 5 times to 0.7 ± 0.1%.

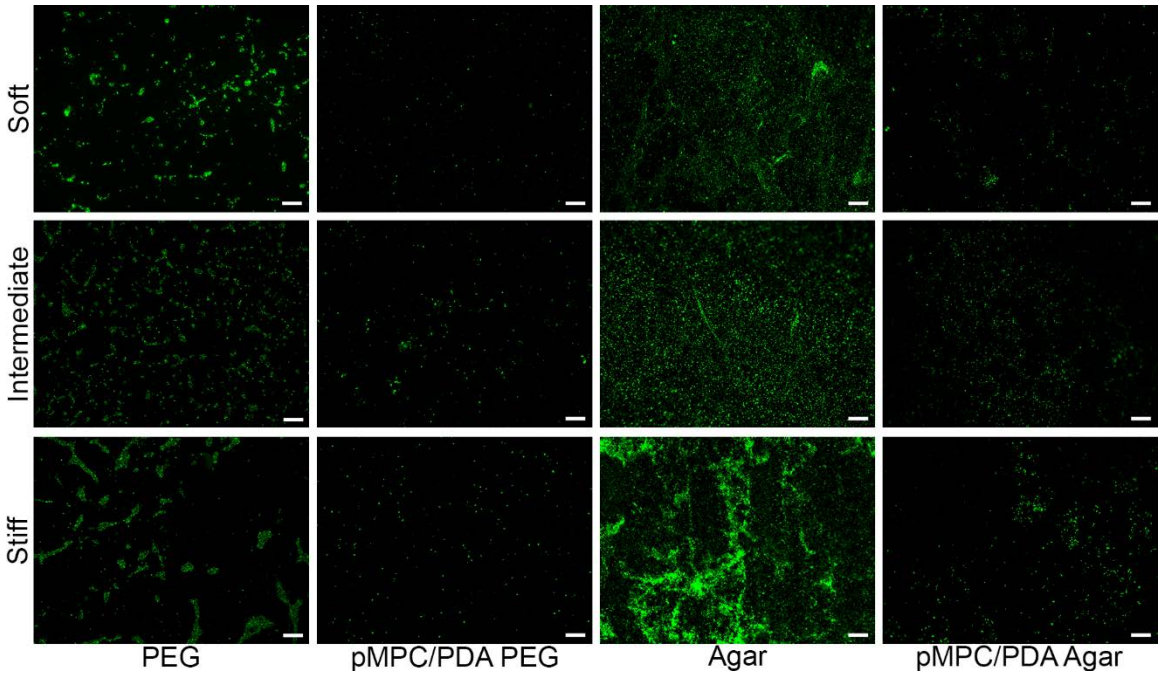

Figure 48: Representative micrographs of *S. aureus* adhesion to unmodified and pMPC/PDA PEG and agar hydrogels with increasing stiffness. A scale bar corresponding to 100 μm is included on each image.

All pMPC/PDA hydrogels displayed significantly less bacterial adhesion than unmodified controls and lacked signs of colony formation from either bacterial species, Figure 49. Interestingly, *E. coli* colony coverage was consistent on all surfaces following pMPC/PDA formation including thin film controls and normally high-fouling agar hydrogels. Quantitatively, *E. coli* adhesion was statistically equivalent on soft, intermediate, and stiff pMPC/PDA PEG hydrogels with colony area coverages of 0.17 ± 0.03%, 0.23 ± 0.04%, and 0.23 ± 0.03%, respectively. These results are analogues to Cheng *et al*., who found that surfaces modified with a long-chain zwitterionic poly(sulfobetaine methacrylate) significantly reduced the colony coverage of *Staphylococcus epidermis* and *Pseudomonas aeruginosa* to a similar extent.[219] *E. coli* attachment was reduced by 5, 7, and 9 times on pMPC/PDA PEG hydrogels compared to control PEG hydrogels. Further, *E. coli* colony coverages of 0.22 ± 0.07%, 0.37 ± 0.13%, and 0.23 ± 0.06% were observed on soft, intermediate, and stiff pMPC/PDA agar hydrogels; values that are statistically equivalent to pMPC/PDA thin film controls (0.22 ± 0.07%) and all pMPC/PDA PEG hydrogels. The improvement in the fouling resistance of pMPC/PDA agar hydrogels is

especially remarkable and demonstrates the strong antifouling properties provided by the pMPC.

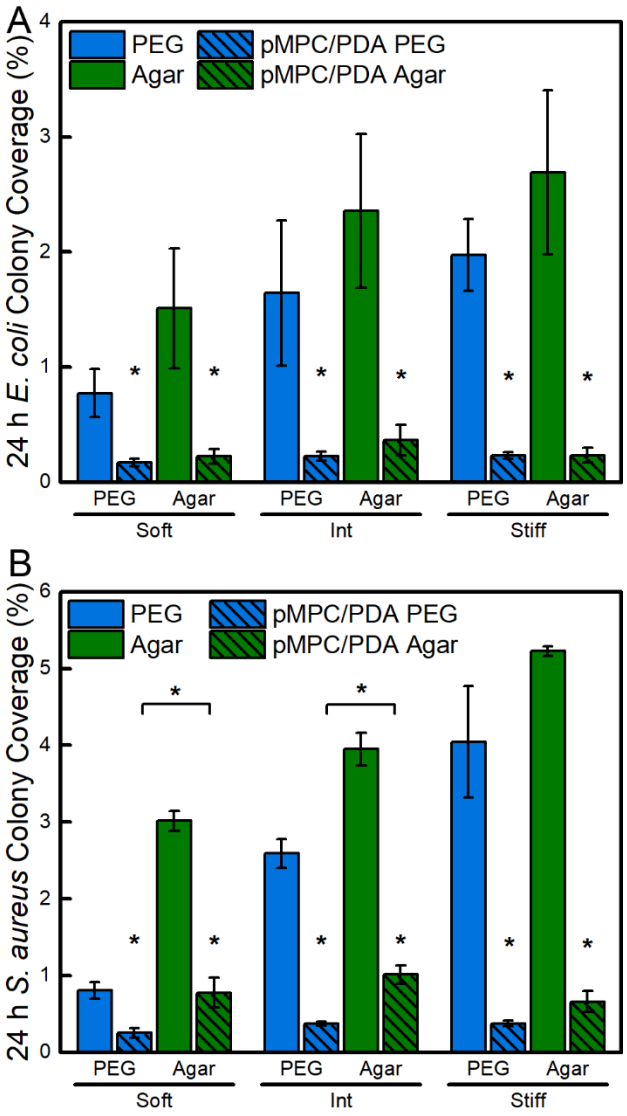

Figure 49: Adhesion of (A) *E. coli* and (B) *S. aureus* on PEG and agar hydrogels with and without PDA and pMPC/PDA incorporation. Hydrogels are grouped by their storage moduli: soft, intermediate, and stiff. The difference between unmodified and pMPC/PDA hydrogels is statistically significant (p-value < 0.01) for all samples. One asterisk (*) denotes P < .01 intra-sample significance and brackets denotes P < .01 significance between hydrogels. Error bars denote standard error.

PMPC/PDA PEG hydrogels exhibited superior resistance to *S. aureus* adhesion relative to pMPC/PDA modified agar or thin film controls. *S. aureus* adhesion was statistically equivalent on soft, intermediate, and stiff pMPC/PDA PEG hydrogels with

colony area coverages of 0.25 ± 0.06%, 0.37 ± 0.02%, and 0.37 ± 0.04% respectively. Notably, soft, intermediate, and stiff pMPC/PDA agar hydrogels displayed *S. aureus* colony area coverages of 0.78 ± 0.20%, 1.0 ± 0.12%, and 0.65 ± 0.14%, respectively. These functionalized agar hydrogels supported 4 times fewer microbes than the control agar hydrogels, but significantly more microbes than the functionalized PEG hydrogels. Further, the pMPC/PDA thin film controls displayed an impressive 9 times reduction in *S. aureus* adhesion, from 6.2 ± 1.0% to 0.68 ± 0.06% *S. aureus* compared to unmodified glass controls, Table 10. Therefore, the superior performance of pMPC/PDA PEG hydrogels likely resulted from a combination of the antifouling activity of each polymer. The increased adhesion of *S. aureus* to pMPC/PDA agar compared to pMPC/PDA PEG is likely due to the unique membrane-bound protein adhesion in *S. aureus* that facilitates adhesion to human tissue, enhancing interaction with the bioinspired MPC structure.[21,100] This is consistent with literature reports describing the variation in *S. aureus* adhesion depending on abiotic materials.[220,221]

Table 10: Total surface colony coverage of *E. coli* and *S. aureus* on control hydrogels (PEG and agar), pMPC/PDA functionalized PEG and agar hydrogels, and glass coverslips.

		E. coli Surface Coverage [%]		*S. aureus* Surface Coverage [%]	
Stiffness	Chemistry	+ PDA	+pMPC/PDA	+ PDA	+pMPC/PDA
Soft	PEG	0.77	0.17	0.81	0.25
Intermediate	PEG	1.64	0.23	2.59	0.37
Stiff	PEG	1.97	0.23	4.05	0.37
Soft	Agar	1.51	0.22	3.02	0.78
Intermediate	Agar	2.36	0.37	3.95	1.01
Stiff	Agar	2.69	0.23	5.23	0.66
Glass	Glass	3.68	0.22	6.19	0.68

7.5 Conclusion and Future Work

We have presented a simple and versatile technique to enhance the fouling resistance of hydrogels with polymer zwitterions, independent of the network structure and mechanical properties of the original hydrogel. A simple solution based approach, a fouling-resistant polymer zwitterion, pMPC, was integrated into PEG and agar hydrogels during hydrogel swelling to facilitate uniform pMPC/PDA incorporation without sacrificing the integrity of the original hydrogel network. The inclusion of this fouling-resistant polymer network successfully reduced fibrinogen adsorption on agar by over 90%, transforming a culture medium for bacteria into a fouling-resistant material. Relative to unmodified PEG and agar hydrogels, *E. coli* and *S. aureus* adhesion was significantly reduced (up to 91%) on all hydrogels following pMPC/PDA formation. PDA-mediated integration of polymer zwitterions offers a simple and versatile platform to enhance the antifouling performance of hydrogels without altering the network structure or mechanical properties of the original hydrogel.

There are a few interesting opportunities for further research stemming from this objective. Extending the use of this hydrogel modification system to catheters would be a natural progression from an application perspective. This would require testing with other hydrogel chemistries that are currently used commercially such as silicone hydrogels. Testing the protein fouling resistance of a pMPC/PDA coated catheter would provide a good benchmark for fouling-resistance compared to commercially available catheters. Integrating antimicrobial functionality into the coating, either through a regenerate release mechanism such as, silver ion eluding zeolites or specific contact killing using cationic chemistry or antimicrobial peptides, would be essential for an extended use application of pMPC/PDA for catheter. A duel-action approach is the standard for catheters today, where released biocides reduce the available bacteria population while the antifouling chemistry inhibits adhesion of the remaining cells.

One interesting commercial application of PDA-functionalized hydrogels could be tinted contact lenses. The melanin-like structure of PDA naturally adsorbs light and is easily transferred throughout hydrogels following successful polymerization. Studies have shown that inhibiting the penetration of light into the eye can reduce the frequency of migraines in light-sensitive patients. When combined with the previously demonstrated

fouling-resistance, pMPC/PDA modified contact lenses hold multiple potential benefits as a modification to current contact lenses.

Alternatively, PDA modification could be harnessed as a platform for other hydrogel applications other than fouling resistance. The use of PDA coatings as a surface modification platform has exploded over the past few years to include a host of secondary modifications to PDA including click chemistry, growth factor immobilization, and surface-initiated atom transfer radical polymerization.[222] Although PDA modification are unable to replace intra-network chemistry, such as degradable networks, surface-based modifications could be easily implemented on different hydrogel material platforms (silk, alginate, PDMS, etc) without the need for specific tailored chemistry.

CHAPTER 8

ANTIFOULING AND ANTIBACTERIAL ACTIVITY OF BIOINSPIRED POLYMERIC FILMS

Adapted from: Li, Y.; John, J.; Kolewe, K. W.; Schiffman, J. D.; Carter, K. R. Scaling up Nature ― Large Area Flexible Biomimetic Surfaces. *ACS Appl. Mater. Interfaces* 2015, 7 (42), 23439–23444.
Dündar, F.; Kolewe, K. W.; Schiffman, J. D.; Watkins, J. J. Bioinspired Photocatalytic Sharkskin via Solvent Assisted Nanoimprint Lithography with Antibacterial and Antifouling Activity. *In preparation*
Arellano, D. L. G.; Kolewe, K. W.; Champagne, V. K.; Burnett, E. K.; Dündar, F.; Schiffman, J. D.; Briseno, A. L. Biocidal Vertically Oriented Nanocrystals Initiated from Pencil-Drawn Graphene. *In preparation*

8.1 Introduction

Nature provides a wealth of inspiration for the design of antifouling and antibacterial surfaces. From the skin of the largest predator in the sea to the wings of tiny insects, naturally developed surface topographies display unique structure-property relationships.[50,72] Developing synthetic analogs or biomimetic materials is a growing field of study; however, recapitulating properties developed over thousands-millions of years is a challenging pursuit. In this chapter, I will briefly discuss my contributions to collaborative projects that developed antifouling and/or antibacterial thin films whose structure was inspired by nature. These projects are; slippery liquid-infused porous surfaces, photocatalytic sharkskin, and nanopillars of death.

8.2 Results and Discussion

8.2.1 Slippery Liquid-Infused Porous Surfaces

Inspired by the self-cleaning surface of the *Nepenthes* pitcher plants, Wong *et al*. developed an analogous synthetic "surface slippery liquid-infused porous surface" (SLIPS).[77] The tips of the pitcher plant's leaves display a hierarchical surface topography that retains liquid between surface features to create a superhydrophobic or "slippery zone" to trap prey.[223] Notably, SLIPS is one of the few surfaces that can prevent mussel adhesion.[224] To fully develop the potential self-cleaning surfaces, their production must be scaled up over a large area in a cost-efficient manner.

8.2.1.1 Evaluation of SLIPS Fouling-Resistance

The antifouling properties of the samples were evaluated using *E. coli* as a model bacteria for attachment. Each sample was placed in a separate well of a 6-well polystyrene plate to which 10 mL of M9 growth media containing ampicillin (100 μg mL−1) was added. Overnight cultures of E. coli (1.0×10^8 cells/mL) grown in Difco Luria–Bertani broth with ampicillin (100 μg/mL) were inoculated into each well and incubated at 37 °C for 2 hr. The growth media was then removed via a sterilized glass pipette and the samples were lightly shaken and rinsed repeatedly three times with sterile phosphate buffered saline solution. The samples were then fixed for 10 min using a fresh 4%-paraformaldhyde, mounted between sterilized 22-mm glass coverslips, and sealed using an equal part mixture of Vaseline, lanoline, and paraffin wax (VALAP). To quantify the attachment of viable bacteria, confocal laser scanning microscopy (CLSM, Nikon-D Eclipse) with a 60× Nikon NF oil immersion objective and a green argon laser were used. Flat PET samples acted as

an internal control to normalize bacterial attachment. For each sample, 10–15 micrographs were randomly acquired with at least 3 parallel replicates. Subsequent image analysis was performed with *ImageJ 1.45* software (National Institutes of Health, Bethesda, MD).

8.2.1.2 Fouling Resistance of SLIPS

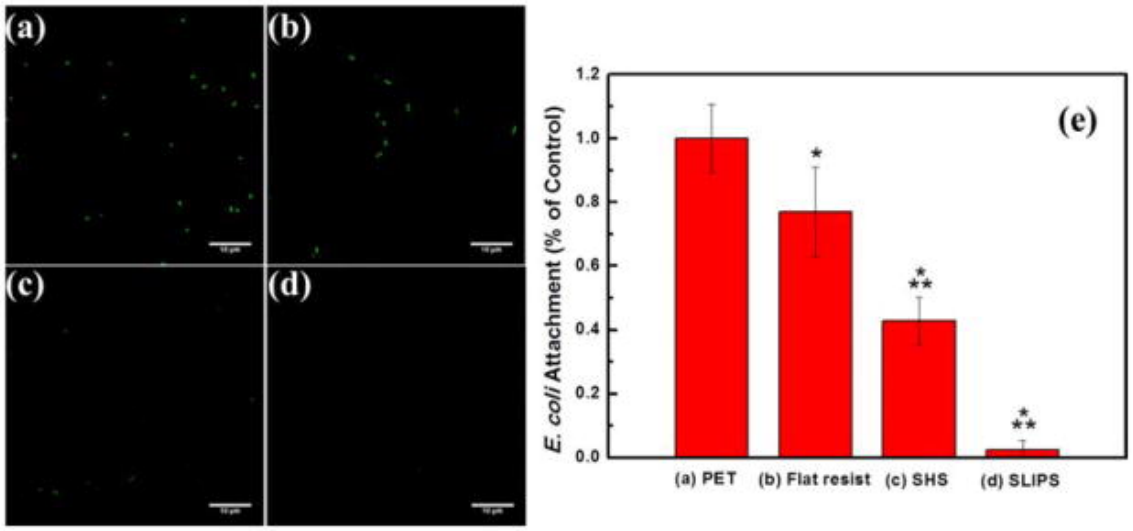

Figure 50: Representative fluorescence micrographs of *E. coli* attachment on (a) PET, (b) flat resist, (c) SHS, (d) SLIPS. (e) Normalized *E. coli* attachment on PET, flat resist, SHS and SLIPS. All values are normalized to the coverage of *E. coli* on the PET control. One and two asterisk(s) (*) and (**) denote statistical significance ($p < 0.01$) compared to the PET control and the flat resist, respectively. Scale bar: 10 μm.

To explore the potential biomimetic applications of the flexible, large area superhydrophobic surface (SHS) and SLIPS manufactured by roll-to-roll nanoimprinting, the anti-biofouling properties were investigated by challenging the surfaces with *E. coli*. As shown in Figure 48, planar resist films exhibited ~20% less bacterial attachment than a bare PET control. SHS reduced *E. coli* adhesion by ~60% compared to planar PET controls. This is consistent with literature where superhydrophobic hierarchically wrinkled patterns resisted the adhesion of *E. coli* and calf pulmonary artery endothelial.[225,226] By coating a layer of lubricant on SHS and creating a SLIPS surface, bacterial adhesion was reduced by 98% compared with the planar PET control. The hydrophobic lubrication layer

of SLIPS creates a boundary layer that limits bacterial diffusion to the PET surface. Non-adherent cells are easily washed away, imbuing SLIPS surfaces with their fouling-resistance.

8.2.2 Photocatalytic Sharkskin

The skin of aquatic animals is naturally designed to reduce drag so the animal can expel as little energy as possible when moving through the water. The adhesion of bacteria and other microorganisms would create substantial drag by disrupting the natural streamlines of the animal, thus the skin of these aquatic creatures frequently display hierarchical topography.[71] Of the various sea creatures whose skin displayed fouling resistance, the best studied are sharks.[227] Sharkskin consists of layers of scales covered in longitudinal ridges, of varied length but consistent spacing. The first synthetic analog of this hierarchical diamond design, Sharklet AF™ was developed by Carman *et al.* and shown to successfully resist the attachment of spores and later modified to resist bacterial adhesion.[228] The primary limitation of these hierarchical materials, like any antifouling surfaces, is long-term prevention of biofilm formation. Although Sharklet AF™ patterned PDMS has been shown to delay biofilm formation compared to planar PDMS, a biofilm will develop with time.[72] Photocatalytic materials are an effective and relatively environmentally friendly class of antibacterial surfaces. One of the best studied of these materials is titanium dioxide (TiO_2). When TiO_2 absorbs UV light, redox reactions with H_2O or OH^- molecules to form reactive hydroxyl radicals and superoxide ions, respectively.[229] Interaction of these radicals with the outer membrane of bacteria induces rupture and subsequent cell death. Thus, a material that displayed the physical structure

derived fouling resistance of sharks and the broad spectrum antibacterial activity of photocatalytic materials could tap into a natural synergistic relationship to improve the overall fouling resistance of the system.

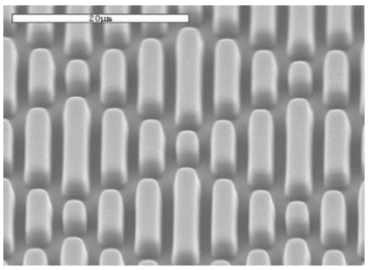

Figure 51: Representative SEM micrograph of the sharkskin patterned surface. The diamond pattern of riblets with a height, width and spacing of ~1.6, 1.2 and 2.6 µm, respectively.

8.2.2.1 Sharkskin Patterned Surface Fouling Evaluation

The fouling resistance of smooth and modified Sharklet AF™ patterned TiO_2 composites and PET controls were evaluated with a modified bacterial attachment assay.[123] The Sharklet AF™ pattern (P) used for this study consisted of a modified structure consisting of riblets with a height, width and spacing of ~1.6, 1.2 and 2.6 µm, respectively, Figure 49. For comparison, the original Sharklet AF™ pattern (P*) was used as a control. The model bacterial species, *E. coli*, was cultured overnight in Luria-Bertani broth, then washed and resuspended in M9 media to a final concentration of (1×10^8 cells/mL). Samples were placed at the base of separate wells in six-well polystyrene plates (Fisher Scientific) and inoculated with 5 mL of E. coli suspension in M9 media. Following a 24 hr incubation at 37 ºC, growth media was removed using a sterilized glass pipette and samples were lightly shaken and rinsed repeatedly with sterile phosphate-buffered saline (PBS). Samples were imaged using 20× and 50× objective on a Zeiss Microscope Axio Imager A2M. The area coverage of bacterial adhesion (%) was quantified by analyzing 10–15

randomly acquired images over at least three parallel replicates using *Image J 1.45* software (National Institutes of Health, Bethesda, MD). Statistical significance was accepted at $p < 0.001$ level. The particle analysis function in *ImageJ* was used to calculate the colony area coverage over the acquired 58716 μm^2 area.[72]

8.2.2.2 Evaluation of Photocatalytic Bactericidal Efficiency

Planar NOA60:TiO_2 films (10:90, 50:50, and 90:10), as well as controls (glass, PET, and NOA60) were placed at the base of separate wells in 6-well polystyrene plates (Fisher Scientific) and inoculated with 5 mL suspension of *E. coli* or *S. aureus* in M9 media, adjusted to a working concentration of 1×10^8 cells/mL. Samples were incubated at 37 °C under UV lamp irradiation for 1 hr (15 cm separation and 365 nm wavelength using F15W/T8 McMaster-Carr). Samples were then stained with propidum iodide (PI) for 5 min, washed, and immediately imaged using a 20× objective on a Zeiss Microscope Axio Imager A2M. The loss of *E. coli* viability was determined through the number of Live (green) and Dead (red) bacteria from 10-15 images over 5+ samples.

8.2.2.3 Fouling-Resistance of Sharklet Pattern Surfaces

The antifouling performance of planar and Sharklet AF™ surfaces was tested using the model organism *E. coli*. Tests were conducted in the dark, to eliminate any contribution from the antibacterial photocatalytic activity of the substrates. Composite TiO_2 materials were prepared were prepared by dispersing TiO_2 nanoparticles within a UV cured Norland Optical Adhesive 60 (NOA60) binding matrix. For readability, TiO_2 composite materials will be referred to by the ratio of NOA60:TiO_2 10:90, 50:50, and 90:10 corresponding to 10, 50, and 90 wt% TiO_2 respectively. Planar or smooth (S) and Sharklet AF™ patterned

(P) surfaces were tested for each composite and a TiO_2-free control (NOA60). PET and glass internal controls were tested in parallel for reference. Sharkskin microstructure films decreased bacterial attachment by ~80% compared to PET controls and ~65% compared to smooth films of the same materials, Figure 50. For example, patterned 10:90 surfaces reduced *E. coli* coverage from 1.7 ± 0.6% on smooth planar films to 0.6 ± 0.2% on the patterned surface. Notably, the area coverage of *E. coli* was found to be statistically equivalent on all patterned surfaces, including TiO_2-free controls. Although the wettability of each surface is affected by the wt% of TiO_2, this indicates that the fouling-resistance of the patterned surfaces to *E. coli* adhesion was independent of chemistry. Decreasing the height and aspect ratio of the surface features (P* vs P) slightly affected *E. coli* adhesion (33% change), yet not a substantial decrease and is consistent with previous Sharklet AF™ studies with larger organisms.

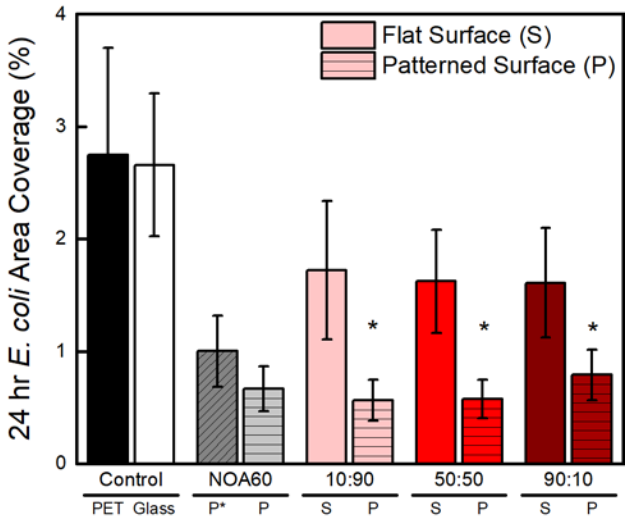

Figure 52: Colony area coverage of *E. coli* adhesion to smooth (S) and Sharklet AF™ patterned (P) films on a PET substrate. An asterisk (*) denotes 95% significance between smooth and patterned samples. Error bars denote standard error.

8.2.2.4 Bactericidal Activity of Planar TiO_2 Composite Surfaces

The antibacterial activity of photocatalytic TiO_2 surfaces was assessed using planar films of each composite. *E. coli* and *S. aureus* were used as model organisms to demonstrate the broad-spectrum bactericidal efficacy of photocatalytic TiO_2 surfaces. After 1 hr of UV light exposure, all TiO_2 composites displayed excellent antibacterial activity against both bacterial species, Figure 51. For example, 10:90 TiO_2:NOA60 composites killed ~90% of both *E. coli* and *S. aureus* adhered to its surface. The antibacterial performance of 50:50 surfaces was slightly reduced with killing efficiencies of 83% and 87% for *E. coli* and *S. aureus*, respectively. The loss in killing efficiency of 50:50 composites was attributed to the aggregation of TiO_2 nanoparticles, confirmed through transmission electron microscopy (TEM) micrographs of the surface of each composite (data not shown). Further, the increased antibacterial performance of 90:10 composites can be attributed to the use of Tetraethyl orthosilicate (TEOS) to stabilize the matrix at high nanoparticle concentration.[230] Although the antibacterial activity was composite surfaces was increased through the use of anatase TiO_2 nanoparticles, superior photocatalytic activity compared to rutile phase TiO_2; antibacterial performance could be further improved by improving nanoparticle dispersion. Evidenced of this is the reduced activity of 50:50 composites compared to the lower wt% 10:90 composites due to nanoparticle aggregation.

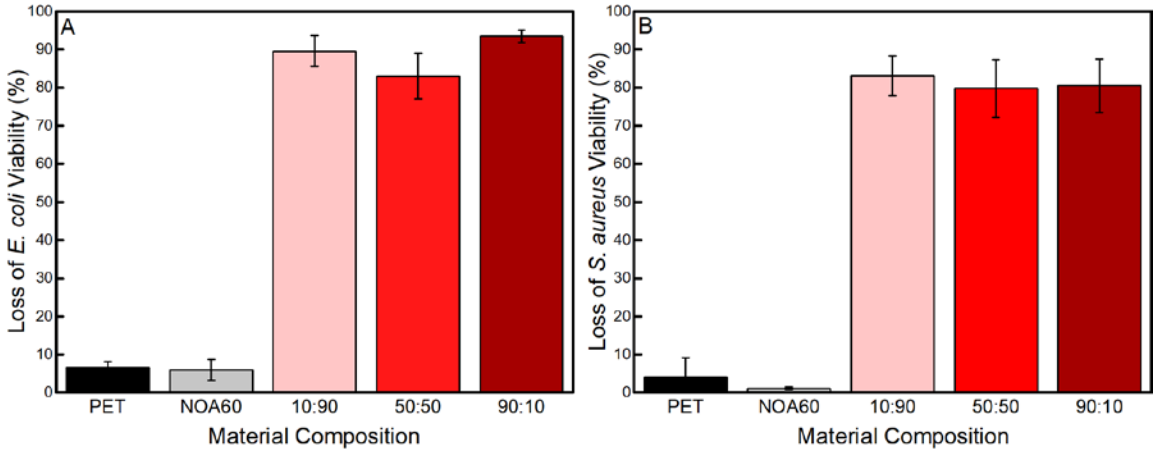

Figure 53: (A) Loss of *E. coli* and (B) *S. aureus* viability after 1 hr of UV irradiation. All tested surfaces were flat films. Error bars denote standard error.

8.2.3 Bioinspired Nanopillars of Death

As described in Chapter 1.2.1.2, a new and unique mechanism to kill bacteria through mechanical rupture was discovered on the surface of cicada and dragonfly wings.[231] Ivanova et al. utilized this principle to design high-aspect ratio inorganic surfaces through ion-beam etching, that achieved exceptional antibacterial activity independent of surface chemistry.[51,52,232] Unfortunately, ion-beam etched surfaces are expensive and low-throughput, leaving room for the development of lower-cost contact bactericidal surfaces. Delving into the field of organic solar cells, a similar surface architecture was previously developed to maximize the interfacial area of photovoltaics.[233] Crystalline nanopillar surfaces were grown using a variety of crystalline chemistries from a wetting layer on graphene substrates. The structure and spacing of the nanostructures can be modified by altering the chemistry and processing parameters of crystal growth to mimic the size and spacing of ion-beam etched surfaces, Figure 52.

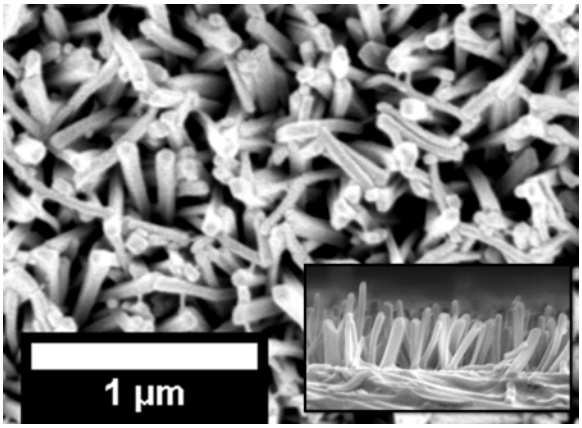

Figure 54: Top-down SEM micrograph of ZnPc nanopillars. Inset depicts a cross-sectional view of pillar orientation.

8.2.3.1 Nanopillar Antibacterial Activity Evaluation

The bactericidal efficiency of substrates was evaluated using a modified adhesion viability assay.[234] *Escherichia coli* K12 MG1655 (*E. coli*) (DSMZ, Leibniz-Institut, Germany) containing a GFP plasmid were cultured overnight in LB media for 12-16 hr, washed with PBS, and resuspended in M9 media. Control and nanopillar substrates were placed at the base of 6-well plates (Fisher Scientific) to which 5 mL of M9 media containing 100 µg/mL of ampicillin was added to select for GFP expressing *E. coli* (1×10^8 cells/mL). Internal controls (glass coverslips) were run in parallel (data not shown). Samples were incubated at 37 °C for a predetermined incubation period then removed and washed with PBS to remove non-adhered cells. PI stain (15 min) identified the dead cells while GFP expressing *E. coli* were considered viable. The loss of E. coli viability was visualized using a Zeiss Microscope Axio Imager A2M (20× magnification, Thornwood, NY). The number of live and dead *E. coli* was quantified using *ImageJ 1.48* software (National Institutes of Health, Bethesda, MD) and the relative viability was calculated by Equation 6:

Equation 6

$$Loss\ of\ E.coli\ Viability\ (\%) = \frac{Dead\ Cells}{Live + Dead\ Cells} \times 100$$

8.2.3.2 Biocidal Activity of ZnPc Nanopillars

The bactericidal efficiency of the ZnPc nanopillars was compared against planar films of ZnPc and graphite Figure 53A, which only demonstrated a baseline loss of *E. coli* viability, 4 ± 0.8 and 8 ± 0.2%, respectively. SEM micrographs indicates minimal E. coli maintain their characteristic rod-like morphology on the planar graphite surface and the ZnPc thin film, (data not shown). The shortest evaporation time (3 min) resulted in an average killing efficiency of 21 ± 9%. The variability of the average pillar length and inter-pillar, likely causes the large range of killing efficiency, 10 – 50% observed on short (3 min) nanopillars. SEM micrographs indicate that the short (<200 nm) nanopillars protrude and deform cell membranes of *E. coli*, but do not create enough tension to induce rupture. However, once the nanopillars were grown for 3.5 min, a substantially greater loss in *E. coli* viability was observed 79 ± 6%. When grown for 4.0 min, the resulting nanopillars further increased killing efficacy with a 90 ± 4% loss in *E. coli* viability. Interestingly, even though the length of nanopillar length increased with evaporation times of 4.5 and 5.0 min, bactericidal efficiency plateaued at ~90%. Even though the length of nanopillars grown for 4.5 and 5.0 min were longer than those grown for 4.0 min, the inter-pillar spacing remained ~1.1 μm for evaporation times of 4.0, 4.5, and 5.0 min. This implies that the force required to induce membrane rupture was not significantly increased with nanopillar length beyond a critical point. This is supported by the biophysical model of bacteria killing associated with cicada wing nanotopography.[49] Notably, the Zn+ ions in ZnPc are covalently bonded

into the crystal structure, thus leeching does not occur nor contribute to the observed bactericidal effect of pillar morphology.

To investigate the bactericidal kinetics, we systematically varied the time that *E. coli* was incubation with the nanopillars deemed to have the most effective topography (evaporation time = 4.0 min), Figure 53B. After 15 min of contact, the shortest time interval that can be tested using the fluorescence-based toxicity assay, a 90 ± 3% loss in *E. coli* viability was achieved. This is statistically equivalent to the loss of E. coli viability after 120 min, 90 ± 4%, suggesting that *E. coli* dies on contact with the nanostructured surface. This is consistent with previous reports on cicada wings where similar loss in bacterial viability was evident after 20 min.[50]

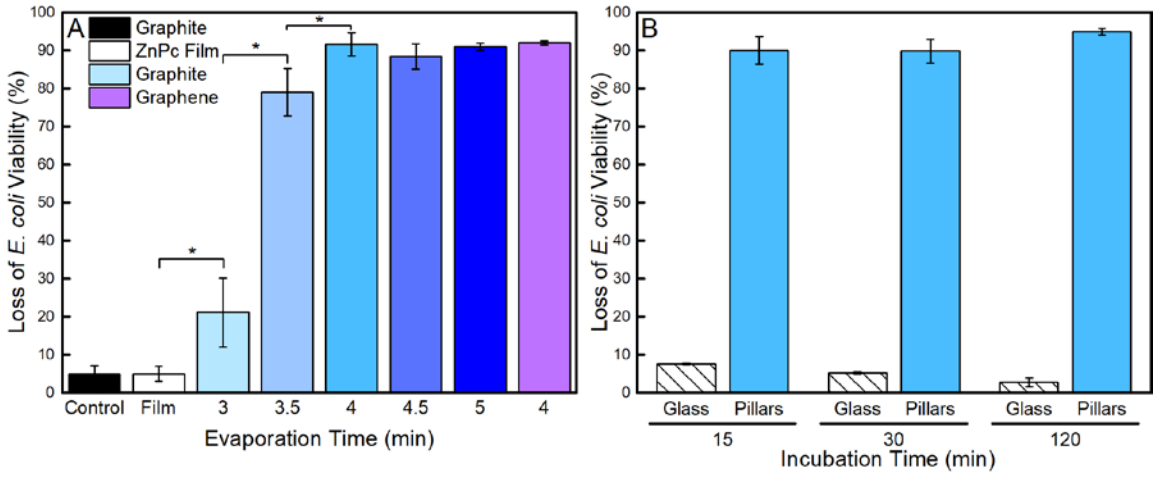

Figure 55: (A) Loss of *E. coli* viability after a 2 h incubation on ZnPc nanopillars as a function of evaporation time. Nanopillars were grown from graphite (shades of blue) and graphene (purple) substrates. Graphite and ZnPc thin film controls are also provided. An asterisk (*) denotes a statistically significant (p value < .05) difference than other samples. (B) Viability of *E. coli* incubated on ZnPc planar films and nanopillars as a function of incubation time. Error bars denote standard error.

8.3 Conclusion

The efficacy of three bioinspired surfaces were shown to significantly reduce the adhesion of bacteria. The efficacy of SLIPS was shown to passively reduce *E. coli* adhesion by 98% through the formation of a lubrication boundary layer at the material surface. Sharklet AF™ patterned TiO_2 composite surfaces were shown to decrease the surface colonization of *E. coli* by ~80% while simultaneously killing over 90% of adhered bacteria through UV induced photocatalytic activity. By optimizing length and the spacing between ZnPc crystalline nanopillars, a 90% killing efficiency was achieved. Each of these bioinspired approaches holds promise as scalable material infection-resistant surface modification platforms.

There are a wide variety of directions future research could follow from these projects. Integrating a released biocidal mechanism that would remain in the lubrication layer of a SLIPS surface could further enhance the performance with synergistic killing and fouling resistance. Although the TiO_2 Sharklet AF™ project already incorporates both antifouling and antibacterial mechanisms in a synergistic fashion, future research could further improve the fouling reduction by optimizing the chemistry and stiffness of the surface. Tuning the stiffness of the surface features could further reduce the ability for bacteria to adhere to Sharklet AF™ patterned surfaces. The use of a different nanoparticle dispersion matrix could simultaneously be used to resist bacterial adhesion while increasing the overall concentration of TiO_2 nanoparticles. If a fouling-resistant surface coating could be used as a dispersion matrix without inhibiting the transport of reactive hydroxyl radicals and superoxide ions following TiO_2 UV exposure, the antifouling and antibacterial mechanisms could be simultaneously optimized.

The specificity of the crystalline nanopillars killing mechanism to gram-negative bacteria, due to membrane-structure, opens interesting opportunities to selectively control the selection and proliferation of gram-positive bacterial species from a mixed species population. Preliminary experiments with *S. aureus* demonstrate little loss of viability, likely due to the membrane-structure and spherical shape of the bacteria. Although there is a biophysical model of the mechanism for cicada wing killing, the surface architecture of the nanopillars used here differ significantly. The random crystal orientation and non-homogeneous inter-pillar spacing are notably different between these surfaces. Thus, further studies into the specifics of the killing mechanisms of the pillars would also be of interest. An alternative research path could investigate the nanopillars on flexible substrates. Beyond the material oriented questions concerning the stretching of the base substrate on nanopillar orientation and viability, testing the interaction of mammalian cells could lead to possible applications in flexible electronics.

CHAPTER 9

CONCLUSION

With the spread of antibiotic resistance and the rise of biofilm-associated HAIs arising from medical devices, there is a need to develop alternative strategies to mitigate the risk of bacterial infection without the use of antibiotics. The chemical properties of surfaces are known to influence bacterial adhesion; thus fouling-resistant coatings are applied to virtually all medical devices today to alter the surface chemistry of medical devices to improve resistance to bacterial contamination. As all materials are comprised of both chemical and physical properties, the effect of a material's physical properties on bacterial adhesion has been relatively unexplored in comparison to the influence of its chemical properties.

The first portion of this work focused on decoupling the physical properties of polymer hydrogels to understand the effect of fundamental material properties on bacterial interaction, independent of chemistry. PEG hydrogels were chosen as a model protein-resistant system while biopolymer agar hydrogels were chosen as a biopolymer "pro-adhesion" chemistry control. PEG and agar hydrogels were synthesized over a wide range of Young's moduli and challenged with two well-characterized bacterial pathogens, *E. coli* and *S. aureus*. The extent of surface colonization of each microbe was assessed after 2 and 24 hr, to monitor both bacterial adhesion and early biofilm formation. The primary finding of this study was that fewer bacteria adhered to softer hydrogels independent of hydrogel chemistry.

The influence of a materials physical properties was further investigated by decoupling the stiffness and thickness of PEG hydrogels. By manipulating the fabrication conditions, a library of hydrogels was produced with a range of stiffness and thickness each over three orders of magnitude. Hydrated AFM was used to ensure the stiffness and morphology of hydrogels remained consistent when manipulating hydrogel thickness. This study produced a previously unreported insight into the depth-sensitivity of *E. coli* and *S. aureus* attachment to soft-thin hydrogels, where each species attachment was influenced by the mechanics of an underlying support layer.

We further probed the effect of material stiffness on bacterial-surface interactions by studying the surface-associated transport of *S. aureus*. The effect of surface stiffness on the surface-associated transport of *S. aureus* was demonstrated for the first time using a series of PEG hydrogels and a chemical control films of PEG brushes. Stiff PEG hydrogels were found to induce significantly more surface engagement compared to chemically similar soft PEG hydrogels and PEG brush controls. Connecting this dynamic study with the previous static adhesion study, increased hydrogel stiffness was found to induce an increased rate of dynamic bacterial surface engagement in flow and an increased rate of permanent adhesion when allowed to settle to a surface. Together these studies indicate that stiffness is an important yet relatively unappreciated parameter in fouling-resistant coating design that can be tuned to non-specifically improve the fouling-resistance of hydrogels.

The second portion of this work was the development of a universal surface modification to limit bacterial adhesion. This collaborative effort produced a super-adhesive composite film comprised of polymer zwitterions and the catechol-adhesive

polydopamine that was demonstrated to effectively coat a variety of surfaces including planar surfaces and three-dimensional porous cellulose nanofibers. This platform was extended for the modification of hydrogels through simple solution-based processing. By harnessing the intrinsic swelling of hydrogels to drive the diffusion of pMPC/PDA, homogeneous functionalization was achieved without altering the rheological properties of the hydrogel. PMPC/PDA functionalized PEG and agar hydrogels displayed excellent resistance to fibrinogen adsorption and significantly reduced the adhesion of *E. coli* and *S. aureus* compared to unmodified hydrogel controls. Due to the non-specific nature of PDA adhesion, this solution based functionalization strategy can theoretically be used to functionalize any hydrogel system to improve its fouling resistance.

A final part of this dissertation explored novel antibacterial and antifouling films and discussed the methodology used to quantify the efficacy of each approach. The fouling resistance of roll-to-roll SLIPS films demonstrated excellent resistance to *E. coli* adhesion over a sustained challenge period. Sharklet AF™ patterned composite films containing the photocatalytic compound TiO_2 displayed synergistic resistance to the adhesion of bacteria due to the patterned microtopography and excellent non-specific biocidal activity following exposure to UV light. This synergistic antibacterial and antifouling performance were shown for soft polymeric films and hard ceramic materials. Finally, a unique contact-initiated killing mechanism using a film of crystalline nanostructures successfully inactivated gram-negative bacterial upon adhesion. Derived from the chemical and physical structure of each film, exploitable relationships with bacterial-surface interactions were investigated that could be used to selectively control bacterial adhesion and colonization.

There is not a single “magic bullet” that has been developed to replace antibiotics in the treatment and prevention of bacterial infections; rather a combination of approaches and practices will be necessary. The hydrogel structure-property relationships developed in this thesis are an example of an antibiotic-free approach towards bacterial infection prevention. To broaden the impact of this work beyond hydrogels, further research will be needed to connect and expand the structure-property relationships found here with other types of materials. The next generation of fouling-resistant materials for healthcare will be designed to integrate multiple materials with complementary or synergistic properties to mitigate the risk of bacterial infection without the use of antibiotics.

CHAPTER 10

SCIENTIFIC CONTRIBUTIONS

The work in this thesis has culminated in various publications, which are listed in this section. Additionally, dissemination of this work has taken place through various conference presentations and on-campus presentations within different organizations. Authors contributed equally (ǂ)

1. Li, Y.; John, J.; Kolewe, K. W.; Schiffman, J. D.; Carter, K. R. Scaling up Nature — Large Area Flexible Biomimetic Surfaces. ACS Appl. Mater. Interfaces 2015, 7 (42), 23439–23444.
2. Dobosz, K. M.ǂ; Kolewe, K. W.ǂ; Schiffman, J. D. Green Materials Science and Engineering Reduces Biofouling: Approaches for Medical and Membrane-Based Technologies. Front. Microbiol. 2015, 6, 1–8.
3. Kolewe, K.W.; Peyton, S. R.; Schiffman, J. D. Fewer Bacteria Adhere to Softer Hydrogels. ACS Appl. Mater. Interfaces 2015, 7 (35), 19562–19569.
4. Sui, S.; Wang, Y.; Kolewe, K.W.; Srajer, V.; Henning, R.; Schiffman, J. D.; Dimitrakopoulos, C.; Perry, S. L. Graphene-Based Microfluidics for Serial Crystallography. Lab Chip 2016, 16, 3082-3096.
5. Chang, C.-C.; Kolewe, K. W.; Li, Y.; Kosif, I.; Freeman, B. D.; Carter, K. R.; Schiffman, J. D.; Emrick, T. Underwater Superoleophobic Surfaces Prepared from Polymer Zwitterion/Dopamine Composite Coatings. Adv. Mater. Interfaces 2016, 3, 1500521.

6. Kolewe, K. W.;‡ Dobosz, K. M.;‡ Rieger K. A.; Chang, C.-C.; Emrick T.; Schiffman, J. D. Antifouling Electrospun Nanofiber Mats Functionalized with Polymer Zwitterions. ACS Appl. Mater. Interfaces 2016, 8 (41), 27585-27593.
7. Sae-un, P.; Kolewe, K.W.; Bai, Y.; Rice, E.; Schiffman, J.D.; Emrick, T.; Hoven, V. Antifouling Stripes Prepared from Clickable Zwitterionic Copolymers. Langmuir 2017, 33 (28), 7028-7035.
8. Kolewe, K. W.; Zhu, J.; Mako, N. R.; Nonnenmann, S. S.; Schiffman, J. D., Bacterial Adhesion is Effected by the Thickness and Stiffness of Poly(ethylene glycol) Hydrogels. Under revisions
9. Kolewe, K. W.; Kalasin, S.; Santore, M. M.; Schiffman, J. D., Mechanically Sensitive Surface Transport of *Staphylococcus aureus* MW2 on Poly(ethylene glycol) Hydrogels and Brushes. In preparation
10. Arellano, D. L. G.; Kolewe, K. W.; Champagne, V. K.; Burnett, E. K.; Dündar, F.; Schiffman, J. D.; Briseno, A. L. Biocidal Vertically Oriented Nanocrystals Initiated from Pencil-Drawn Graphene. In preparation
11. Birch, N. P.; Kolewe, K. W.; Digiovanni, T.; Champagne, V. K.; Schiffman, J. D. Self-assembled antibacterial metal nanoparticles in alkyd-based paints. In Preparation
12. Dündar, F.; Kolewe, K. W.; Homyak, B.; Schiffman, J. D.; Watkins, J. J. Bioinspired Photocatalytic Sharkskin via Solvent Assisted Nanoimprint Lithography with Antibacterial and Antifouling Activity. In preparation
13. Shave, M. S.; Kolewe, K. W.; Raman, V.; Forbes, N.; Schiffman, J. D.; Santore, M. M. Effects of *Escherichia coli* Motility and Surface Mechanics on Behavior in Flow. In preparation.

14. Sharma, A.; Kwak, J.; Kolewe, K. W.; Schiffman, J. D.; Forbes, N.; Lee, J. In Vitro Reconstituted Natural Mucins Recapitulate pH and Ion Dependent Biophysical Barrier to Bacteria and Small Molecule Diffusion. In preparation
15. Bai, Y.; Kolewe, K. W.; Chang, C.-C.; Schiffman, J.D.; Emrick, T. Bacteria Pick-up with Zwitterionic Droplets. In preparation

REFERENCES

(1) Fleming, A. On the Antibacterial Action of Cultures of a Penicillium, with Special Reference to Their Use in the Isolation of B. Influenzae. 1929. *Br. J. Exp. Pathol.* **1929**, *10*, 226–236.

(2) Ventola, C. L. The Antibiotic Resistance Crisis: Part 1: Causes and Threats. *P T A peer-reviewed J. Formul. Manag.* **2015**, *40*, 277–283.

(3) Arias, C. A.; Murray, B. E. Antibiotic-Resistant Bugs in the 21st Century — A Clinical Super-Challenge. *N. Engl. J. Med.* **2009**, *360*, 439–443.

(4) Zimlichman, E.; Henderson, D.; Tamir, O.; Franz, C.; Song, P.; Yamin, C. K.; Keohane, C.; Denham, C. R.; Bates, D. W. Health Care–Associated Infections. *JAMA Intern. Med.* **2013**, *173*, 2039.

(5) CDC. Antibiotic Resistance Threats in the United States, 2013. **2013**.

(6) Saint, S. Clinical and Economic Consequences of Nosocomial Catheter-Related Bacteriuria. *Am. J. Infect. Control* **2000**, *28*, 68–75.

(7) O'Grady, N. P.; Alexander, M.; Burns, L. A.; Dellinger, E. P.; Garland, J.; Heard, S. O.; Lipsett, P. A.; Masur, H.; Mermel, L. A.; Pearson, M. L.; *et al.* Guidelines for the Prevention of Intravascular Catheter-Related Infections. *Clin. Infect. Dis.* **2011**.

(8) Goede, M. R.; Coopersmith, C. M. Catheter-Related Bloodstream Infection. *Surgical Clinics of North America*, 2009, *89*, 463–474.

(9) Römling, U.; Kjelleberg, S.; Normark, S.; Nyman, L.; Uhlin, B. E.; Åkerlund, B. Microbial Biofilm Formation: A Need to Act. *J. Intern. Med.* **2014**, *276*, 98–110.

(10) Costerton, J. W. *The Role of Biofilms in Device-Related Infections*; **2007**.

(11) Von Eiff, C.; Jansen, B.; Kohnen, W.; Becker, K. Infections Associated with Medical Devices: Pathogenesis, Management and Prophylaxis. *Drugs* **2005**, *65*, 179–214.

(12) Hall-Stoodley, L.; Costerton, J. W.; Stoodley, P. Bacterial Biofilms: From the Natural Environment to Infectious Diseases. *Nat. Rev. Microbiol.* **2004**, *2*, 95–108.

(13) Costerton, J. W. Bacterial Biofilms: A Common Cause of Persistent Infections. *Science.* **1999**, *284*, 1318–1322.

(14) An, Y. H.; Friedman, R. J. Concise Review of Mechanisms of Bacterial Adhesion to Biomaterial Surfaces. *J. Biomed. Mater. Res.* **1998**, *43*, 338–348.

(15) van Loosdrecht, M. C.; Lyklema, J.; Norde, W.; Zehnder, a J. Influence of Interfaces on Microbial Activity. *Microbiol. Rev.* **1990**, *54*, 75–87.

(16) Poortinga, A. T.; Bos, R.; Norde, W.; Busscher, H. J. *Electric Double Layer Interactions in Bacterial Adhesion to Surfaces*. **2002**, *47*, 1-32.

(17) Hermansson, M. The DLVO Theory in Microbial Adhesion. *Colloids Surfaces B Biointerfaces* **1999**, *14*, 105–119.

(18) Hori, K.; Matsumoto, S. Bacterial Adhesion: From Mechanism to Control. *Biochem. Eng. J.* **2010**, *48*, 424–434.

(19) Katsikogianni, M.; Missirlis, Y. F. Concise Review of Mechanisms of Bacterial Adhesion to Biomaterials and of Techniques Used in Estimating Bacteria-Material Interactions. *Eur. Cell. Mater.* **2004**, *8*, 37–57.

(20) Foster, T. J.; Höök, M. Surface Protein Adhesins of Staphylococcus Aureus. *Trends Microbiol.* **1998**, *6*, 484–488.

(21) Götz, F. Staphylococcus and Biofilms. *Molecular Microbiology*, **2002**, *43*, 1367–1378.

(22) Francius, G.; Polyakov, P.; Merlin, J.; Abe, Y.; Ghigo, J.-M.; Merlin, C.; Beloin, C.; Duval, J. F. L. Bacterial Surface Appendages Strongly Impact Nanomechanical and Electrokinetic Properties of Escherichia Coli Cells Subjected to Osmotic Stress. *PLoS One* **2011**, *6*, e20066.

(23) Bullitt, E.; Makowski, L. Structural Polymorphism of Bacterial Adhesion Pili. *Nature* **1995**, *373*, 164–167.

(24) Thomas, W. E. Mechanochemistry of Receptor-Ligand Bonds. *Curr. Opin. Struct. Biol.* **2009**, *19*, 50–55.

(25) Persat, A.; Inclan, Y. F.; Engel, J. N.; Stone, H. A.; Gitai, Z. Type IV Pili Mechanochemically Regulate Virulence Factors in Pseudomonas Aeruginosa. *Proc. Natl. Acad. Sci. U. S. A.* **2015**, *112*, 7563–7568.

(26) Costerton, J. W.; Lewandowski, Z.; Caldwell, D. E.; Korber, D. R.; LappinScott, H. M. Microbial Biofilms. *Microb. Biofilms.* **1995**, *49*, 711–745.

(27) Mah, T. F. C.; O'Toole, G. A. Mechanisms of Biofilm Resistance to Antimicrobial Agents. *Trends Microbiol.* **2001**, *9*, 34–39.

(28) Singh, R.; Paul, D.; Jain, R. Biofilms: Implications in Bioremediation. *TRENDS Microbiol.* **2006,** *14*, 389-397.

(29) Chmielewski, R. a. N.; Frank, J. F. Biofilm Formation and Control in Food Processing Facilities. *Compr. Rev. Food Sci. Food Saf.* **2003**, *2*, 22–32.

(30) Davies, D. Understanding Biofilm Resistance to Antibacterial Agents. *Nat. Rev. Drug Discov.* **2003**, *2*, 114–122.

(31) Stoodley, P.; Sauer, K.; Davies, D. G.; Costerton, J. W. Biofilms as Complex Differentiated Communities. *Annu. Rev. Microbiol.* **2002**, *56*, 187–209.

(32) Flemming, H.-C.; Wingender, J. The Biofilm Matrix. *Nat. Rev. Microbiol.* **2010**, *8*, 623–633.

(33) Dunne, W. Bacterial Adhesion: Seen Any Good Biofilms Lately? *Clin. Microbiol. Rev.* **2002**, *15*.

(34) Stewart, P. S.; Costerton, J. W. Antibiotic Resistance of Bacteria in Biofilms. *Lancet* **2001**, *358*, 135–138.

(35) Renner, L. D.; Weibel, D. B. Physicochemical Regulation of Biofilm Formation. *MRS Bull.* **2011**, *36*, 347–355.

(36) Fundeanu, I.; van der Mei, H. C.; Schouten, A. J.; Busscher, H. J. Polyacrylamide Brush Coatings Preventing Microbial Adhesion to Silicone Rubber. *Colloids Surfaces B Biointerfaces* **2008**, *64*, 297–301.

(37) Harding, J. L.; Reynolds, M. M. Combating Medical Device Fouling. *Trends Biotechnol.* **2014**, *32*, 140–146.

(38) Burt, S. Essential Oils: Their Antibacterial Properties and Potential Applications in Foods--a Review. *Int. J. Food Microbiol.* **2004**, *94*, 223–253.

(39) Kavanaugh, N. L.; Ribbeck, K. Selected Antimicrobial Essential Oils Eradicate Pseudomonas Spp. and Staphylococcus Aureus Biofilms. *Appl. Environ. Microbiol.* **2012**, *78*, 4057–4061.

(40) Hazer, D. B.; Mut, M.; Dinçer, N.; Saribas, Z.; Hazer, B.; Ozgen, T. The Efficacy of Silver-Embedded Polypropylene-Grafted Polyethylene Glycol-Coated Ventricular Catheters on Prevention of Shunt Catheter Infection in Rats. *Childs. Nerv. Syst.* **2012**, *28*, 839–846.

(41) Hetrick, E. M.; Schoenfisch, M. H. Reducing Implant-Related Infections: Active Release Strategies. *Chem. Soc. Rev.* **2006**, *35*, 780–789.

(42) Xiu, Z. M.; Zhang, Q. B.; Puppala, H. L.; Colvin, V. L.; Alvarez, P. J. J. Negligible Particle-Specific Antibacterial Activity of Silver Nanoparticles. *Nano Lett.* **2012**, *12*, 4271–4275.

(43) Rieger, K. A.; Cho, H. J.; Yeung, H. F.; Fan, W.; Schiffman, J. D. Antimicrobial Activity of Silver Ions Released from Zeolites Immobilized on Cellulose Nanofiber Mats. *ACS Appl. Mater. Interfaces* **2016**, *8*, 3032–3040.

(44) Silver, S. Bacterial Silver Resistance: Molecular Biology and Uses and Misuses of Silver Compounds. *FEMS Microbiol. Rev.* **2003**, *27*, 341–353.

(45) Finley, P. J.; Norton, R.; Austin, C.; Mitchell, A.; Zank, S.; Durham, P. Unprecedented Silver Resistance in Clinically Isolated Enterobacteriaceae: Major Implications for Burn and Wound Management. *Antimicrob. Agents Chemother.* **2015**, *59*, 4734–4741.

(46) Gunawan, C.; Marquis, C. P.; Amal, R.; Harry, E. J. Widespread Nanosilver Use: Genuine Potential for Microbial Resistance. *Perspective* **2017**, *11*, 3438–3445.

(47) Brunet, N. a; Lyon, D. Y.; Alvarez, P. J. J. Comparative Photoactivity and Antibacterial Properties of C 60 Fullerenes and Titanium Dioxide Nanoparticles. *Environ. Sci. Technol.* **2009**, *43*, 4355–4360.

(48) Li, Y.; Zhang, W.; Niu, J.; Chen, Y. Mechanism of Photogenerated Reactive Oxygen Species and Correlation with the Antibacterial Properties of Engineered Metal-Oxide Nanoparticles. *ACS Nano* **2012**, *6*, 5164–5173.

(49) Pogodin, S.; Hasan, J.; Baulin, V. A.; Webb, H. K.; Truong, V. K.; Phong Nguyen, T. H.; Boshkovikj, V.; Fluke, C. J.; Watson, G. S.; Watson, J. A.; *et al.* Biophysical Model of Bacterial Cell Interactions with Nanopatterned Cicada Wing Surfaces. *Biophys. J.* **2013**, *104*, 835–840.

(50) Ivanova, E. P.; Hasan, J.; Webb, H. K.; Truong, V. K.; Watson, G. S.; Watson, J. A.; Baulin, V. A.; Pogodin, S.; Wang, J. Y.; Tobin, M. J.; *et al.* Natural Bactericidal Surfaces: Mechanical Rupture of Pseudomonas Aeruginosa Cells by Cicada Wings. *Small* **2012**, *8*, 2489–2494.

(51) Ivanova, E. P.; Hasan, J.; Webb, H. K.; Gervinskas, G.; Juodkazis, S.; Truong, V. K.; Wu, A. H. F.; Lamb, R. N.; Baulin, V. A.; Watson, G. S.; *et al.* Bactericidal Activity of Black Silicon. *Nat. Commun.* **2013**, *4*, 2838.

(52) Ostrikov, K.; Macgregor-ramiasa, M.; Cavallaro, A.; Sengstock, C.; Lopian, M.; Motemani, Y. Influence of Nanoscale Topology on Bactericidal Efficiency of Black Silicon Surfaces. *Nanotechnology* **2017**, *28*, 1–9.

(53) Peppas, N. A.; Keys, K. B.; Torres-Lugo, M.; Lowman, A. M. Poly (Ethylene Glycol)-Containing Hydrogels in Drug Delivery. *J. Control. Release* **1999**, *62*, 81–87.

(54) Kingshott, P.; Griesser, H. J. Surfaces That Resist Bioadhesion. *Curr. Opin. Solid State Mater. Sci.* **1999**, *4*, 403–412.

(55) Kane, R. S.; Deschatelets, P.; Whitesides, G. M. Kosmotropes Form the Basis of Protein-Resistant Surfaces. *Langmuir* **2003**, *19*, 2388–2391.

(56) Banerjee, I.; Pangule, R. C.; Kane, R. S. Antifouling Coatings: Recent Developments in the Design of Surfaces That Prevent Fouling by Proteins, Bacteria, and Marine Organisms. *Adv. Mater.* **2011**, *23*, 690–718.

(57) Hucknall, A.; Rangarajan, S.; Chilkoti, A. In Pursuit of Zero: Polymer Brushes That Resist the Adsorption of Proteins. *Adv. Mater.* **2009**, *21*, 2441–2446.

(58) Schlenoff, J. B. Zwitteration: Coating Surfaces with Zwitterionic Functionality to Reduce Nonspecific Adsorption. *Langmuir* **2014**, *30*, 9625–9636.

(59) Chen, S.; Li, L.; Zhao, C.; Zheng, J. Surface Hydration: Principles and Applications toward Low-Fouling/nonfouling Biomaterials. *Polymer (Guildf).* **2010**, *51*, 5283–5293.

(60) Hower, J. C.; Bernards, M. T.; Chen, S.; Tsao, H. K.; Sheng, Y. J.; Jiang, S. Hydration of "Nonfouling" functional Groups. *J. Phys. Chem. B* **2009**, *113*, 197–201.

(61) Ueda, T.; Oshida, H.; Kurita, K.; Ishihara, K.; Nakabayashi, N. Perparation of 2-Methacryloyloxyethyl Phosphorylcholine Copolymers with Alkyl Methacrylates and Their Blood Compatibility. *Polymer Journal*, **1992**, *24*, 1259–1269.

(62) Jiang, S.; Cao, Z. Ultralow-Fouling, Functionalizable, and Hydrolyzable Zwitterionic Materials and Their Derivatives for Biological Applications. *Adv. Mater.* **2010**, *22*, 920–932.

(63) Keefe, A. J.; Brault, N. D.; Jiang, S. Suppressing Surface Reconstruction of Superhydrophobic PDMS Using a Superhydrophilic Zwitterionic Polymer. *Biomacromolecules* **2012**, *13*, 1683-1687.

(64) Zhang, Z.; Chao, T.; Liu, L. Y.; Cheng, G.; Ratner, B. D.; Jiang, S. Zwitterionic Hydrogels: An in Vivo Implantation Study. *J. Biomater. Sci. Ed.* **2009**, *20*, 1845–1859.

(65) Zhang, L.; Cao, Z.; Bai, T.; Carr, L.; Ella-Menye, J.-R.; Irvin, C.; Ratner, B. D.; Jiang, S. Zwitterionic Hydrogels Implanted in Mice Resist the Foreign-Body Reaction. *Nat. Biotechnol.* **2013**, *31*, 553–556.

(66) Cao, B.; Li, L.; Tang, Q.; Cheng, G. The Impact of Structure on Elasticity, Switchability, Stability and Functionality of an All-in-One Carboxybetaine Elastomer. *Biomaterials* **2013**, *34*, 7592–7600.

(67) Ning, J.; Li, G.; Haraguchi, K. Synthesis of Highly Stretchable, Mechanically Tough, Zwitterionic Sulfobetaine Nanocomposite Gels with Controlled Thermosensitivities. *Macromolecules* **2013**, *46*, 5317–5328.

(68) Yin, H.; Akasaki, T.; Lin Sun, T.; Nakajima, T.; Kurokawa, T.; Nonoyama, T.; Taira, T.; Saruwatari, Y.; Ping Gong, J. Double Network Hydrogels from Polyzwitterions: High Mechanical Strength and Excellent Anti-Biofouling Properties. *J. Mater. Chem. B* **2013**, *1*, 3685–3693.

(69) Carr, L. R.; Zhou, Y.; Krause, J. E.; Xue, H.; Jiang, S. Uniform Zwitterionic Polymer Hydrogels with a Nonfouling and Functionalizable Crosslinker Using Photopolymerization. *Biomaterials* **2011**, *32*, 6893–6899.

(70) Cao, B.; Tang, Q.; Li, L.; Humble, J.; Wu, H.; Liu, L.; Cheng, G. Switchable Antimicrobial and Antifouling Hydrogels with Enhanced Mechanical Properties. *Adv. Healthc. Mater.* **2013**, *2*, 1096–1102.

(71) Magin, C. M.; Cooper, S. P.; Brennan, A. B. Non-Toxic Antifouling Strategies. *Mater. Today* **2010**, *13*, 36–44.

(72) Chung, K. K.; Schumacher, J. F.; Sampson, E. M.; Burne, R. a; Antonelli, P. J.; Brennan, A. B. Impact of Engineered Surface Microtopography on Biofilm Formation of Staphylococcus Aureus. *Biointerphases* **2007**, *2*, 89–94.

(73) Rizzello, L.; Cingolani, R.; Pompa, P. P. Nanotechnology Tools for Antibacterial Materials. *Nanomedicine (Lond).* **2013**, *8*, 807–821.

(74) Bazaka, K.; Crawford, R. J.; Ivanova, E. P. Do Bacteria Differentiate between Degrees of Nanoscale Surface Roughness? *Biotechnol. J.* **2011**, *6*, 1103–1114.

(75) Scardino, A. J.; de Nys, R. Mini Review: Biomimetic Models and Bioinspired Surfaces for Fouling Control. *Biofouling* **2011**, *27*, 73–86.

(76) Perera-Costa, D.; Bruque, J. M.; González-Martín, M. L.; Gómez-García, A. C.; Vadillo-Rodríguez, V. Studying the Influence of Surface Topography on Bacterial Adhesion Using Spatially Organized Microtopographic Surface Patterns. *Langmuir* **2014**, *30*, 4633–4641.

(77) Wong, T.-S.; Kang, S. H.; Tang, S. K. Y.; Smythe, E. J.; Hatton, B. D.; Grinthal, A.; Aizenberg, J. Bioinspired Self-Repairing Slippery Surfaces with Pressure-Stable Omniphobicity. *Nature* **2011**, *477*, 443–447.

(78) Langer, R.; Tirrell, D. a. Designing Materials for Biology and Medicine. *Nature* **2004**, *428*, 487–492.

(79) Hoffman, A. S. Hydrogels for Biomedical Applications. *Adv. Drug Deliv. Rev.* **2002**, *64*, 18–23.

(80) Varshosaz, J.; Zaki, M. R.; Minaiyan, M.; Banoozadeh, J. Preparation, Optimization, and Screening of the Effect of Processing Variables on Agar Nanospheres Loaded with Bupropion HCl by a D-Optimal Design. *Biomed Res. Int.* **2015**, *2015*.

(81) Matsuo, M.; Tanaka, T.; Ma, L. Gelation Mechanism of Agarose and κ-Carrageenan Solutions Estimated in Terms of Concentration Fluctuation. *Polymer (Guildf).* **2002**, *43*, 5299–5309.

(82) Xiong, J. Y.; Narayanan, J.; Liu, X. Y.; Chong, T. K.; Chen, S. B.; Chung, T. S. Topology Evolution and Gelation Mechanism of Agarose Gel. *J. Phys. Chem. B* **2005**, *109*, 5638–5643.

(83) Maaloum, M.; Pernodet, N.; Tinland, B. Agarose Gel Structure Using Atomic Force Microscopy: Gel Concentration and Ionic Strength Effects. *Electrophoresis* **1998**, *19*, 1606–1610.

(84) Belas, R. Biofilms, Flagella, and Mechanosensing of Surfaces by Bacteria. *Trends Microbiol.* **2014**, *22*, 1–11.

(85) Ellison, C.; Brun, Y. V. Mechanosensing : A Regulation Sensation. *Curr. Biol.* **2014**, *25*, R113–R115.

(86) Grozea, C. M.; Walker, G. C. Approaches in Designing Non-Toxic Polymer Surfaces to Deter Marine Biofouling. *Soft Matter* **2009**, *5*, 4088-4100.

(87) Gu, H.; Ren, D. Materials and Surface Engineering to Control Bacterial Adhesion and Biofilm Formation: A Review of Recent Advances. *Front. Chem. Sci. Eng.* **2014**, *8*, 20–33.

(88) Dobosz, K. M.; Kolewe, K. W.; Schiffman, J. D. Green Materials Science and Engineering Reduces Biofouling: Approaches for Medical and Membrane-Based Technologies. *Front. Microbiol.* **2015**, *6*, 1–8.

(89) Meel, C.; Kouzel, N.; Oldewurtel, E. R.; Maier, B. Three-Dimensional Obstacles for Bacterial Surface Motility. *Small* **2012**, *8*, 530–534.

(90) Bakker, D. P.; Van der Plaats, a.; Verkerke, G. J.; Busscher, H. J.; Van der Mei, H. C. Comparison of Velocity Profiles for Different Flow Chamber Designs Used in Studies of Microbial Adhesion to Surfaces. *Appl. Environ. Microbiol.* **2003**, *69*, 6280–6287.

(91) Lichter, J. a; Thompson, M. T.; Delgadillo, M.; Nishikawa, T.; Rubner, M. F.; Van Vliet, K. J. Substrata Mechanical Stiffness Can Regulate Adhesion of Viable Bacteria. *Biomacromolecules* **2008**, *9*, 1571–1578.

(92) Saha, N.; Monge, C.; Dulong, V.; Picart, C.; Glinel, K. Influence of Polyelectrolyte Film Stiffness on Bacterial Growth. *Biomacromolecules* **2013**, *14*, 520–528.

(93) Song, F.; Ren, D. Stiffness of Cross-Linked Poly(dimethylsiloxane) Affects Bacterial Adhesion and Antibiotic Susceptibility of Attached Cells. *Langmuir* **2014**, *30*, 10354–10362.

(94) Mata, A.; Fleischman, A. J.; Roy, S. Characterization of Polydimethylsiloxane (PDMS) Properties for Biomedical Micro/nanosystems. *Biomed. Microdevices* **2005**, *7*, 281–293.

(95) Lin-Gibson, S.; Bencherif, S.; Cooper, J. a; Wetzel, S. J.; Antonucci, J. M.; Vogel, B. M.; Horkay, F.; Washburn, N. R. Synthesis and Characterization of PEG Dimethacrylates and Their Hydrogels. *Biomacromolecules* **2004**, *5*, 1280–1287.

(96) Trappmann, B.; Gautrot, J. E.; Connelly, J. T.; Strange, D. G. T.; Li, Y.; Oyen, M. L.; Cohen Stuart, M. a.; Boehm, H.; Li, B.; Vogel, V.; *et al.* Extracellular-Matrix Tethering Regulates Stem-Cell Fate. *Nat. Mater.* **2012**, *11*, 742–742.

(97) Oyen, M. L. Mechanical Characterisation of Hydrogel Materials. *Int. Mater. Rev.* **2014**, *59*, 44–59.

(98) Beloin, C.; Roux, A.; Ghigo, J. Escherichia Coli Biofilms. *Curr Top Microbiol Immunol.*, **2008**, 249–289.

(99) Krishnan, S.; Weinman, C. J.; Ober, C. K. Advances in Polymers for Anti-Biofouling Surfaces. *J. Mater. Chem.* **2008**, *18*, 3405–3413.

(100) Beloin, C.; Houry, A.; Froment, M.; Ghigo, J. M.; Henry, N. A Short-Time Scale Colloidal System Reveals Early Bacterial Adhesion Dynamics. *PLoS Biol.* **2008**, *6*, 1549–1558.

(101) Lawrence, E. L.; Turner, I. G. Materials for Urinary Catheters: A Review of Their History and Development in the UK. *Med. Eng. Phys.* **2005**, *27*, 443–453.

(102) Herrick, W. G.; Nguyen, T. V; Sleiman, M.; McRae, S.; Emrick, T. S.; Peyton, S. R. PEG-Phosphorylcholine Hydrogels as Tunable and Versatile Platforms for Mechanobiology. *Biomacromolecules* **2013**, *14*, 2294–2304.

(103) Liu, V. A.; Bhatia, S. N. Three-Dimensional Patterning of Hydrogels Containing Living Cells. *Biomed Microdevices* **2002**, *4*, 257–266.

(104) Ayyad, O.; Muñoz-Rojas, D.; Agulló, N.; Borrós, S.; Gómez-Romero, P. High-Concentration Compact Agar Gels from Hydrothermal Synthesis. *Soft Matter* **2010**, *6*, 2389-2391.

(105) Shull, K. R.; Ahn, D.; Chen, W.-L.; Flanigan, C. M.; Crosby, A. J. Axisymmetric Adhesion Tests of Soft Materials. *Macromol. Chem. Phys.* **1998**, *199*, 489–511.

(106) Canal, T.; Peppas, N. Correlation between Mesh Size and Equilibrium Degree of Swelling of Polymeric Networks. *J. Biomed. Mater. Res.* **1989**, *23*, 1183-1193.

(107) Pang, Y. Y.; Schwartz, J.; Thoendel, M.; Ackermann, L. W.; Horswill, A. R.; Nauseef, W. M. Agr-Dependent Interactions of Staphylococcus Aureus USA300 with Human Polymorphonuclear Neutrophils. *J. Innate Immun.* **2010**, *2*, 546–559.

(108) Fletcher, M.; Loeb, G. I. Influence of Substratum Characteristics on the Attachment of a Marine Pseudomonad to Solid Surfaces Influence of Substratum Characteristics on the Attachment of a Marine Pseudomonad to Solid Surfaces. *Appl. Enviromental Microbiol.* **1979**, *37*, *67-72*.

(109) Schiffman, J. D.; Wang, Y.; Giannelis, E. P.; Elimelech, M. Biocidal Activity of Plasma Modified Electrospun Polysulfone Mats Functionalized with Polyethyleneimine-Capped Silver Nanoparticles. *Langmuir* **2011**, *27*, 13159–13164.

(110) Fux, C. a; Wilson, S.; Stoodley, P. Detachment Characteristics and Oxacillin Resistance of Staphoccocus Aureus Biofilm Emboli in an In Vitro Catheter Infection Model. *J. Bacteriol.* **2004**, *186*, 4486–4491.

(111) Peyton, S. R.; Kalcioglu, Z. I.; Cohen, J. C.; Runkle, A. P.; Van Vliet, K. J.; Lauffenburger, D. a; Griffith, L. G. Marrow-Derived Stem Cell Motility in 3D Synthetic Scaffold Is Governed by Geometry along with Adhesivity and Stiffness. *Biotechnol. Bioeng.* **2011**, *108*, 1181–1193.

(112) Clarke, S. R.; Foster, S. J. Surface Adhesins of Staphylococcus Aureus. *Advances in Microbial Physiology*, **2006**, *51*, 187–224.

(113) Sauer, K.; Camper, A. K. Characterization of Phenotypic Changes in Pseudomonas Putida in Response to Surface-Associated Growth Characterization of Phenotypic Changes in Pseudomonas Putida in Response to Surface-Associated Growth. *J. Bacteriol.* **2001**, *183*, 6579–6589.

(114) Herrwerth, S.; Eck, W.; Reinhardt, S.; Grunze, M. Factors That Determine the Protein Resistance of Oligoether Self-Assembled Monolayers - Internal Hydrophilicity, Terminal Hydrophilicity, and Lateral Packing Density. *J. Am. Chem. Soc.* **2003**, *125*, 9359–9366.

(115) Galluzzi, M.; Biswas, C. S.; Wu, Y.; Wang, Q.; Du, B.; Stadler, F. J. Space-Resolved Quantitative Mechanical Measurements of Soft and Supersoft Materials by Atomic Force Microscopy. *NPG Asia Mater.* **2016**, *8*, e327.

(116) González-Méijome, J. M.; López-Alemany, A.; Almeida, J. B.; Parafita, M. A.; Refojo, M. F. Microscopic Observation of Unworn Siloxane-Hydrogel Soft Contact Lenses by Atomic Force Microscopy. *J. Biomed. Mater. Res. - Part B Appl. Biomater.* **2006**, *76*, 412–418.

(117) Kim, S. H.; Opdahl, A.; Marmo, C.; Somorjai, G. a. AFM and SFG Studies of pHEMA-Based Hydrogel Contact Lens Surfaces in Saline Solution: Adhesion, Friction, and the Presence of Non-Crosslinked Polymer Chains at the Surface. *Biomaterials* **2002**, *23*, 1657–1666.

(118) Lira, M.; Santos, L.; Azeredo, J.; Yebra-Pimentel, E.; Real Oliveira, M. E. C. D. Comparative Study of Silicone-Hydrogel Contact Lenses Surfaces before and after Wear Using Atomic Force Microscopy. *J. Biomed. Mater. Res. - Part B Appl. Biomater.* **2008**, *85*, 361–367.

(119) Barbucci, R.; Pasqui, D.; Favaloro, R.; Panariello, G. A Thixotropic Hydrogel from Chemically Cross-Linked Guar Gum: Synthesis, Characterization and Rheological Behaviour. *Carbohydr. Res.* **2008**, *343*, 3058–3065.

(120) Tronci, G.; Grant, C. A.; Thomson, N. H.; Russell, S. J.; Wood, D. J. Multi-Scale Mechanical Characterization of Highly Swollen Photo-Activated Collagen Hydrogels. *J. R. Soc. Interface* **2015**, *12*, 20141079.

(121) O'Toole, G. A.; Wong, G. C. L. Sensational Biofilms: Surface Sensing in Bacteria. *Curr. Opin. Microbiol.* **2016**, *30*, 139–146.

(122) Truong, V. K.; Lapovok, R.; Estrin, Y. S.; Rundell, S.; Wang, J. Y.; Fluke, C. J.; Crawford, R. J.; Ivanova, E. P. The Influence of Nano-Scale Surface Roughness on Bacterial Adhesion to Ultrafine-Grained Titanium. *Biomaterials* **2010**, *31*, 3674–3683.

(123) Kolewe, K.; Peyton, S. R.; Schiffman, J. D. Fewer Bacteria Adhere to Softer Hydrogels. *ACS Appl. Mater. Interfaces* **2015**, *7*, 19562–19569.

(124) Zodrow, K. R.; Schiffman, J. D.; Elimelech, M. Biodegradable Polymer (PLGA) Coatings Featuring Cinnamaldehyde and Carvacrol Mitigate Biofilm Formation. *Langmuir* **2012**, *28*, 13993–13999.

(125) Drira, Z.; Yadavalli, V. K. Nanomechanical Measurements of Polyethylene Glycol Hydrogels Using Atomic Force Microscopy. *J. Mech. Behav. Biomed. Mater.* **2013**, *18*, 20–28.

(126) Costa, K. D.; Yin, F. C. Analysis of Indentation: Implications for Measuring Mechanical Properties with Atomic Force Microscopy. *J. Biomech. Eng.* **1999**, *121*, 462–471.

(127) Stammen, J. A.; Williams, S.; Ku, D. N.; Guldberg, R. E. Mechanical Properties of a Novel PVA Hydrogel in Shear and Unconfined Compression. *Biomaterials* **2001**, *22*, 799–806.

(128) Busscher, H. J.; van der Mei, H. C. How Do Bacteria Know They Are on a Surface and Regulate Their Response to an Adhering State? *PLoS Pathog.* **2012**, *8*, 1–3.

(129) Bos, R.; Van Der Mei, H. C.; Busscher, H. J. Physico-Chemistry of Initial Microbial Adhesive Interactions - Its Mechanisms and Methods for Study. *FEMS Microbiol. Rev.* **1999**, *23*, 179–229.

(130) Tuson, H. H.; Weibel, D. B. Bacteria–surface Interactions. *Soft Matter* **2013**, *9*, 4368–4380.

(131) Anselme, K.; Davidson, P.; Popa, A. M.; Giazzon, M.; Liley, M.; Ploux, L. The Interaction of Cells and Bacteria with Surfaces Structured at the Nanometre Scale. *Acta Biomater.* **2010**, *6*, 3824–3846.

(132) Iscla, I.; Wray, R.; Blount, P. The Oligomeric State of the Truncated Mechanosensitive Channel of Large Conductance Shows No Variance in Vivo. *Protein Sci.* **2011**, *20*, 1638–1642.

(133) Li, Z. J.; Mohamed, N.; Ross, J. M. Shear Stress Affects the Kinetics of Staphylococcus Aureus Adhesion to Collagen. *Biotechnol. Prog.* **2000**, *16*, 1086–1090.

(134) Islam, N.; Kim, Y.; Ross, J. M.; Marten, M. R. Proteomic Analysis of Staphylococcus Aureus Biofilm Cells Grown under Physiologically Relevant Fluid Shear Stress Conditions. *Proteome Sci.* **2014**, *12*, 21.

(135) Chen, Y.; Norde, W.; Mei, H. C. Van Der; Busscher, H. J. Bacterial Cell Surface Deformation under External Loading. *MBio* **2012**, *3*, 1–7.

(136) Persat, A.; Nadell, C. D.; Kim, M. K.; Ingremeau, F.; Siryaporn, A.; Drescher, K.; Wingreen, N. S.; Bassler, B. L.; Gitai, Z.; Stone, H. A. The Mechanical World of Bacteria. *Cell* **2015**, *161*, 988–997.

(137) Soyer, M.; Duménil, G. Introducing Shear Stress in the Study of Bacterial Adhesion. *J. Vis. Exp.* **2011**, e3241.

(138) Nilsson, L. M.; Thomas, W. E.; Trintchina, E.; Vogel, V.; Sokurenko, E. V. Catch Bond-Mediated Adhesion without a Shear Threshold: TRIMANNOSE VERSUS MONOMANNOSE INTERACTIONS WITH THE FimH ADHESIN OF ESCHERICHIA COLI. *J. Biol. Chem.* **2006**, *281*, 16656–16663.

(139) Thomas, W. E.; Trintchina, E.; Forero, M.; Vogel, V.; Sokurenko, E. V. Bacterial Adhesion to Target Cells Enhanced by Shear Force. *Cell* **2002**, *109*, 913–923.

(140) Anderson, B. N.; Ding, A. M.; Nilsson, L. M.; Kusuma, K.; Tchesnokova, V.; Vogel, V.; Sokurenko, E. V; Thomas, W. E. Weak Rolling Adhesion Enhances Bacterial Surface Colonization. *J. Bacteriol.* **2007**, *189*, 1794–1802.

(141) Thomas, W. E.; Nilsson, L. M.; Forero, M.; Sokurenko, E. V; Vogel, V. Shear-Dependent "Stick-and-Roll" Adhesion of Type 1 Fimbriated Escherichia Coli. *Mol. Microbiol.* **2004**, *53*, 1545–1557.

(142) Weaver, W. M.; Dharmaraja, S.; Milisavljevic, V.; Di Carlo, D. The Effects of Shear Stress on Isolated Receptor-Ligand Interactions of Staphylococcus Epidermidis and Human Plasma Fibrinogen Using Molecularly Patterned Microfluidics. *Lab Chip* **2011**, *11*, 883–889.

(143) Ding, a. M.; Palmer, R. J.; Cisar, J. O.; Kolenbrander, P. E. Shear-Enhanced Oral Microbial Adhesion. *Appl. Environ. Microbiol.* **2010**, *76*, 1294–1297.

(144) Henrichsen, J. Bacterial Surface Translocation: A Survey and a Classification. *Bacteriol. Rev.* **1972**, *36*, 478–503.

(145) Kearns, D. B. A Field Guide to Bacterial Swarming Motility. *Nat. Rev. Microbiol.* **2010**, *8*, 634–644.

(146) Son, K.; Brumley, D. R.; Stocker, R. Live from under the Lens: Exploring Microbial Motility with Dynamic Imaging and Microfluidics. *Nat. Rev. Microbiol.* **2015**, *13*, 761–775.

(147) Skerker, J. M.; Berg, H. C. Direct Observation of Extension and Retraction of Type IV Pili. *Proc. Natl. Acad. Sci. U. S. A.* **2001**, *98*, 6901–6904.

(148) Uyama, Y.; Kato, K.; Ikada, Y. *Surface Modification of Polymers by Grafting*; **1998**; *137*, 1-39.

(149) Schneider, K. Mechanical Properties of Polymers at Surfaces and Interfaces. *Polym. Surfaces Interfaces* **2008**, 139–160.

(150) Gon, S.; Bendersky, M.; Ross, J. L.; Santore, M. M. Manipulating Protein Adsorption Using a Patchy Protein-Resistant Brush. *Langmuir* **2010**, *26*, 12147–12154.

(151) Roosjen, A.; Van Der Mei, H. C.; Busscher, H. J.; Norde, W. Microbial Adhesion to Poly(ethylene Oxide) Brushes: Influence of Polymer Chain Length and Temperature. *Langmuir* **2004**, *20*, 10949–10955.

(152) Gon, S.; Fang, B.; Santore, M. M. Interaction of Cationic Proteins and Polypeptides with Biocompatible Cationically-Anchored PEG Brushes. *Macromolecules* **2011**, *44*, 8161–8168.

(153) Fu, Z.; Santore, M. M. Poly(ethylene Oxide) Adsorption onto Chemically Etched Silicates by Brewster Angle Reflectivity. *Colloids Surfaces A Physicochem. Eng. Asp.* **1998**, *135*, 63–75.

(154) Wertz, C. F.; Santore, M. M. Adsorption and Relaxation Kinetics of Albumin and Fibrinogen on Hydrophobic Surfaces: Single-Species and Competitive Behavior. *Langmuir* **1999**, *15*, 8884–8894.

(155) Kalasin, S.; Santore, M. M. Engineering Nanoscale Surface Features to Sustain Microparticle Rolling in Flow. *ACS Nano* **2015**, *9*, 4706–4716.

(156) Fang, B.; Gon, S.; Nüsslein, K.; Santore, M. M. Surfaces for Competitive Selective Bacterial Capture from Protein Solutions. *ACS Appl. Mater. Interfaces* **2015**, *7*, 10275–10282.

(157) Schindelin, J.; Arganda-Carreras, I.; Frise, E.; Kaynig, V.; Longair, M.; Pietzsch, T.; Preibisch, S.; Rueden, C.; Saalfeld, S.; Schmid, B.; *et al.* Fiji: An Open-Source Platform for Biological-Image Analysis. *Nat. Methods* **2012**, *9*, 676–682.

(158) Goldman, A. J.; Cox, R. G.; Brenner, H. Slow Viscous Motion of a Sphere Parallel to a Plane wall—I Motion through a Quiescent Fluid. *Chemical Engineering Science*, 1967, *22*, 637–651.

(159) Guégan, C.; Garderes, J.; Le Pennec, G.; Gaillard, F.; Fay, F.; Linossier, I.; Herry, J. M.; Fontaine, M. N. B.; Réhel, K. V. Alteration of Bacterial Adhesion Induced by the Substrate Stiffness. *Colloids Surfaces B Biointerfaces* **2014**, *114*, 193–200.

(160) Chang, Y.; Shih, Y. J.; Lai, C. J.; Kung, H. H.; Jiang, S. Blood-Inert Surfaces via Ion-Pair Anchoring of Zwitterionic Copolymer Brushes in Human Whole Blood. *Adv. Funct. Mater.* **2013**, *23*, 1100–1110.

(161) Kyomoto, M.; Moro, T.; Takatori, Y.; Kawaguchi, H.; Nakamura, K.; Ishihara, K. Self-Initiated Surface Grafting with poly(2-Methacryloyloxyethyl Phosphorylcholine) on Poly(ether-Ether-Ketone). *Biomaterials* **2010**, *31*, 1017–1024.

(162) Kuang, J.; Messersmith, P. B. Universal Surface-Initiated Polymerization of Antifouling Zwitterionic Brushes Using a Mussel-Mimetic Peptide Initiator. *Langmuir* **2012**, *28*, 7258–7266.

(163) Zhang, Z.; Chao, T.; Chen, S.; Jiang, S. Superlow Fouling Sulfobetaine and Carboxybetaine Polymers on Glass Slides. *Langmuir* **2006**, *22*, 10072–10077.

(164) Futamura, K.; Matsuno, R.; Konno, T.; Takai, M.; Ishihara, K. Rapid Development of Hydrophilicity and Protein Adsorption Resistance by Polymer Surfaces Bearing Phosphorylcholine and Naphthalene Groups. *Langmuir* **2008**, *24*, 10340–10344.

(165) Seo, J. H.; Matsuno, R.; Takai, M.; Ishihara, K. Cell Adhesion on Phase-Separated Surface of Block Copolymer Composed of poly(2-Methacryloyloxyethyl Phosphorylcholine) and Poly(dimethylsiloxane). *Biomaterials* **2009**, *30*, 5330–5340.

(166) Holmlin, R. E.; Chen, X.; Chapman, R. G.; Takayama, S.; Whitesides, G. M. Zwitterionic SAMs That Resist Nonspecific Adsorption of Protein from Aqueous Buffer. *Langmuir* **2001**, *17*, 2841–2850.

(167) Lee, H.; Dellatore, S. M.; Miller, W. M.; Messersmith, P. B. Mussel-Inspired Surface Chemistry for Multifunctional Coatings. *Science* **2007**, *318*, 426–430.

(168) Liebscher, J.; Mrówczyński, R.; Scheidt, H. A.; Filip, C.; Hădade, N. D.; Turcu, R.; Bende, A.; Beck, S. Structure of Polydopamine: A Never-Ending Story? *Langmuir* **2013**, *29*, 10539–10548.

(169) Van De Walle, E.; Van Nieuwenhove, I.; Vanderleyden, E.; Declercq, H. A.; Gellynck, K.; Schaubroeck, D.; Ottevaere, H.; Thienpont, H.; DeVos, W. H.; Cornelissen, M.; *et al.* Polydopamine–Gelatin as Universal Cell-Interactive Coating for Methacrylate-Based Medical Device Packaging Materials: When Surface Chemistry Overrules Substrate Bulk Properties. *Biomacromolecules* **2016**, *17*, 56–68.

(170) Ding, Y.; Weng, L.-T.; Yang, M.; Yang, Z.; Lu, X.; Huang, N.; Leng, Y. Insights into the Aggregation/Deposition and Structure of a Polydopamine Film. *Langmuir* **2014**, *30*, 12258–12269.

(171) Della Vecchia, N. F.; Luchini, A.; Napolitano, A.; D'Errico, G.; Vitiello, G.; Szekely, N.; D'Ischia, M.; Paduano, L. Tris Buffer Modulates Polydopamine Growth, Aggregation, and Paramagnetic Properties. *Langmuir* **2014**, *30*, 9811–9818.

(172) McCloskey, B. D.; Park, H. B.; Ju, H.; Rowe, B. W.; Miller, D. J.; Chun, B. J.; Kin, K.; Freeman, B. D. Influence of Polydopamine Deposition Conditions on Pure Water Flux and Foulant Adhesion Resistance of Reverse Osmosis, Ultrafiltration, and Microfiltration Membranes. *Polymer (Guildf).* **2010**, *51*, 3472–3485.

(173) Chang, C.-C.; Kolewe, K. W.; Li, Y.; Kosif, I.; Freeman, B. D.; Carter, K. R.; Schiffman, J. D.; Emrick, T. Underwater Superoleophobic Surfaces Prepared from Polymer Zwitterion/Dopamine Composite Coatings. *Adv. Mater. Interfaces* **2016**, *3*, 521–530.

(174) Persano, L.; Camposeo, A.; Tekmen, C.; Pisignano, D. Industrial Upscaling of Electrospinning and Applications of Polymer Nanofibers: A Review. *Macromol. Mater. Eng.* **2013**, *298*, 504–520.

(175) Gangwal, S.; Wright, M. Nanofibres: New Scalable Technology Platform for Producing Polymeric Nanofibres. *Filtr. Sep.* **2013**, *50*, 30–33.

(176) Deitzel, J. .; Kleinmeyer, J.; Harris, D.; Beck Tan, N. . The Effect of Processing Variables on the Morphology of Electrospun Nanofibers and Textiles. *Polymer (Guildf).* **2001**, *42*, 261–272.

(177) Moghadam, B. H.; Haghi, A. K.; Kasaei, S.; Hasanzadeh, M. Computational-Based Approach for Predicting Porosity of Electrospun Nanofiber Mats Using Response Surface Methodology and Artificial Neural Network Methods. *J. Macromol. Sci. Part B Phys.* **2015**, *54*, 1404–1425.

(178) Barnes, C. P.; Sell, S. A.; Boland, E. D.; Simpson, D. G.; Bowlin, G. L. Nanofiber Technology: Designing the next Generation of Tissue Engineering Scaffolds. *Adv. Drug Deliv. Rev.* **2007**, *59*, 1413–1433.

(179) Wang, X.; Ding, B.; Li, B. Biomimetic Electrospun Nanofibrous Structures for Tissue Engineering. *Mater. Today* **2013**, *16*, 229–241.

(180) Najafabadi, A. H.; Tamayol, A.; Annabi, N.; Ochoa, M.; Mostafalu, P.; Akbari, M.; Nikkhah, M.; Rahimi, R.; Dokmeci, M. R.; Sonkusale, S.; *et al.* Biodegradable Nanofibrous Polymeric Substrates for Generating Elastic and Flexible Electronics. *Adv. Mater.* **2014**, *26*, 5823–5830.

(181) Lee, J.; Jung, J.; Cho, Y. H.; Yadav, S. K.; Baek, K. Y.; Park, H. B.; Hong, S. M.; Koo, C. M. Fouling-Tolerant Nanofibrous Polymer Membranes for Water Treatment. *ACS Appl. Mater. Interfaces* **2014**, *6*, 14600–14607.

(182) Ma, H.; Hsiao, B. S.; Chu, B. Functionalized Electrospun Nanofibrous Microfiltration Membranes for Removal of Bacteria and Viruses. *J. Memb. Sci.* **2014**, *452*, 446–452.

(183) Baker, J. S.; Dudley, L. Y. Biofouling in Membrane Systems — A Review. *Desalination* **1998**, *118*, 81–89.

(184) Huang, L.; Arena, J. T.; Manickam, S. S.; Jiang, X.; Willis, B. G.; McCutcheon, J. R. Improved Mechanical Properties and Hydrophilicity of Electrospun Nanofiber Membranes for Filtration Applications by Dopamine Modification. *J. Memb. Sci.* **2014**, *460*, 241–249.

(185) Brown, R. H.; Hunley, M. T.; Allen, M. H.; Long, T. E. Electrospinning Zwitterion-Containing Nanoscale Acrylic Fibers. *Polymer (Guildf).* **2009**, *50*, 4781–4787.

(186) Lalani, R.; Liu, L. Synthesis, Characterization, and Electrospinning of Zwitterionic Poly(sulfobetaine Methacrylate). *Polymer (Guildf).* **2011**, *52*, 5344–5354.

(187) Emerick, E.; Grant, S.; Bernards, M. Electrospinning of Sulfobetaine Methacrylate Nanofibers. *Chem. Eng. Process Tech.* **2013**, *1003*.

(188) Lalani, R.; Liu, L. Electrospun Zwitterionic Poly(sulfobetaine Methacrylate) for Nonadherent, Superabsorbent, and Antimicrobial Wound Dressing Applications. *Biomacromolecules* **2012**, *13*, 1853–1863.

(189) Ye, S. H.; Hong, Y.; Sakaguchi, H.; Shankarraman, V.; Luketich, S. K.; DAmore, A.; Wagner, W. R. Nonthrombogenic, Biodegradable Elastomeric Polyurethanes with Variable Sulfobetaine Content. *ACS Appl. Mater. Interfaces* **2014**, *6*, 22796–22806.

(190) Mele, E.; Heredia-Guerrero, J. A.; Bayer, I. S.; Ciofani, G.; Genchi, G. G.; Ceseracciu, L.; Davis, A.; Papadopoulou, E. L.; Barthel, M. J.; Marini, L.; *et al.* Zwitterionic Nanofibers of Super-Glue for Transparent and Biocompatible Multi-Purpose Coatings. *Sci. Rep.* **2015**, *5*, 14019.

(191) Jiang, K.; Long, Y.-Z.; Chen, Z.-J.; Liu, S.-L.; Huang, Y.-Y.; Jiang, X.; Huang, Z.-Q. Airflow-Directed in Situ Electrospinning of a Medical Glue of Cyanoacrylate for Rapid Hemostasis in Liver Resection. *Nanoscale* **2014**, *6*, 7792–7798.

(192) Liu, S.-L.; Long, Y.-Z.; Huang, Y.-Y.; Zhang, H.-D.; He, H.-W.; Sun, B.; Sui, Y.-Q.; Xia, L.-H. Solventless Electrospinning of Ultrathin Polycyanoacrylate Fibers. *Polym. Chem.* **2013**, *4*, 5696–5700.

(193) Zhu, J.; Su, Y.; Zhao, X.; Li, Y.; Zhang, R.; Fan, X.; Ma, Y.; Liu, Y.; Jiang, Z. Constructing a Zwitterionic Ultrafiltration Membrane Surface via Multisite Anchorage for Superior Long-Term Antifouling Properties. *RSC Adv.* **2015**, *5*, 40126–40134.

(194) Huang, J.; Wang, D.; Lu, Y.; Li, M.; Xu, W. Surface Zwitterionically Functionalized PVA-Co-PE Nanofiber Materials by Click Chemistry. *RSC Adv.* **2013**, *3*, 20922.

(195) Huang, C.-J.; Chu, S.-H.; Wang, L.-C.; Li, C.-H.; Lee, T. R. Bioinspired Zwitterionic Surface Coatings with Robust Photostability and Fouling Resistance. *ACS Appl. Mater. Interfaces* **2015**, *7*, 23776–23786.

(196) Rieger, K. A.; Thyagarajan, R.; Hoen, M. E.; Yeung, H. F.; Ford, D. M.; Schiffman, J. D.; Persano, L.; Camposeo, A.; Tekmen, C.; Pisignano, D.; *et al.* Transport of Microorganisms into Cellulose Nanofiber Mats. *RSC Adv.* **2016**, *6*, 24438–24445.

(197) Bhuchar, N.; Deng, Z.; Ishihara, K.; Narain, R. Detailed Study of the Reversible Addition–fragmentation Chain Transfer Polymerization and Co-Polymerization of 2-Methacryloyloxyethyl Phosphorylcholine. *Polym. Chem.* **2011**, *2*, 632-639.

(198) Senbil, N.; He, W.; Démery, V.; Dinsmore, A. D. Effect of Interface Shape on Advancing and Receding Fluid-Contact Angles around Spherical Particles. *Soft Matter* **2015**, *11*, 4999–5003.

(199) Ma, Z.; Kotaki, M.; Ramakrishna, S. Electrospun Cellulose Nanofiber as Affinity Membrane. *J. Memb. Sci.* **2005**, *265*, 115–123.

(200) Frey, M. W. Electrospinning Cellulose and Cellulose Derivatives. *Polym. Rev.* **2008**, *48*, 378–391.

(201) Xie, J.; Michael, P. L.; Zhong, S.; Ma, B.; MacEwan, M. R.; Lim, C. T. Mussel Inspired Protein-Mediated Surface Modification to Electrospun Fibers and Their Potential Biomedical Applications. *J. Biomed. Mater. Res. - Part A* **2012**, *100*, 929–938.

(202) Yang, H.; Lan, Y.; Zhu, W.; Li, W.; Xu, D.; Cui, J.; Shen, D.; Li, G. Polydopamine-Coated Nanofibrous Mats as a Versatile Platform for Producing Porous Functional Membranes. *J. Mater. Chem.* **2012**, *22*, 16994–17001.

(203) Sundaram, H. S.; Han, X.; Nowinski, A. K.; Brault, N. D.; Li, Y.; Ella-Menye, J. R.; Amoaka, K. A.; Cook, K. E.; Marek, P.; Senecal, K.; *et al.* Achieving One-Step Surface Coating of Highly Hydrophilic Poly(Carboxybetaine Methacrylate) Polymers on Hydrophobic and Hydrophilic Surfaces. *Adv. Mater. Interfaces* **2014**, *1*, 1–8.

(204) Sileika, T. S.; Kim, H. Do; Maniak, P.; Messersmith, P. B. Antibacterial Performance of Polydopamine-Modified Polymer Surfaces Containing Passive and Active Components. *ACS Appl. Mater. Interfaces* **2011**, *3*, 4602–4610.

(205) Miller, D. J.; Araújo, P. a.; Correia, P. B.; Ramsey, M. M.; Kruithof, J. C.; van Loosdrecht, M. C. M.; Freeman, B. D.; Paul, D. R.; Whiteley, M.; Vrouwenvelder, J. S. Short-Term Adhesion and Long-Term Biofouling Testing of Polydopamine and Poly(ethylene Glycol) Surface Modifications of Membranes and Feed Spacers for Biofouling Control. *Water Res.* **2012**, *46*, 3737–3753.

(206) Araújo, P. A.; Miller, D. J.; Correia, P. B.; Van Loosdrecht, M. C. M.; Kruithof, J. C.; Freeman, B. D.; Paul, D. R.; Vrouwenvelder, J. S. Impact of Feed Spacer and Membrane Modification by Hydrophilic, Bactericidal and Biocidal Coating on Biofouling Control. *Desalination* **2012**, *295*, 1–10.

(207) Tateishi, T.; Kyomoto, M.; Kakinoki, S.; Yamaoka, T.; Ishihara, K. Reduced Platelets and Bacteria Adhesion on Poly(ether Ether Ketone) by Photoinduced and Self-Initiated Graft Polymerization of 2-Methacryloyloxyethyl Phosphorylcholine. *J. Biomed. Mater. Res. - Part A* **2014**, *102*, 1342–1349.

(208) Sui, S.; Wang, Y.; Kolewe, K.; Srajer, V.; Henning, R.; Schiffman, J. D.; Dimitrakopoulos, C.; Perry, S. L. Graphene-Based Microfluidics for Serial Crystallography. *Lab Chip* **2016**, *16*, 3082-3096.

(209) Liu, Y.; Ai, K.; Lu, L. Polydopamine and Its Derivative Materials: Synthesis and Promising Applications in Energy, Environmental, and Biomedical Fields. *Chem. Rev.* **2014**, *114*, 5057–5115.

(210) Hong, S.; Na, Y. S.; Choi, S.; Song, I. T.; Kim, W. Y.; Lee, H. Non-Covalent Self-Assembly and Covalent Polymerization Co-Contribute to Polydopamine Formation. *Adv. Funct. Mater.* **2012**, *22*, 4711–4717.

(211) Birch, N. P.; Barney, L. E.; Pandres, E.; Peyton, S. R.; Schiffman, J. D. Thermal-Responsive Behavior of a Cell Compatible Chitosan/pectin Hydrogel. *Biomacromolecules* **2015**, *16*, 1837–1843.

(212) Rahbani, J.; Behzad, A. R.; Khashab, N. M.; Al-Ghoul, M. Characterization of Internal Structure of Hydrated Agar and Gelatin Matrices by Cryo-SEM. *Electrophoresis* **2013**, *34*, 405–408.

(213) Seliktar, D. Designing Cell-Compatible Hydrogels. *Science* **2012**, *336*, 13–17.

(214) Haque, M. A.; Kurokawa, T.; Gong, J. P. Super Tough Double Network Hydrogels and Their Application as Biomaterials. *Polymer (Guildf).* **2012**, *53*, 1805–1822.

(215) Kolewe, K. W.; Dobosz, K. M.; Rieger, K. A.; Chang, C.-C.; Emrick, T.; Schiffman, J. D. Antifouling Electrospun Nanofiber Mats Functionalized with Polymer Zwitterions. *ACS Appl. Mater. Interfaces* **2016**, *8*, 27585-27593.

(216) Tsai, W. B.; Grunkemeier, J. M.; Horbett, T. A. Human Plasma Fibrinogen Adsorption and Platelet Adhesion to Polystyrene. *J. Biomed. Mater. Res.* **1999**, *44*, 130–139.

(217) Chen, H.; Chen, Q.; Hu, R.; Wang, H.; Newby, B. Z.; Chang, Y.; Zheng, J. Mechanically Strong Hybrid Double Network Hydrogels with Antifouling Properties. *J. Mater. Chem. B* **2015**, *3*, 5426–5435.

(218) Cui, J.; Ju, Y.; Liang, K.; Ejima, H.; Lörcher, S.; Gause, K. T.; Richardson, J. J.; Caruso, F. Nanoscale Engineering of Low-Fouling Surfaces through Polydopamine Immobilisation of Zwitterionic Peptides. *Soft Matter* **2014**, *10*, 2656–2663.

(219) Cheng, G.; Zhang, Z.; Chen, S.; Bryers, J. D.; Jiang, S. Inhibition of Bacterial Adhesion and Biofilm Formation on Zwitterionic Surfaces. *Biomaterials* **2007**, *28*, 4192–4199.

(220) Gungor, B.; Esen, Ş.; Gök, A.; Yilmaz, H.; Malazgirt, Z.; Leblebicioğlu, H. Comparison of the Adherence of E.Coli and S. Aureus to Ten Different Prosthetic Mesh Grafts: In Vitro Experimental Study. *Indian J. Surg.* **2010**, *72*, 226–231.

(221) Hsieh, Y. -L; Merry, J. The Adherence of Staphylococcus Aureus, Staphylococcus Epidermidis and Escherichia Coli on Cotton, Polyester and Their Blends. *J. Appl. Bacteriol.* **1986**, *60*, 535–544.

(222) Kang, S. M.; Hwang, N. S.; Yeom, J.; Park, S. Y.; Messersmith, P. B.; Choi, I. S.; Langer, R.; Anderson, D. G.; Lee, H. One-Step Multipurpose Surface Functionalization by Adhesive Catecholamine. *Adv. Funct. Mater.* **2012**, *22*, 2949–2955.

(223) Wang, L.; Zhou, Q. Surface Hydrophobicity of Slippery Zones in the Pitchers of Two Nepenthes Species and a Hybrid. *Sci. Rep.* **2016**, *6*, 19907.

(224) Amini, S.; Kolle, S.; Petrone, L.; Ahanotu, O.; Sunny, S.; Sutanto, C. N.; Hoon, S.; Cohen, L.; Weaver, J. C.; Aizenberg, J.; *et al.* Preventing Mussel Adhesion Using Lubricant-Infused Materials. *Science.* **2017**, *673*, 668–673.

(225) Freschauf, L. R.; McLane, J.; Sharma, H.; Khine, M. Shrink-Induced Superhydrophobic and Antibacterial Surfaces in Consumer Plastics. *PLoS One* **2012**, *7*, 1–7.

(226) Rahmawan, Y.; Jang, K.-J.; Moon, M.-W.; Lee, K.-R.; Suh, K.-Y. Anti-Biofouling Coating by Wrinkled, Dual-Roughness Structures of Diamond-like Carbon (DLC). *Biochip J.* **2009**, *3*, 143–150.

(227) Kirschner, C. M.; Brennan, A. B. Bio-Inspired Antifouling Strategies. *Annu. Rev. Mater. Res.* **2012**, *42*, 211–229.

(228) Carman, M. L.; Estes, T. G.; Feinberg, A. W.; Schumacher, J. F.; Wilkerson, W.; Wilson, L. H.; Callow, M. E.; Callow, J. A.; Brennan, A. B. Engineered Antifouling Microtopographies – Correlating Wettability with Cell Attachment. *Biofouling* **2006**, *22*, 11–21.

(229) Kubacka, A.; Diez, M. S.; Rojo, D.; Bargiela, R.; Ciordia, S.; Zapico, I.; Albar, J. P.; Barbas, C.; Martins dos Santos, V. a P.; Fernández-García, M.; *et al.* Understanding the Antimicrobial Mechanism of TiO_2-Based Nanocomposite Films in a Pathogenic Bacterium. *Sci. Rep.* **2014**, *4*, 4134.

(230) Guan, K. Relationship between Photocatalytic Activity, Hydrophilicity and Self-Cleaning Effect of TiO2/SiO2 Films. *Surf. Coatings Technol.* **2005**, *191*, 155–160.

(231) Hasan, J.; Crawford, R. J.; Ivanova, E. P. Antibacterial Surfaces: The Quest for a New Generation of Biomaterials. *Trends Biotechnol.* **2013**, *31*, 295–304.

(232) Ostrikov, K.; Macgregor-Ramiasa, M.; Cavallaro, A.; Ostrikov, K. (Ken); Vasilev, K. Bactericidal Effects of Plasma-Modified Surface Chemistry of Silicon Nanograss. *J. Phys. D. Appl. Phys.* **2016**, *49*, 304001.

(233) Zhang, Y.; Diao, Y.; Lee, H.; Mirabito, T. J.; Johnson, R. W.; Puodziukynaite, E.; John, J.; Carter, K. R.; Emrick, T.; Mannsfeld, S. C. B.; *et al.* Intrinsic and Extrinsic Parameters for Controlling the Growth of Organic Single-Crystalline Nanopillars in Photovoltaics. *Nano Lett.* **2014**, *14*, 5547–5554.

(234) Rieger, K. a; Schiffman, J. D. Electrospinning an Essential Oil: Cinnamaldehyde Enhances the Antimicrobial Efficacy of Chitosan/poly(ethylene Oxide) Nanofibers. *Carbohydr. Polym.* **2014**, *113*, 561–568.